REDESIGN OF A COMPOSITE SPORTS CAR TO ACCOMMODATE A BATTERY ELECTRIC POWERTRAIN FOR TYPE APPROVAL IN THE EUROPEAN UNION

Master Thesis
A.P.C. Urlings

15 March 2017

Confidentiality Notice

In this report all used confidential information provided by Roding Automobile GmbH or its suppliers are omitted. General available information is included, however brand names and cost are not provided since this is proprietary information. The research will be presented using normalised values, rounded values or cost ratios.

Abstract

Since 2008, Roding Automobile GmbH has been developing composite products and small series vehicles. Both are combined in their flagship the Roding Roadster, a medium sized two-seater sports car. This research project was set up to combine a lightweight chassis design with the increasing demand for battery electric vehicles. The goal of this research was to get a better understanding of the consequences of the integration of a battery electric powertrain on the chassis layout and its type approval in the European Union.

The Roding Roadster, which is developed and produced by Roding Automobile GmbH, was used as reference throughout this research. The original Roding Roadster uses an internal combustion engine to drive the vehicle. In this research, this powertrain was withdrawn to accommodate a battery electric powertrain. The general layout and suspension of the original vehicle were used as starting point for the redesign.

Based on the legislation for type approval within the European Union, requirements and tests were extracted which apply to electric passenger cars. These tests were transformed to static load cases, which were used to give an estimation of the chassis behaviour under collision loads and other approval tests. To analyse the load transfer during the prescribed collisions, the inertia relief method was used. This method uses inertial loads instead of supports to bring a system in static equilibrium.

Along with these load cases, design envelopes were constructed, to create a set of criteria to create a measure for the concept. Using these requirements and measuring criteria, several concepts were created for at first the powertrain and later the structural chassis. A trade-off based on the costs and weight distribution resulted in the use of four in-wheel motors in combination with a REESS (Rechargeable Energy Storage System) in the middle tunnel and rear section of the vehicle. To guarantee adequate grounding, a concept utilizing the conductive property of aluminium honeycomb was developed and tested. Measurements supported compliance with European legislation and resulted in an estimation method for different geometries.

It was decided that the frontal substructure and passenger compartment do not require major alterations to serve as chassis for the battery electric version, based on their layout and structural performance. For this reason, only the metal rear substructure is replaced by a composite substructure. This is combined with an integral REESS structure, which can be easily assembled and is adaptable for different vehicles and battery modules. For this structure the performance was analysed and reviewed during the defined collision tests. The most limiting points, such as the suspension connections and manufacturing, were developed in further detail. This resulted in a vehicle with an estimated kerb weight of 1467kg.

This final concept indicates that it is feasible to create a battery electric version of the Roding Roadster, and that only minor adjustments are required to the frontal substructure and the passenger compartment. That is why, this research provides relevant insight in the implications of accommodating a battery electric powertrain in a composite sports car. It is suggested further research should be performed to create a more accurate structural analysis which enables manufacturers to check suitability for type approval, early in the development process. Furthermore it is concluded that different automotive projects can benefit from the researched decision-making methods and concepts developed in this project.

Preface

According to Nikola Tesla, dependency on fossil fuel would eventually turn on us. This thesis provides a tiny link in the transition towards more sustainable, electric transport. The research was performed at Roding Automobile GmbH in Roding, Germany as part of my studies at the Aerospace Engineering faculty at Delft University of Technology. It is a mandatory element of the Master of Science curriculum within the Aerospace Structures and Materials group. The work was performed at Roding Automobile GmbH from the September 1st 2016 till March 2nd 2017.

"Electric power is everywhere present in unlimited quantities and can drive the world's machinery without the need of coal, oil, gas, or any other of the common fuels."

- Nikola Tesla

Roding Automobile GmbH has given me the opportunity to perform my internship and literature study prior to this research project. I would like to thank Managing Director Dipl.-Ing. G. Riedl for giving me the opportunity to come to Roding and my supervisor Dipl.-Ing. W. Frank for the advice and guidance throughout this period. Further I would like to thank Dr.ir. J.M.J.F. van Campen as supervisor from Delft University of Technology, for bringing me into contact with Roding Automobile GmbH, his support, feedback and knowledge throughout this research. I would like to thank all employees of Roding Automobile GmbH for the opportunity to work in the professional environment of their company, which gave me a lot of valuable experience for my further career and insight in the commercial environment. At last I would like to thank C. Ligthart as well, for her comments and feedback during the creation of this thesis report.

Toine Urlings BSc
Roding, 15 March 2017

Table of Contents

Nomenclature

Symbols

Symbol	Unit	Description
$\hat{a}_x, \hat{a}_y, \hat{a}_z$	g	Threshold acceleration components
$\bar{a}_x, \bar{a}_y, \bar{a}_z$	g	50ms average vehicle acceleration components
A	m^2	Cross sectional area
ASI	-	Acceleration Severity Index
I	A	Current
I_{zz}	m^2*kg	Mass moment of inertia
ℓ	m	Length
R	Ω	Electrical resistance
r_i	m	Distance from the rotation axis
T	N*m	Torque
U	V	Voltage
V_f	-	Fibre volume ratio
α	rad/s^2	Angular acceleration
γ	-	Shear strain
ε	-	Strain
κ	m^{-1}	Curvature
τ	s	Period of loading
ω	Hz	Natural frequency
m_i	kg	Component mass

Acronyms

Acronym	Description
AC	Alternating Current
AFP	Automated Fibre Placement
ASI	Acceleration Severity Index
ATL	Automated Tape Laying
AWD	All-Wheel Drive
BEV	Battery Electric Vehicle
BMS	Battery Management System
CAD	Computer-Aided Design
CEN	European Committee for Standardization (organisation)
CFRP	Carbon Fibre Reinforced Plastic
CLT	Classical Laminate Theory
CG	Centre of Gravity
DC	Direct Current
DIN	Deutsches Institut für Normung (organisation)
EC	European Commission (organisation)
ECE	see UNECE
EMI	Electromagnetic Interference
EU	European Union (organisation)
FBD	Free Body Diagram
FE	Finite Element
FIA	Federation Internationale de l'Automobile (organisation)
gsm	Gram per Square Meter
HIC	Head Injury Criterion (similar to HPC)
HP RTM	High Pressure Resin Transfer Moulding
HPC	Head Performance Criterion (similar to HIC)
HV	High Voltage
HVAC	Heating, Ventilation and Air Conditioning
ICE	Internal Combustion Engine
ICEV	Internal Combustion Engine Vehicle
Li-ion	Lithium ion
LP RTM	Low Pressure Resin Transfer Moulding
LV	Low Voltage

Acronym	Description
Mass dis.	Mass distribution
M_1	Passenger car comprising not more than nine seats (driver included)
mln.	Million
n/a	Not Applicable
OEM	Original Equipment Manufacturer
pc.	Piece
Qty.	Quantity
RA	Roding Automobile GmbH (organisation)
REESS	Rechargeable Energy Storage System
Ref.	Reference
Res.	Resistance
RESS	Similar to REESS, both are used haphazardly in UNECE legislations [1]
Rivnut	Blind Rivet Nut
rpm	Revolutions per Minute
RTM	Resin Transfer Moulding
RWD	Rear Wheel Drive
SAE	Society of Automotive Engineers (organisation)
SMC	Sheet Moulding Compound
Src.	Source
UNECE	United Nations Economic Commission for Europe (organisation)
USA	United States of America
VAC	Volt Alternating Current
VDC	Volt Direct Current

1 Introduction

In the last decades composite knowledge and usage has increased immensely due to its high specific strength and stiffness. The possibility to use the superior properties of composites for weight reduction resulted in the introduction of composites in the commercial automotive industry by McLaren in the early 90's. [2] Since then, carbon fibre consumption in the automotive market grew explosively and it currently undergoes an annual growth of 12.6%. [3, 4]

Since its founding in 2008, Roding Automobile GmbH has developed a lot of knowledge about composites in primarily the automotive industry. Along with that, the company is involved in the development of several prototypes and test vehicles for electric driven cars. This research was created by Roding Automobile GmbH to explore the feasibility of combining these technologies in composite chassis for a battery electric version of their Roding Roadster sports car. The achievements by Roding Automobile GmbH and development in the automotive industry can be used to move towards the development of more advanced vehicles. The objective of this research is to come up with a concept for the composite chassis of the Roding Roadster which accommodates a battery electric powertrain, and is suitable for type approval within the European Union to facilitate series production. The purpose of this project is to improve know-how on the implications of type approval for Roding Automobile GmbH. This is emphasised on the requirements for collision tests and electric vehicles. In this research this will be specifically evaluated for the development of a battery electric, composite based sports car. Supplementary to the gathered knowledge on the Roding Roadster, the outcome of this research is expected to give more insight in electric vehicle development and legislation for passenger cars in general.

This report will present an overview of the performed research, development and analysis of the composite chassis for a battery electric sports car. To be able to develop a more realistic vehicle, the Roding Roadster was used as starting point and reference vehicle. Multiple steps are discussed to develop a final chassis concept which can be used to create an electric sports car with the desired characteristics. Furthermore the chassis was analysed using finite element analysis to get an insight in the performances under, for example, collision load cases. This research should answer the question how the Roding Roadster could best be outlined, when it is redesigned as a battery electric vehicle and what chassis concept suits this layout best.

To start, Chapter 2 defines the standards and assumptions which are applied throughout this report. Chapter 3 will represent a short summary of the literature study, performed at the start of this project. Chapter 4 will draw the outlines of the research, by giving a short overview of the background information driving the project and summing up the requirements. Chapter 5 will show the development of the design envelope along with supporting research for the development of the vehicle. Subsequently, this chapter will elaborate on legislation and analysis methods. To perform the structural analysis in Chapter 6, this chapter first describes how the load cases used in this research were determined. Chapter 7 will be used to elaborate on the vehicle concepts, divided into powertrain concepts and chassis concepts. At the end of this chapter the best concept is chosen using a trade-off. Chapter 8 will go into more detail on the chosen concept and elaborate on some relevant design details. This final design will be then reviewed in Chapter 9. Chapter 10 presents the conclusions of the research, which will be followed by a set of recommendations for further development of composite based electric sports cars and the Roding Roaster in general in Chapter 11.

2 Standards and Assumptions

In this chapter general assumptions and conditions are presented which will be used throughout this research report. This includes the definition of a three-dimensional reference system and the units used in general.

2.1 Axis Systems

Throughout this report a right-handed axis system is used unless described differently. The origin of this axis system is defined as the intersection between the longitudinal plane of symmetry and the line between the centre points of both front wheels in rest. The horizontal vehicle centreline in opposite direction from the forward direction of travel defines x-axis. The z-axis is defined towards zenith. This global axis system is visualised in Figure 2.1. Where relevant, the principle directions of this axis system are visualised in figures throughout the research. For the sake of clarity, the origin is mostly not visualised at the global origin.

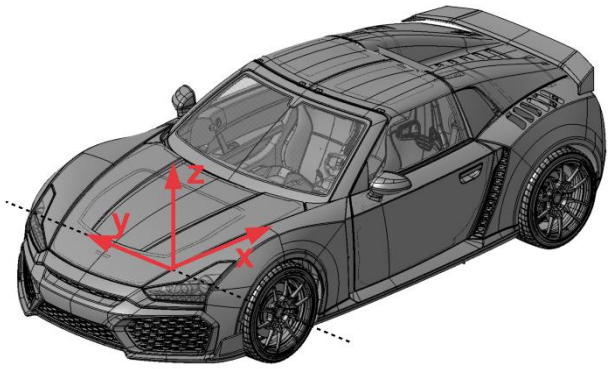

Figure 2.1 Global vehicle axis system

2.2 Units of Measurement

This report will use measures based on the International System of Units (SI units), unless described differently. Forces will be displayed in Newton, using the orientation of the vehicle axis system discussed in Section 2.1. Moments are considered positive when counter clockwise. Prices are all calculated in Euros, where values in US Dollars are converted with an exchange rate of 0.89.

2.3 Safety Factors

A conservative approach for the load determinations, and the 1.25 load factor to account for dynamic overshoot in combination with inertia relief, were used within the created models. Besides these measures, no safety factors were applied on both the material properties and the loads. This was done to report unbiased results, since the scope of this project was to give an estimation of the structural performance. Further research should elaborate on the product quality, analysis accuracy and the required safety margins depending on each load case.

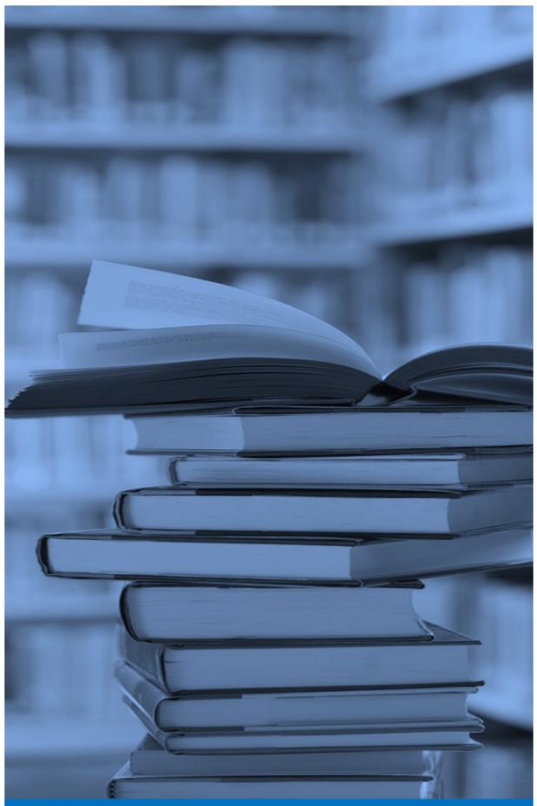

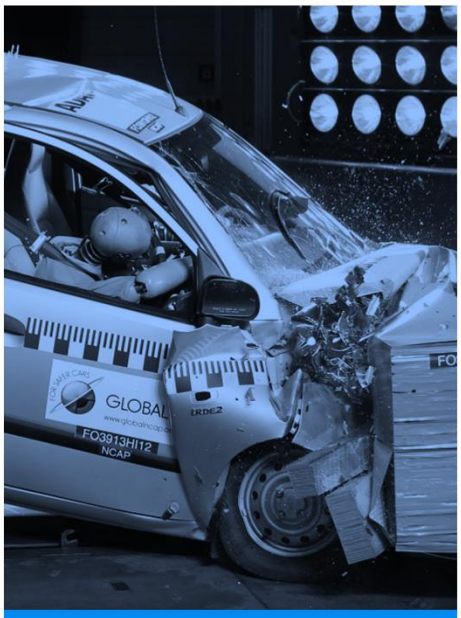

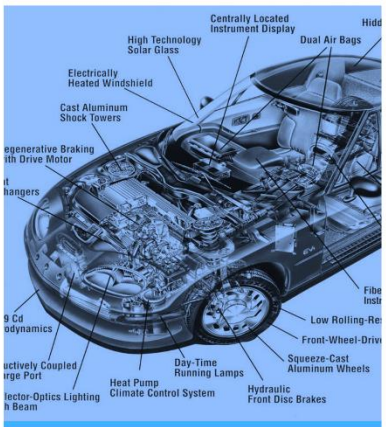

3 Literature Review

As preparation for this research project a literature study was performed from June 1st to August 31st 2016. [1] This chapter will give a brief overview of the most important information which was found. At first a summary on main passenger car components will be presented. Components specific for BEVs (Battery Electric Vehicles) will be presented separately.

For cars produced in series, a set of regulations must be met to qualify for type approval. In this chapter the regulations related to the chassis of the vehicle are outlined according to legislation in the European Union. This is followed by a quick overview on manufacturing methods for composites. At last this chapter will give insight in the investigated methods for structural analysis, which will be worked out in more detail throughout this research project.

Electric powertrains improved significantly over the last 30 years. Simultaneously the use of fibre reinforced composites increased. [5, 6] This resulted in the interest of the automotive industry for both technologies. In 2013 BMW introduced the i3, which was the first large-series production consumer car making extensive use of composites in primary car structures. [7] The higher specific properties of composite materials enabled a substantial weight reduction. Since a limited range is often seen as the biggest downside of BEVs (Battery Electric Vehicles) when selecting a car, decrease in weight and therefore power consumption is very advantageous for electric transportation.

3.1 Vehicle Components

In order to develop a passenger car, some basic knowledge on main vehicle components must be gathered first. A list of the major components in passenger cars is drafted below. Common components for passenger cars will be assigned first and will be followed with a brief description for BEV specific components.

3.1.1 General Vehicle Components

Chassis: In the automotive industry the chassis is defined as the primary structure of a vehicle. Its main functions is to protect the occupants and transfer loads between the suspensions which are mounted to the chassis. The first composite based chassis was used in the early 80's. [2] In history several chassis concepts were used. For composite based chassis, a monocoque concept is often used as basis, often combined with metal sub-frames. In a monocoque the exterior fulfils additionally the function of main structure, which is often applied to reduce weight. The weight reduction due to the use of composite monocoque chassis can typically add up to 40% with respect to aluminium chassis and 60% with respect to steel chassis. [8]

Suspension: The suspension is defined as "the system of tires, tire air, springs, shock absorbers and linkages that connects a vehicle to its wheels and allows relative motion between the two." [9] This research will be limited to the use of the double wishbone suspensions which are also used in the Roding Roadster. This suspension layout is used since it allows careful control of the kinematics. An example of such a configuration can be seen in Figure 3.1.

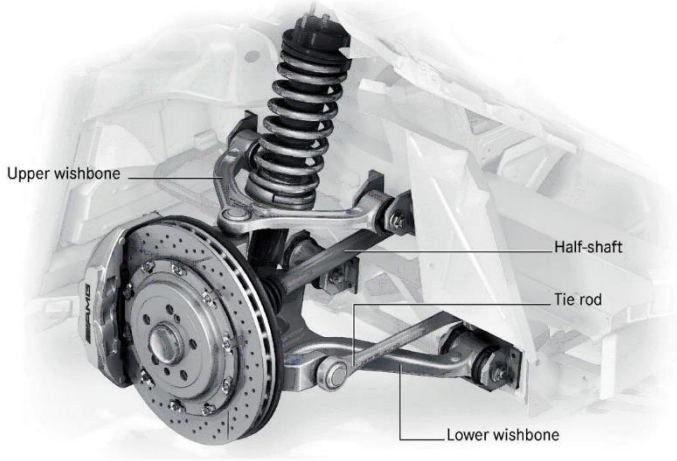

Figure 3.1 Double wishbone suspension configuration [10]

Steering System: The system which enables the driver to control the direction of the vehicle will be adapted from the conventional Roding Roadster. This system makes use of a rack and pinion combination connected to the suspension with a tie rod to fix the direction of the wheel.

Braking system: The brake system will, when possible, be adapted from the conventional Roding Roadster. This system consists of brake discs with hydraulic callipers, a pedal connected to the brake cylinder with brake booster and an ABS-block (Anti Blocking System) to improve safety.

Vehicle Control System: A vehicle control system combines inputs like the throttle setting and the state of the powertrain, to control and monitor the state of the vehicle. Most modern vehicles have such a system available to improve performance and safety.

Low Voltage Electronics: Most modern vehicles have complicated electric systems to monitor and control the vehicle or to increase comfort. Since these operate at a lower current level this system is often referred to as low voltage (LV) electronics in vehicles which also contain high voltage (HV) electrics. This includes for example safety systems, windscreen wipers, electric locking systems and infotainment. These systems are all powered and connected using an extensive wiring loom.

Auxiliary battery: For practicality and safety reasons some LV components should operate when the vehicle is turned off. For this reason an auxiliary battery is present in the LV system. This auxiliary battery is used in both internal combustion engine vehicles (ICEV) as in electric vehicles, however in ICEVs the power is generated using a small generator, where in BEVs energy is obtained from the electric system.

Interior: The interior influences the chassis design with respect to seating position, seatbelts and ergonomics. For this reason some interior aspects should be taken into account in the chassis design. It is also important to note that for aesthetic and weight saving reasons, sports cars manufacturers (and Roding Automobile GmbH) make minimal use of lining. This however demands high quality finish of the composite products, which should be taken into account when choosing manufacturing methods.

Bodywork/Body panels and closures: Bodywork is the name for exterior panelling of vehicles. In a semi-monocoque the chassis replaces parts of this bodywork. Remaining panels can be made of carbon fibre or glass fibre composites to make stiff but light panels. Hoods, doors and lids are called closures. They do have a structural function, however this is neglected in this chassis development.

Heating, Ventilation and Air Conditioning (HVAC): Most vehicles, as well as the Roding Roadster, have a heating HVAC system for passenger comfort. In ICEVs the HVAC system uses the heat and propulsion from the engine. Due to the lack of an engine in an electric vehicle, it costs more energy to include a HVAC system. For this reason the HVAC system should be accounted for when designing the electric system in detail.

Cooling system: Besides the heating and cooling of the passenger compartment most vehicles contain a cooling system for the powertrain. Besides coolant hoses, this system typically contains a radiator and a pump which are often combined with the HVAC system. A lot of the High Voltage (HV) components require liquid cooling, however the total cooling capacity of BEVs is typically lower than for ICEVs.

3.1.2 Battery Electric Vehicle Components

Motor: Where conventional cars use combustion engines to power the vehicle, electric cars make use of at least one electric motor. There are different types of electric motors using different working principles. For electric vehicles AC (Alternating Current) motors are commonly used for its higher reliability, efficiency and lower weight. Synchronous AC motors suit BEVs best. [11] Depending on their design, electric motors require a gearbox to operate in their most optimal rpm range (Revolutions per Minute) and reach the required top speed, power and torque.

Inverter (also called motor controller): Since batteries provide direct current (DC), the use of AC electric motors requires an additional component to convert the electric power. This device is called an inverter and should match the characteristics of the motor. An input signal defines the output power setting, so the motor controller can match this.

REESS (Rechargeable Energy Storage System): The energy source can be seen as the basis of a BEV, since it provides the power the vehicle requires to drive. The size and weight of the REESS are mainly defined by the required capacity, which defines the vehicle its range and performance. During the literature study it was found that lithium-ion batteries are by far the best choice for BEVs at the moment. [11] REESS is a more general term which is often used as the name for the energy source in electric vehicles since it is not limited to chemical batteries.

DC/DC converter: Since the LV electronics operate at a lower current level than the powertrain, an additional power source is required. To power the low voltage system a BEV uses a converter instead of a generator for increased efficiency. This converter is also used to charge the auxiliary battery.

Charger: As the conventional power grid provides AC, electricity should be converted to DC to charge the REESS. Most BEVs carry this device around to be able to charge at more locations.

Vacuum pump: In ICEVs the brake force is amplified using a vacuum assisted brake booster. Since the engine air intake cannot be used to provide suction. A small vacuum pump is required to complete the braking system in electric vehicles.

3.2 Type Approval within the European Union

For series manufactured vehicles it is not required to approve each vehicle separately, to exploit street legal vehicles. Instead this can be done for the vehicle type in general using type approval. Within the European Union (EU) this type approval is based on adapted regulations from the United Nations Economic Commission for Europe (UNECE) and can be found under directive 2007/46/EC. [1, 12]

The legislation under this European Directive is compulsory for type approval in the EU, however, the manufacturer can apply for an “EC type-approval of small series” under Article 22. [12] When for a vehicle type, less than 1,000 M_1 vehicles (passenger cars) are registered annually, this article can be used to reduce the requirements for type approval. The most important changes in small series type

approval are that the criteria for occupant and pedestrian protection criteria do not have to be met (ECE R94, ECE R95 and ECE R102). This is done to eliminate collision test, which are a major expense for vehicles in small series production. Frontal collision and lateral collision will however be described since it will give a good insight in the requirements of chassis produced in large series, which was a rationale for the initiation of this research. The most relevant passages influencing the chassis design will be described below. [12, 13, 14]

ECE R12 - Protective steering: To limit the amount of harm the steering wheel can do to a driver, the steering column may not move more than 12.7cm backwards and 12.7cm upwards when driving into a concrete barrier at 48.3km/h. Besides this requirement, the possibility to receive an electric shock throughout this test must be non-existent. In small series type approval the manufacturer must meet the main requirements of ECE R17 in a way acknowledged by the approving authority.

ECE R14 - Safety-belt anchorages: This regulation sets requirements for allowed types of safety belts. In a conventional three-point safety belt, the vehicle structure must withstand 13500N on the torso strap and lower belt at the same moment. When the belt anchorages are (partially) mounted to the seat, the described loads should be applied along with a 20g acceleration of the seat. The anchorage points should be able to withstand the loads, “allowing permanent deformation and partial failure”. [1]

ECE R17 - Seat approval: Since off-the-shelf seats are used at Roding Automobile GmbH which comply with ECE R17, testing of the anchorage points is the remainder of ECE R17. This can be done by a frontal collision into a concrete barrier at 50km/h, or a cheaper 20g inertia resistance test. The conditions are satisfied when the anchorages hold the loads and show no failure.

ECE R34 – Prevention of fire risk: For approval of fuel tanks, the vehicle should conform to ECE R34. However the exclusion of this test in the absence of a fuel tank is not elaborated on. For this reason it is not clear if and how electric vehicles should meet these requirements.

The regulation states several requirements for the frontal, lateral (ECE R94 and ECE R95) and an additional rear end collision test. The rear collision defines a 1,100 kg test vehicle impacting the vehicle at 50 km/h from the rear, using a rigid impacting surface. This test can also be replaced by an analysis or substituted test that shows conformity. During the tests no fire maintained by the fuel may occur and leakage of fuel is limited.

ECE R94 - Frontal collision: This regulation dictates a frontal collision throughout which de occupant protection is evaluated. At 56km/h the vehicle is driven forward into a deformable barrier with an overlap op 40%. The occupant protection is defined by a number of requirements and numerical evaluations for injury. Besides accessibility and direct harm from components in the passenger compartment, the allowed vehicle deceleration is most important for the overall chassis design. This is mainly limited by the Head Injury Criterion (HIC, similar to HPC), which should be less than 1,000.

ECE R95 - Lateral collision: A lateral collision is defined similarly to ECE R94. In this collision a 950kg test vehicle collides at 50km/h into the side of the vehicle around the position of the driver. The most important criterion is here also the maximum allowed HIC, being 1,000. The colliding element of the test vehicle is covered with a deformable barrier.

ECE R100 - Electric vehicles: Since July 2016, the European Parliament made ECE R100 mandatory for type approval of vehicles with an electric powertrain. [15] The first section of this regulation states requirements on electrical safety of the total vehicle, the second section defines regulation which should be met for the REESS.

For electrical safety it is stated that using defined probes, one cannot touch parts which are energised. Also all exposed conductive parts which belong the HV system should be grounded to the chassis with a resistance of less than 0.1Ω to prevent indirect shocks.

The REESS construction must be approved by a set of tests. This can be done as part of the ECE R94 and ECE R95 collision test, or by separately defined component based tests. These component based tests includes a mechanical shock and crush test. During both tests the isolation should also be intact and there should be no evidence of fire, explosion or electrolyte leakage. During the mechanical shock test, the REESS should “remain within its boundaries” as well. [1] Besides these tests, a thermal shock and vibration test are required to approve the REESS. When flammable electrolytes (Lithium Ion REESS cells included) are used, an additional fire resistance test must be carried out in addition.

ECE R125 - Forward field of vision: This regulation dictates four requirements for the forward field of vision. This influences the chassis design since it limits the construction geometry. These limits mainly influence the “A” pillars, which are defined as the frontal roof supports, including non-transparent parts. The following requirements are defined:

- A minimal transparent area defines the minimal size of the windscreen.
- The “A” pillars are limited in geometry by a maximum angle of obstruction.
- Within a well-defined area, no obstruction is allowed that blocks the view. This requirements excludes "A" pillars, vents, side window division bars, radio antennas, rear-view mirrors and windscreen wipers.
- A maximum height of the steering wheel is defined to limit obstruction of the view.

3.3 Composite Manufacturing

For the production of composite components in small series different manufacturing techniques were investigated. For a relative complex part as a vehicle chassis with annual production rates up to 1,000 parts, it is unlikely to use automated tape laying or automated fibre placement. The reason is that the required investment in machinery and development is very high and relatively complex geometries in this project are not expected to be very suitable. Due to high initial costs, wet compression moulding and HP RTM (High Pressure Resin Transfer Moulding) are more suitable for automated mass production. Open moulding and wet lay-up are excluded since these create components which do not have the quality consistency and visual quality which are desired. SMC-pressing (sheet moulding compound) and thermoplastic forming do also not create high visual quality parts, but create cheap constant quality parts quickly. Therefore, for non-visual parts, this process might be suitable in the required production range. Since this process would be used in specific components, investment costs might be covered by outsourcing the production of these specific components.

Braiding, pultrusion and filament winding are production processes which create advantages for very specific geometries and applications. For this reason these processes might be the solution for specific problems, although they are not expected to serve as main manufacturing method. In the end hand lay-up, vacuum infusion and LP RTM appear to be the most promising manufacturing methods since they are very adaptable processes, suitable for the required production rate.

3.4 Structural Analysis

A chassis can be either analysed analytically or numerically. During the literature study, multiple techniques were combined to form a methods to assess the structural performance of the chassis in the concept phase. For the analytical part the Classical Laminate Theory (CLT) will be used to create realistic lay-up stacks. Numerical analyses can be done using Finite Element (FE) methods in Catia or Ansys Workbench.

These numerical analyses can be performed to check the structural performance for three main categories of load cases: collision load cases, regulatory load cases and operational load cases. Operational load cases describe the loads when driving the vehicle. Since the periods of these load cases are relatively long, these loads will be analysed statically. The same holds for most regulatory load cases. However for crash analyses the inertia of the vehicle will influence the loads during impact significantly. This influence can be included using the principle of inertia relief. This method can be used to create a relatively simple static FE analysis, instead of an expensive dynamic FE analysis to estimate load during impact. The principle of this method is to apply a set of accelerations to bring an unconstraint system in static equilibrium. [16, 17, 18] A detailed description of the used methods for analysis used in this research is given in Chapter 6. In this chapter the load cases are explained into detail as well.

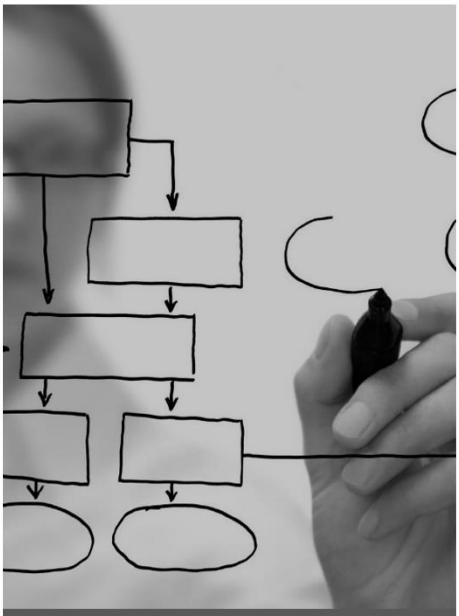

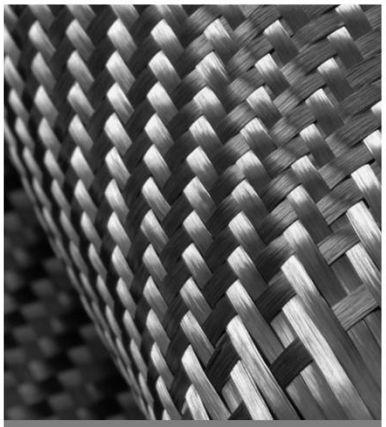

Project Definition

4

This chapter will outline the context of the project, to draw a picture of the desired output. The background will be described briefly by introducing the conventional Roding Roadster. This is done to give a better understanding of Roding Automobile GmbH, the Roding Roadster and the performed research. At last the requirements for the researched vehicle will be set.

4.1 Context of Research Project

Roding Automobile GmbH is an automotive company which has developed a lot of knowledge about composites since 2008, when it was founded. Roding Automobile GmbH, in collaboration with the in-house composite production company, SK Carbon, developed a carbon based sports car called Roding Roadster (Figure 4.1 and Figure 4.2). The evolution of the automotive market towards electric transport resulted in the development of multiple electric vehicles at Roding Automobile GmbH. These vehicles were developed to serve as prototypes, test fleets or show cars. This encouraged the desire for a series produced electric version of their flagship. This project should show the main obstacles which must be overcome in the chassis design of a composite BEV (Battery Electric Vehicle), and what the best solution would be, using the current Roding Roadster configuration. The design will be directed towards type approval, which is limited to type approval in the EU.

Despite the fact that the concept will be developed for manufacturing in small series (500-1000 vehicles per year), this project is also laid out to create a better understanding of European type approval in general. It is estimated, that a project like this will result in a duration of production of approximately 7 years.

The Roding Roadster is a good starting point for an electric vehicle, since it is more often used as modular vehicle platform for prototypes and small series derivatives (as seen in Figure 4.4). For this reason the redesign will not only be used to create a single new vehicle, but can potentially also be used to base future projects upon. The methods developed in this research also have the potential to be used to develop concepts in future projects of Roding Automobile GmbH.

Figure 4.1 Roding Roadster, courtesy of RA

Figure 4.2 Roding Roadster, rear view, courtesy of RA

4.2 Roding Roadster

The conventional Roding Roadster is a medium sized two-seater sports car developed and produced by Roding Automobile GmbH. In modern cars a roadster refers to a two-seat car with no permanent roof and a sporting appearance. After the prototype phase the vehicle first came to market in 2012. This rear-wheel-drive vehicle has a transversely-mounted mid-engine configuration and was created as a sports car to suit “individualists” and “sport drivers”. This roadster is designed to symbolise a strong personality and sporty handling in an innovative and lightweight car.

Figure 4.3 Monocoque chassis of Roding Roadster, courtesy of RA

The vehicle is constructed around a CFRP (Carbon Fibre Reinforced Plastic) monocoque, as seen in Figure 4.3. This is done to make optimal use of the higher specific properties of CFRP with respect to metals by creating high end composite products in-house. Due to this company profile of Roding Automobile GmbH, the use of composites is limited to the CFRP unless product specific arguments advocate otherwise. Up till now only 15 Roding Roadsters were produced. However, its monocoque is seen as the main part the modular chassis in Figure 4.4. Using these modules, Roding Automobile GmbH is able to produce customer specific vehicles such as prototypes, show cars or test fleets within minimal lead times based on the Roding Roadster.

The monocoque is produced out of different components which are bonded together. These components are produced by a combination of RTM, vacuum infusion or hand lay-up. This combination was executed as such to get familiar with different production processes. To create a relatively simple concept which is suitable for multiple production methods, all composite parts are designed without sandwich constructions. To give a better impression of the complete chassis assembly, an exploded view of the chassis is shown in Figure 4.5. In this figure, metal parts are visualised in grey and composite parts are visualised in black, red and blue (for better visualisation). The method of assembling the separate components to form the passenger compartment was patented by Roding Automobile GmbH. [19]

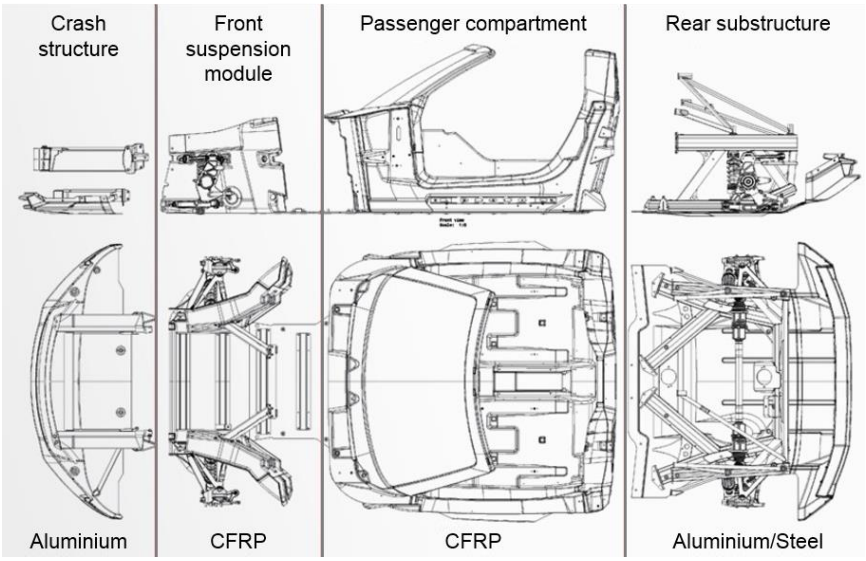

Figure 4.4 Modular Roding Roadster chassis, courtesy of RA

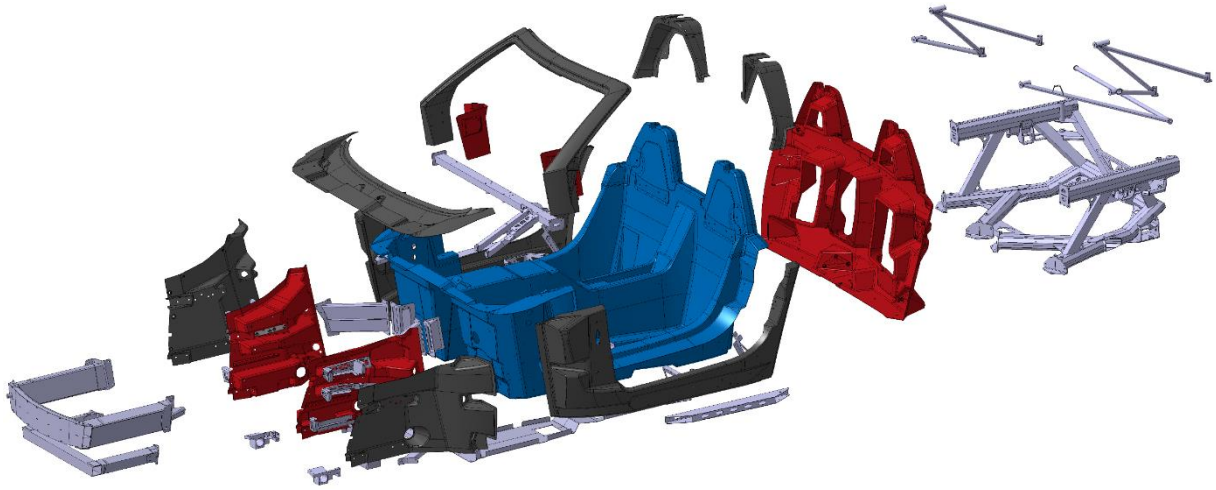

Figure 4.5 Exploded view of the Roding Roadster chassis

4.3 Requirements

For the development of the Roding Roadster, Roding Automobile GmbH created a customer profile to suit the car, consisting of “individualists” and “sport drivers”. This profile resulted in a practical and

luxurious sports car, with racing capabilities. To create a car matching this segment, a vehicle with a bear carbon chassis was chosen to save weight and add to the appearance. The BEV version of this car should fit in the same segment as the original Roding Roadster. For the electric version, the following requirements are added by Roding Automobile GmbH:

- The vehicle should have approximately 300+ hp (~225kW) nominal power output.
- The REESS should have a capacity of approximately 70kWh. One should be able to take the car for a trip, since it is a sports car. For this reason range should be extended beyond everyday use. It is assumed that this will be possible with a REESS capacity of approximately 70kWh.
- A charger should be built in to enable AC charging.
- Since the car should project luxury, exposed carbon fibre parts of the chassis should look neat.
- The general layout should be similar to the Roding Roadster. When possible the same suspension will be used.
- The two-piece detachable roof of the Roding Roadster system should be included.
- Comparable or better handling than the conventional Roding Roadster are required.

5 Supporting Research and Legal Requirements

In this chapter fundamental boundaries will be created to get a better scope for the project and base the chassis on. Ergonomics and regulations will be researched to create the design envelope. Furthermore, a link between regulations and collision load cases will be established. In combination with a section on static collision analysis, this can be used to determine the collision load cases later in this research.

At last the legal requirements which specifically apply to electric vehicles will be researched. To comply with regulation ECE R100 in composite vehicles, the risk of electrical shocks must be ruled out. For this requirement different grounding concepts will be created and tested in Section 5.4.

5.1 Ergonomics and Suspension Envelopes

In this section the design envelope will be fixed. This is done by creating a model which combines the current Roding Roadster suspension with an analysis of ergonomics. A CAD master part will be constructed from these data, which is the basis for the chassis model.

5.1.1 Occupants Sizing and Head Clearance

While designing a vehicle it is important to consider occupants throughout the process. Since everyone is different, statistical standards are often used to design a vehicle suitable for as many people as possible. The Society of Automotive Engineers (SAE) developed different mannequins based on the population of the United States of America (USA). In this research the SAE 95th percentile male is used in combination with the SAE 5th percentile female. These percentiles are often used to define the extremes for ergonomics in the automotive industry and is also used by the UNECE for regulatory purposes. [1] The 95th percentile means that 95% of men are smaller than this male model, so the largest 5% are not covered. Since statically women are smaller, the SAE 5th percentile female is used to evaluate small drivers in a similar fashion. The American population based percentiles are used since these are used for type approval in the EU as well. [1].

Using this information, a number of available mannequin CAD-models at Roding Automobile GmbH were verified to match the set percentiles. [20] From this verification both the correct SAE 95th percentile male and the SAE 5th percentile female were selected for use during this research. The position of the occupants is defined by the Seat Reference Point (SRP). This is the pivot point in the hip of the occupant as defined in SAE standard J4002. [21] To visualise this during the design process, a CAD master part is generated which combines fixed data and relevant geometries. In the CAD master part the SRP is defined by the seat position of the ICE (Internal Combustion Engine) Roding Roadster in combination with the information of the seat manufacturer. [22] This point is also being used as reference point to position regulatory geometries.

These occupant models are placed in a position which falls in a range of comfortable positions as seen in Figure 5.1, which is in line with other literature. [23] The same model will be used for the driver and the passenger. For clarity, in most images the driver position will be used to visualise the 95th percentile male in the most aft seating position as seen in Figure 5.2. The passenger position will be used to visualise the 5th percentile female in the most forward seating position.

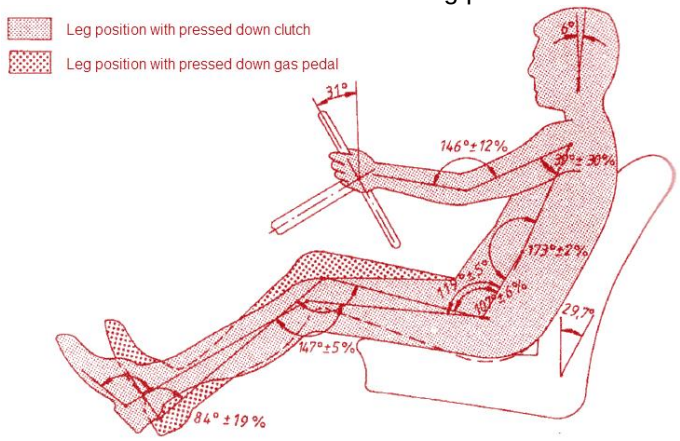

Figure 5.1 Comfort position for driver [24]

In this research, collisions will be analysed to check the structural performance of the chassis using external loads. These load cases will neglect the behaviour of the occupant. To be able to guarantee no excessive injuries to the occupants, it is required to check that the heads of the occupants cannot reach harmful objects. [11] SAE standard J1052 is used to describe an ellipse which covers either 95% or 99% of the head position contours of the population of the USA. [25] To prevent occupants from touching the vehicle surfaces, an offset of 30 mm was constructed around the 99% contour. This contour is positioned in the vehicle as described in SAE J1052 for seats with a horizontal adjustment higher than 133mm. The result can be seen in Figure 5.2.

5.1.2 Suspension and Wheel Envelopes

The suspension is visualised in the CAD master part to make sure the chassis does not interfere. This includes an envelope for the wheels in which the most extreme positions of the wheels are visualised

by applying the maximum amount of travel and steering in both directions. This is done using the standard 18 inch tires used for the Roding Roadster and can be seen in Figure 5.2.

Figure 5.2 Ergonomic models and suspension

5.2 Regulations and Type Approval

In Section 3.2 a short overview was given of the regulations which must be met for type approval in the EU. [1, 11] In this section a visualisation of these regulations will be created in the CAD master part first. This can later be used to evaluate general vehicle lay-outs. Afterwards, a method is described to check the load cases based with respect to the defined injury criteria in legislation.

5.2.1 CAD Master Part

To create concepts which are in line with these regulations, the CAD master part is also used to visualise these where possible. These visualisations can be seen in Figure 5.3.

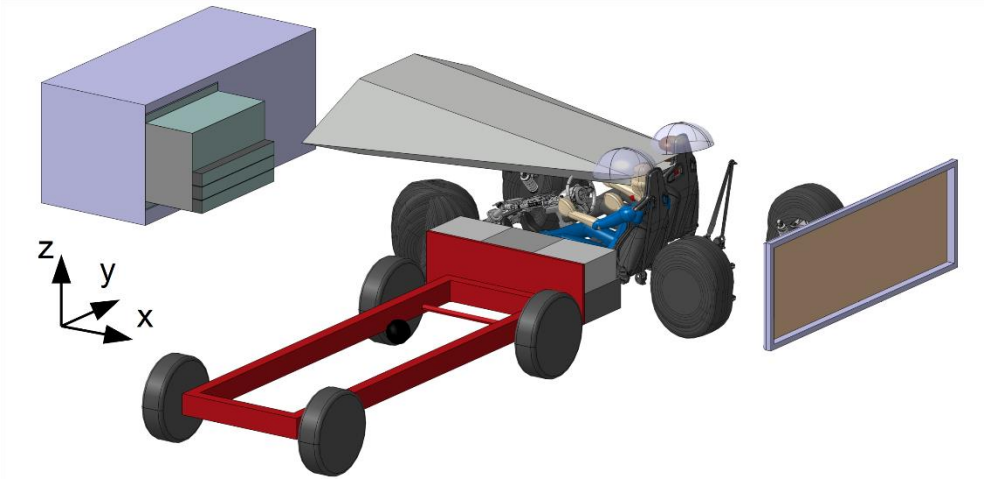

Figure 5.3 Regulations for type approval in the EU visualised in CAD master part

Most noticeable in this figure are the crash barriers visualised in front, besides and behind the vehicle. These barriers represent the barriers defined in the regulations for the frontal collision (ECE R94), lateral collision (ECE R95) and the rear collision for the prevention of fire risk (ECE R34). The CAD master part was created to position these barriers with respect to the vehicle as defined in the corresponding regulation. This visualisation can be used to examine the area of impact and create the chassis geometry accordingly. Additionally the four requirements for the forward view regulation (ECE R125) are visualised in the CAD master part to be able to check the compliance of different concepts easily. In Figure 5.3 only the geometry for the minimal transparent surface is shown for ECE R125 to give a clean overview.

The components of this CAD master part were constructed independently. Using a different vehicle with a comparable but fixed model available, the overlapping components in the CAD master part were verified. This confirmed the correctness of regulation components in the model, since it only showed

differences for the SAE head position contours. The origin of this difference was found to be in the incorrect positioning of this component in the verification model.

5.2.2 Injury Criteria

The requirements for the collision tests defined in ECE R94 and ECE R95 are based on the level of protection of the occupants. These are defined using so called injury criteria. To check the performance of the chassis, load cases will be defined in Section 6.1. However, it is important to check whether the applied loads are allowable for the occupants according to legislation.

The main injury criterion in legislation is the HIC (Head Injury Criterion). In this research the maximum allowable HIC is linked to global vehicle accelerations. It must be noted that when global vehicle accelerations are used to describe injury, additional harm due to hazardous obstacles are not taken into consideration. For this reason the head position contours are defined CAD master part to create an envelope which must be kept clear.

For type approval of large series, the HIC-value is limited to 1,000 for both ECE R94 and ECE R95. [1] Research was done by Sturt and Fell, as well as Shoojati to link this HIC to the Acceleration Severity Index (ASI). [26, 27] ASI evaluates the risk of injury based on vehicle motion only, by comparing accelerations to a reference acceleration using Formula 5.1. As long as the occupant cannot collide with any hazardous obstacles, it is assumed that the relation between HIC and ASI hold for both the frontal and lateral collision.

$$ASI\ (t) = \left[\left(\frac{\bar{a}_x}{\hat{a}_x}\right)^2 + \left(\frac{\bar{a}_y}{\hat{a}_y}\right)^2 + \left(\frac{\bar{a}_z}{\hat{a}_z}\right)^2\right]^{\frac{1}{2}}$$

5.1 [26, 27, 28]

In this formula, $\bar{a}_x$, $\bar{a}_y$ and $\bar{a}_z$ are defined as the 50ms average vehicle acceleration components. $\hat{a}_x$, $\hat{a}_y$ and $\hat{a}_z$ represent the threshold accelerations for each component, which leaves ASI dimensionless. For safety belt wearing occupants, the reference accelerations are given in Table 5.1, according to the European Committee for Standardization (CEN).

Table 5.1 Threshold accelerations ASI [29]

Threshold acceleration components	Acceleration [g]
$\hat{a}_x$	12
$\hat{a}_y$	9
$\hat{a}_z$	10

According to Shoojati (Figure 5.4) an ASI of approximately 1.95 represents a HIC of 1,000. According to Sturt and Fell (Figure 5.5) an ASI of about 2.08 represents the same HIC value when using the “worst case trend”. Since a lower ASI is being more conservative, the ASI of 1.95 is the value used throughout this research. According Figure 5.4 an even lower value would be described in a “worst case trend line”. Since this trend cannot be created accurately, this fact is ignored in this research.

For a frontal collision an ASI of 1.95 would result in a maximum allowed 50ms average acceleration of 230m/s^2 in x-direction. In the y-direction, a 50ms average acceleration or deceleration of 172m/s^2 is allowed. This acceleration will be used to limit the loads for the lateral collision, according to ECE R95.

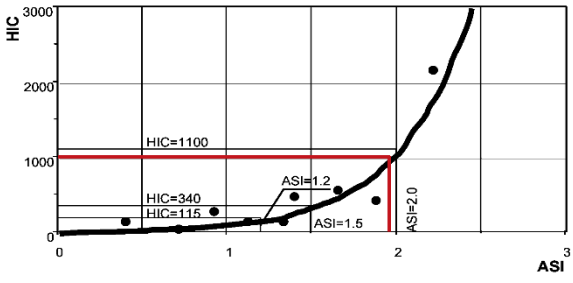

Figure 5.4 HIC-ASI relation according to Shoojati -edited- [27]

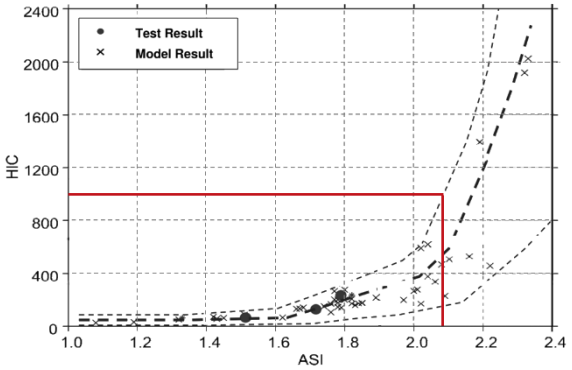

Figure 5.5 HIC-ASI relation according to Sturt and Fell -edited- [26]

5.3 Static Collision Analysis

For the collisions described in legislation only a simplified analysis is performed, to give an estimation of the introduced loads and load paths in the chassis. These loads are analysed statically to reduce complexity, since analysis methods of non-linear behaviour of fibre reinforced materials are still under development and are much more difficult to apply. [11] To estimate the loads during a collision more realistically, the method of inertia relief is used to represent the loads due to inertial effects, instead of assuming an arbitrary support. To model these inertia loads realistically, the weight distribution should be modelled accurately. [17, 18, 30]

Research has shown that the deviation in stresses further away from the applied load increases. However, at more distant areas, other load cases are expected to be more determining for the structure at these locations. To show reliable results using inertia relief, the natural frequency of the system should be considered as well. To create an accurate model, the period of the impact should be much larger than the period of resonant frequency. When this is not the case, the dynamic overshoot will become too high. Nevertheless, a load factor of 1.25 is advised to reckon for the dynamic overshoot. This value is based on the maximum dynamic overshoot, with the ratio between the impact period and the natural frequency period of 2.2. [16]

It might seem that equal results can be achieved by replacing inertia relief and the applied load by a deceleration and support at the original point of load introduction. However in practice this support would prevent deformation of the surface it is applied to. This is particularly undesirable in a lateral collision, where the behaviour of this region is of great interest. Another reason to use the inertia relief function instead of an acceleration is that when the applied force is not in line with the centre of gravity, inertia relief will compensate this with an angular acceleration counteracting the existing moment. This is realistic since an eccentric load will create a rotation which creates a larger acceleration and therefore higher load on the more outward components. When no inertia relief would be applied this effect is more difficult to take into account.

This method will be applied for the frontal, lateral and rear-end collision load case. More accurate descriptions on the application of this method for each load case can be found in the designated subsections of Section 6.1. For verification of the structural model including inertia relief, the results of the structural analysis will be compared to an existing model. Section 6.2.3 will elaborate on the expected differences between both models, whether or not these differences depend on the use of inertia relief. At last, Section 6.2.3 will compare these expected differences with the collected results.

5.4 Carbon Fibre Components in Electrical Systems

Since Roding Automobile GmbH is a company with a lot of experience and interest in CFRP (Carbon Fibre Reinforced Plastic) production, it might be feasible to cover parts of the high voltage system by CFRP housings. This might for example be beneficial for the REESS (Rechargeable Energy Storage System) housing, to create a weight efficient structure. Since carbon fibre is a conductive material, the use of carbon fibre in electric vehicles must be analysed for type approval according to ECE R100. [12, 31] This is evaluated to be aware of possible restrictions for the concept development.

5.4.1 Complications due to Carbon Fibre Usage

The most important requirement in regulation ECE R100 is that “all exposed conductive parts in the high voltage busses should be connected to the electrical chassis with a resistance lower than 0.1Ω” to avert indirect shocks. [1] However, in carbon fibre structures the CFRP is not likely to be conductive enough to fall within the stated limits, when evaluating the specific resistance of CFRP for a quasi-isotropic lay-up (0.231Ωcm). [31] This is a lay-up in which the properties are almost similar in all directions. This is the best reference value since quasi-isotropic lay-ups are often used in the Roding Roadster chassis for simplicity reasons. Based on this value it is assumed that no significantly sized carbon fibre component based on this specific resistance falls below 0.1Ω.

The electrical chassis is a conductive part which is set as the reference potential. This electrical chassis is chosen by the manufacturer, but is commonly represented by the chassis for metal based vehicles. Since in the case of a CFRP chassis there is no highly conductive chassis, it is most logical to choose the negative side of the wire loom as electrical chassis. This is done since it is the same terminal which is connected through the chassis within metal chassis vehicles. [32] For additional safety the carbon

fibre monocoque can still be connected to this electrical chassis. An additional cable can be used to connect the conductive parts to this wire loom, as long as the resistance in low enough.

The poor resistance of carbon fibres is also the reason that CFRP chassis are not used as negative terminal, which is usually done in metal chassis vehicles. Besides bad connectivity, Roding Automobile GmbH experienced that the use of the carbon fibre body as conductor causes disturbances in signals as well. For this reason, both positive and negative leads of the high and low voltage system are connected using cables in composite vehicles. This means more cables are required, increasing weight.

5.4.2 Solutions for Type Approval of Carbon Fibre Components

Possible options for components to comply with regulation ECE R100 can be seen in Figure 5.6. [1] The use of non-conductive materials is a solution which is self-evident and will be assessed in the material choice. However, as explained before, CFRP components are conductive but have a too high resistance for type approval, so other solutions must be consulted. Making carbon fibre parts “not exposed” can be done by isolating the parts with for example a layer of fibreglass material. An additional nonconductive housing enclosing the components is seen as a trivial solution, since this would increase weight severely. The other proposed solutions to make sure the conductive part is not exposed bring problems for most joints. For example, in this case all metal bolts should be isolated additionally since they are able to contact the carbon fibre within a drilled hole. For this reason Roding Automobile GmbH previously decided to not make use of this group of solutions. At last CFRP parts can be grounded to the chassis instead of isolating them.

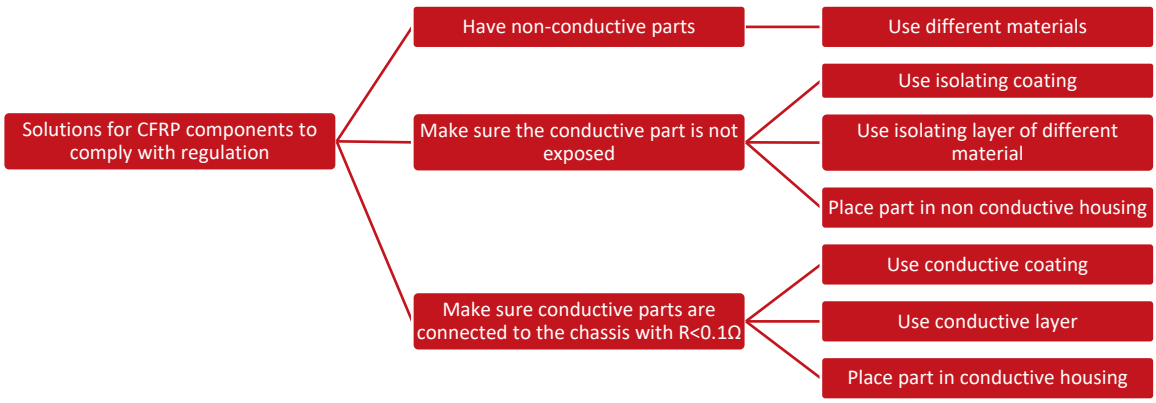

Figure 5.6 Design option tree to satisfy electrical grounding requirements

One can argue that a carbon fibre housing which is entirely covered by the chassis and body panels cannot be reached with the defined probe. For this reason one can state that this component is not exposed and technically this already fulfils the requirements. This neglects the loophole that a not exposed part can be conductively connected to an exposed component which is not part of the HV (High Voltage) busses. To prevent hazardous situations, this is decided to be not satisfactory. For this reason a REESS which might be presented as not exposed will be regarded as exposed in this research. For other HV components it is assumed that the used components have an adequate grounding connection when required, since off-the-shelf components will be used here.

Placing the part in a conductive housing is probably a heavy solution, since this would mean an additional housing is required. This serves actually the same function as a conductive layer which can be included in the product at a higher weight. For example expanded metal foils or meshes can be used to do this, in a similar fashion to lightning strike protection in composite aircraft. [33]

Roding Automobile GmbH is experienced by grounding carbon fibre parts using conductive EMI-Coatings (Electromagnetic Interference). This conductive coating is sprayed onto the finished product to create a conductive layer which has a low enough resistance to comply with regulations. Such coating is made out of a carrier coating with a metallic filler as seen in Figure 5.7 and Figure 5.8. The coating in Figure 5.7 is based on a copper filler as used by Roding Automobile GmbH. Due to the absence of an electrolyte and the microscopic surface area of the metallic particles, these coatings were not prone to any problems with galvanic corrosion. For this reason this aspect is neglected. The resistance of the coating in Figure 5.7 was measured using the method described Appendix A. This coating has a satisfactory average resistance of 0.058Ω, measured over two eyelets (Figure 5.14) bolted onto the coating over a distance of 425mm and an unspecifiable large width (since it was measured in the flange

region of a 5mm thick carbon fibre reinforced product). The method in Appendix A will be used to measure resistance lower than 1Ω throughout this research unless mentioned differently. For higher resistances, the resistance measurement setting of the ELV VC 98B multimeter was used [34]. It must be noted that resistance is inversely proportional to the cross-sectional area and directly proportional to the length between both measurement points, based on Formula 5.2. In this formula, R represents resistance, ρ is specific resistance, ℓ specimen length and A cross sectional area.

$$R = \rho * \frac{\ell}{A}$$

5.2 [35]

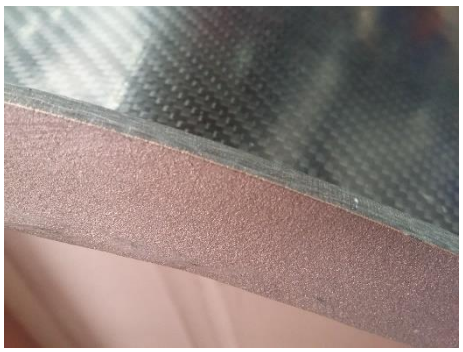

Figure 5.7 Copper based EMI coating on carbon

Figure 5.8 Zinc based EMI coating

During the installation of this product, the grounding of this method was proven to be grounded adequately in combination with contact resistances and the resistance through the thickness of carbon fibre in this product. This was measured using a milliohm meter in a previous project at Roding Automobile GmbH. However, resistances were close to the 0.1Ω maximum permissible value when measuring between the CFRP REESS cover and the used aluminium space frame representing the electrical chassis. These two components were connected by a contact surface of the chassis and the EMI coating of approximately 0.3m^2. For this reason, depending on the application this coating should be checked to have adequately performance.

Another coating which was tested is shown in Figure 5.8. This sample used an EMI coating based on zinc. No further research was done for this sample due to durability problems of the coating. On this picture it can be seen that coating chips can be easily winkled out for different substrates. When these chips end up in the electrical system this could cause major shortcut problems. A different supplier of zinc based EMI coating showed to apply coatings without this problem. [36] This coating was measured at 4.5mΩ over 78mm and a width of 85mm on a 1mm thick carbon substrate. Even without compensating for the decrease in carbon thickness and sample width, this measurement shows a two times higher conductivity than the copper based coating per unit length. Since this coating is higher in cost, the necessity of this higher conductivity should be reviewed when choosing between both coatings.

The disadvantages of the mentioned EMI coatings are the high costs and the addition of a step in the production process. For this reason other solutions are investigated. The additional production step can be avoided by using the EMI-coating to coat a core material. This way the coating process has less influence on the production rate, since bulk material is coated instead of coating end products. [36] A second benefit is that the price from coated foam is about a quarter of the price from coating products, depending on the foam thickness. [32, 37] Using for example a bigHead® fastener this conductive core can be connected. [38] These fasteners, as seen in Figure 5.9, are studs or other fixings welded to a flange or head. A ground wire can be screwed onto the bigHead® to connect a wire to the conductive core as seen in Figure 5.11. Two bigHead® fasteners combined (bolt and nut version) were used to ensure a connection on both sides of the core. This concept is evaluated in more detail in Section 5.4.3.

A second concept using a conductive core is developed using aluminium honeycomb. This is a core material made out of folded aluminium film used for composite sandwich structures. This material is used for its high specific properties and is conductive since it is made out of aluminium. A connection can be made by bolting a cable into a blind rivet nut or rivnut (Figure 5.10). This is a rivet with an internal thread, which can be installed in a predrilled hole with single side access by deforming the rivet. These rivnuts are commonly used in sheet metal products but can also be applied in composite parts already used by Roding Automobile GmbH. The rivnut expands in the core to create a durable connection as seen in Figure 5.12. This concept is evaluated in more detail in Section 5.4.4.

Figure 5.9 bigHead® fastener

Figure 5.10 Compressed and uncompressed rivnut

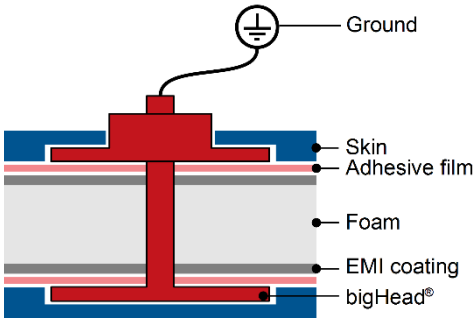

Figure 5.11 Grounding concept using foam core

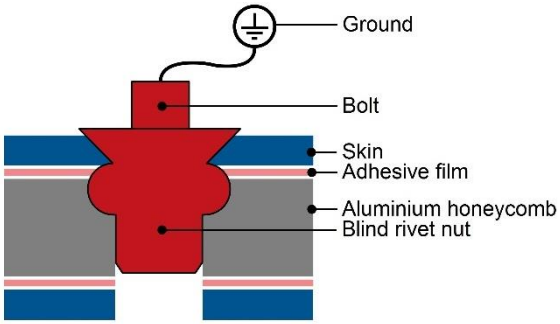

Figure 5.12 Grounding concept using honeycomb core

5.4.3 Testing the bigHead® Fastener Grounding Concept

The connection between the bigHead® fastener and core was measured using glass fibre reinforced skins using a hand-lay-up process cured in the autoclave. This was done using glass fibres to evaluate only the connection between the bigHead® and the core. This resistance for a single sample was measured to be 2.9Ω. This value is promising since in this case the bad connection is due to the thin layer of adhesive film containing a glass fibre carrier. This problem can be solved by using a conductive connecting medium in between the fasteners and the core, so no adhesive film is required here and resin cannot flow in between to create an isolating layer. This means bigHead® will be combined using this conductive medium before laminating the product to ensure a good connection.

For this connecting medium, different carriers with two different conductive filler materials were used, namely graphite and silver. Graphite powder was manually mixed with epoxy adhesive and epoxy resin, which are both not conductive. [39] It was tried to mix as much graphite powder as possible into the carrier to maximise conductivity. For the epoxy adhesive 2:1 graphite epoxy ratio by volume was judged best, based on the thixotropy. For the resin a 4:1 ratio was chosen. Both bulk materials measured resistances in the range of kilo-ohms over a distance of 10mm with a cross section of 15mm^2. The silver filler was applied using a conductive ink pen, which is mainly used to repair circuit boards. [40]

Since it was expected that the silver filled ink would perform best, a test sample was created using this connecting medium first. This sample consisted only of the core material, the conductive filler and the bigHead® fasteners. This was done because the fibre reinforced facings are not required to produce the sample and their effect on the result is expected to be marginal. During resistance measurement of this sample the coating burned out and broke the connection. This was at a location different from the connection. The hypothesis for this problem is that the coating would be locally too thin. This results in a large local resistance and therefore current, which heats the coating until it burns out. This is seen as a large risk since the quality of the coating is more difficult to guarantee and check when applied to a rough foam base material. For this reason, this solution is not suitable since it is expected that the coating on a foam core would not be reliable. This is different from the coating on the end product, since here the quality coating can be inspected or repaired. The successful resistance measurements for a half specimen are shown in Figure 5.13. For the measurements a line is plotted for the worst measurements to be able to estimate resistance in a worst-case scenario. For this extrapolation the formula of this line is enclosed in the figure. A first order trend is used based on the direct proportional relation between length and resistance. The resistance at zero length shows the connection resistance.

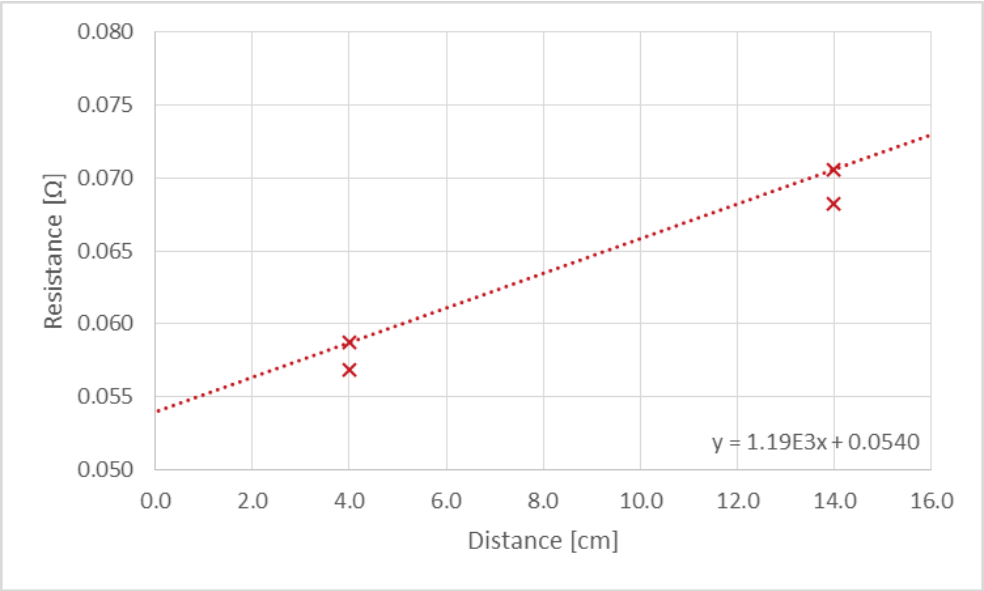

Figure 5.13 Half specimen resistance over distance plot for EMI coated foam, plate width 230mm

5.4.4 Testing the Blind Rivet Nut Grounding Concept

The advantage of rivnut as connection point is that they can be installed after production. Therefore laminating the products is not made more difficult. Installation is done using a special tool into a predrilled hole. One must make sure that the diameter of the rivet is bigger than the width of the honeycomb cells to ensure connection. Due to the expansion of the rivet during installation the connection is made. For honeycomb plates with a cell size of 9.5 mm in a batch of 50 M6 rivnuts, no rivet was measured to have not contacted the honeycomb. Connections were also not prevented by the presence of resin. In the 50 tested rivets one outlier was found, which had a poorer connectivity. This will be discussed later in this section.

For the first measurements a sandwich plate is used with the following representative lay-up made out of common materials for Roding Automobile GmbH (symmetric around the honeycomb core):

- 4 layers of 630gsm carbon fibre epoxy biaxial prepreg to laminate a skin of approximately 2.5mm thick with the layers in the following directions: [45, 0, 45, 0]
- 1 layer 250gsm adhesive film with 30 gsm glass fibre carrier
- 1 layer 10mm thick aluminium honeycomb

Connections are made using stainless steel M6 rivnuts, a pressed cable eyelet and an M6 bolt as seen in Figure 5.14.

Figure 5.14 Connection of ground wire to rivnut, using an eyelet

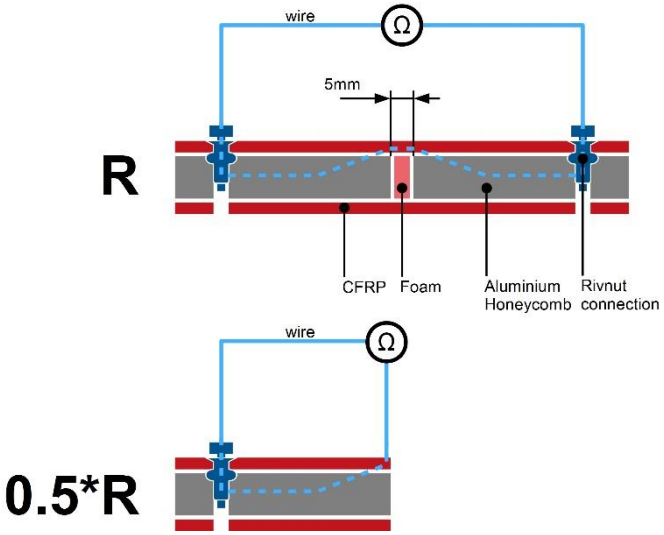

Figure 5.15 Schematic overview of half specimen resistance equality

Half specimen resistance for different specimen lengths are shown in Figure 5.16, for a 280mm wide plate. In these results the resistances in combination with one rivnut were taken out. This was done since high resistances in combination with other rivnuts indicated a poor connection. These outliers are plotted in grey and are not included to create trend lines. The results show, as expected, a larger resistance when the distance increases. Therefore large products might require distributed connection points to have a resistance lower than 0.1Ω. By extrapolating the blue trend line towards a distance of zero, the average connection resistance is known to be around 0.3mΩ. This can be used to calculate the resistance of the poor connection, by assuming a 0.3mΩ connection resistance for the “not-poor” connection point. The poor connection was calculated to be approximately 2.9mΩ. Although the conductivity for this rivnut is still relatively high, a redundant connection can always be made in the product to prevent poor connections. The advantage of this concept is that after measuring the resistance of each vehicle, not complying components can still be repaired by installing an additional connection point. By measuring only a single poor connection in a group of 50 rivnuts and having a simple repair method, the reliability is concluded to be sufficient.

As explained before, the red line shows a relation for the resistance with respect to distance for the worst case connections, excluding the outliers. This relation can be used to estimate resistance from a plate section.

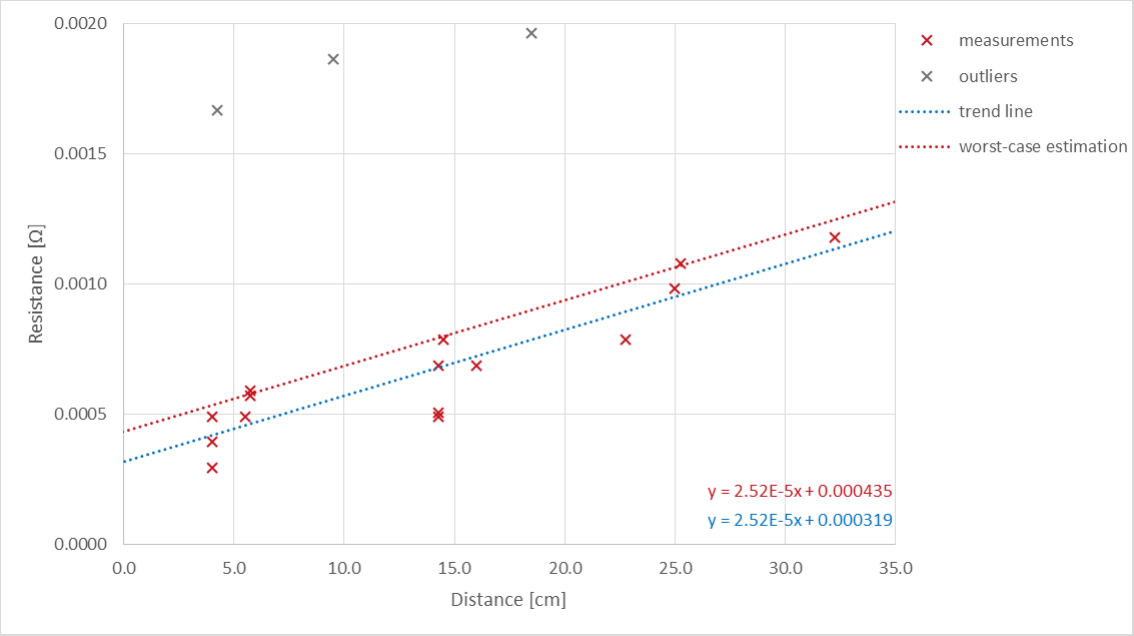

Figure 5.16 Half specimen resistance over distance plot for aluminium honeycomb sandwich, plate width 280mm

Since this measurement shows the resistance from a connection point with respect to the most conductive point in the middle of the specimen, this measurement does not yet show the suitability of this concept. To be able to proof the concept, the resistance between a rivnut and the carbon fibre must be known. To do this, a similar test panel with the same lay-up was produced were the honeycomb core is interrupted in the middle of the panel by a 5mm wide isolating strip of foam core as seen in the top section of Figure 5.15. This plate was produced with a width of 350mm. The foam forces the current to run through at least a short distance of CFRP. This results into a resistance measurement over a short piece of carbon fibre in combination with a connection between carbon fibre and the aluminium core material on both sides. It is assumed that the half specimen resistance including the 2.5mm CFRP along the foam is the same as the resistance “0.5 R” through the 2.5mm thick skin in a contentious plate (Figure 5.15). Using this assumption accurate measurements were done, showing the resistance of a half specimen which can be compared with the resistance from a point on the skin up to a rivnut connection point. Results are shown in Figure 5.17.

From these measurements it can be seen that within the design space of 0.1Ω it is possible to create a concept using an aluminium honeycomb as conductor. It must be noted that connections between different pieces of honeycomb might increase resistance rapidly. Without additional research it is therefore advised to use a separate connection point for all separate honeycomb sections. Whether monolithic parts (fibre reinforced sections without core material) of a structure are connected with a low

enough resistance can be researched using the same method, using specimen with a wider segment without honeycomb material. For this research, the monolithic segment of carbon fibre can be estimated using the earlier mentioned specific resistance for a woven carbon fibre epoxy material in a quasi-isotropic lay-up, 0.231Ωcm. [31] For example, increasing the width of the foam strip in this test with 5cm for both half specimens would add 0.066Ω, based on Formula 5.2. Using this method, small monolithic parts in the structure can be estimated roughly for compliance. Using geometric ratios, changes in specimen size can be estimated using Formula 5.2 as well.

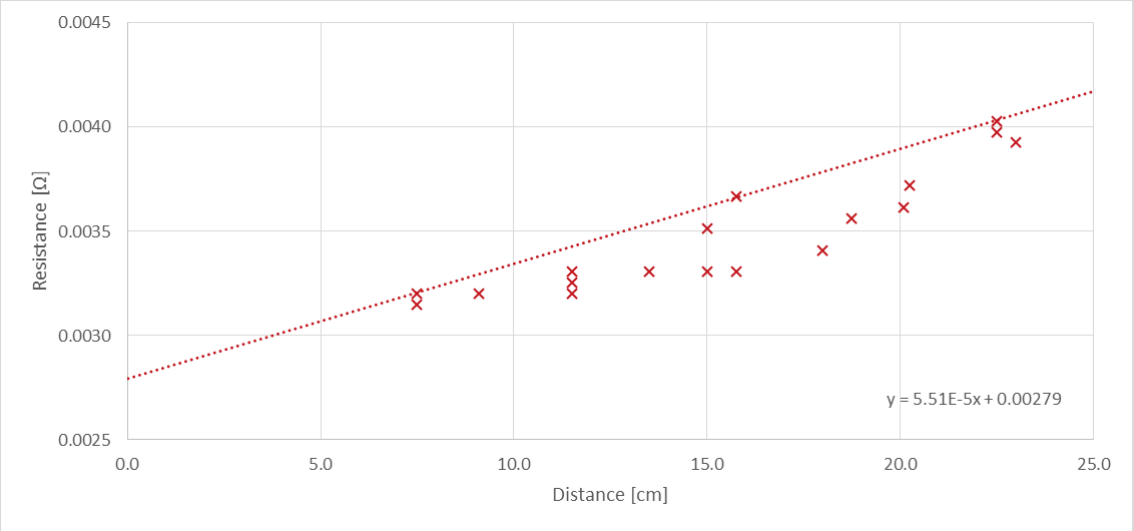

Figure 5.17 Half specimen resistance over distance plot for sandwich with honeycomb separated by 5mm foam, plate width 350mm

5.4.5 Galvanic Corrosion in Rivnut Grounding Concept

A weak spot in this concept is the risk of galvanic corrosion. Since different conducting materials are connected this should be investigated. In this concept, aluminium and carbon fibre can form a couple which is very sensitive for corrosion. [11] Besides a coupled material, an electrolyte is essential for galvanic corrosion. For this reason this method is applied to a rivnut installed in a blind hole on the inner side of the REESS housing. This means that this connection is separated from the outside environment, since the REESS is sealed. In most REESS systems a small membrane is installed to allow air and water vapour to escape, while preventing water from entering. Besides that, this concept depends on the connection between the aluminium honeycomb and the rivnut. The inevitable connection between the carbon fibre and the aluminium honeycomb on which this concept is based, does not add any additional risks when exploited.

Rivnuts can be made out of different materials, such as steel, stainless steel or aluminium. Aluminium rivnuts can be chosen to prevent dissimilar materials at the connection between the core and rivnut. This can however create problems at the small interface of the rivnut and the carbon fibre facing. Further research might be performed to assess the severity of this connection. As long as this is not guaranteed, a small carbon fibre patch might be replaced by a glass fibre reinforced material during lamination. This way, an aluminium rivnut can use the same connecting principle, while not being in contact with the carbon fibre directly. Based on the specific resistance of carbon fibre it is concluded that the elimination of the direct connection between the carbon fibre and the rivnut does not influence the main conduction principle via the honeycomb material. For this reason it is assumed that differences in resistance measurements for rivnuts in a small glass fibre reinforced patch are negligible.

5.4.6 Conclusion of Grounding Concepts

It can be seen that besides the unsuitability of the bigHead® Fastener Grounding Concept, the rivnut concept performs well with respect to its resistance properties. For manufacturing this concept is also an easier solution, since rivnuts are installed easily after laminating. It must be noted that the use of honeycomb core material is not possible for all manufacturing methods, since in for example RTM and vacuum infusion the cells would completely fill with resin. For common manufacturing methods, this only leaves hand lay-up, according to the selection in Section 3.3. Other parts should be coated to comply to regulation with either the zinc or copper based coating.

6 Structural Analysis

With the project boundaries set and supporting research executed, a method must be developed to assess the structural performance of the chassis. In this chapter this will be elaborated on.

At first, the load cases which the chassis must be able to transfer, will be defined in this chapter. This will be done for the operational load cases, the collision load cases and the other regulatory load cases. These load cases were selected to be the leading load cases in the structural performance of the chassis. A structural model will be constructed to evaluate these load cases.

In the second part of this chapter, the structural model will be verified by comparison with an already available model for a frontal collision of the current Roding Roadster chassis.

After this verification, the analyses of the frontal and lateral collision for the current chassis are used to point out the strong and weak points of the chassis. Later these analyses will be used to determine what components of the current chassis might be adopted.

6.1 Load cases

For the development of the chassis concept, it is useful to take the Roding Roadster chassis as a reference. To assess the performance of this chassis, a reference analysis is performed. This will be done in Section 6.2. To be able to do this, the load cases used for structural analysis will be defined in this section. The main part of these load cases are based on legislation. The remaining load cases are used to describe other relevant loads on the body, such as the extreme loads during driving, which will be explained first.

6.1.1 Cruising and Extreme Driving Conditions

During a constant velocity, loads can be analysed under gravitational loads (1g). This load case represents cruising conditions, but will probably not be a design driving due to the relatively low loads. This load case is defined, since in some cases it might be interesting to know specific stresses or deformations in this “normal” condition. For small disturbance an elevated vertical gravitational acceleration of 1.25g is used to define this load case, instead of 1.00g.

More important are the extreme loads occurring during driving, which will be named the extreme driving load case. For driving sports cars the structural performance is expected to be stiffness dominated. For this reason, driving conditions will be analysed as well, since it is expected that the structure of the REESS (Rechargeable Energy Storage System) can influence the chassis stiffness significantly.

These loads are defined by combining the maximum loads in all directions. To do this, this load case combines maximum braking, maximal cornering and a vertical acceleration due to driving over a bump or through a pothole. For the ICE (Internal Combustion Engine) Roding Roadster under normal conditions, the slip limit for braking was determined 0.71g and cornering is limited to 1.4g. [32] For the maximum vertical acceleration different literature sources describe values ranging from 2.5g to 3g. [41, 42, 43] To incorporate misuse, these values are rounded up to 1g longitudinal, 2g lateral and 4g vertical simultaneously.

With this modelled acceleration, the suspension connection points will be used to support the vehicle. At each connection point, a fixed displacement in the load bearing direction on all suspension members is constructed. This is most realistic, since all connection points are mounted to the chassis with a spherical bearing. The supports at the suspension points are applied to the suspension position at rest, which is obtained from the CAD master part. In Figure 6.1 the free body diagram is shown for this load case. The arrows in black show the direction of fixed displacement. The applied supports for these fixed displacements are highlighted in red, based on the suspension connection points. The spheres in this figure represent the point loads for all component weights included in the model. These are included to apply the accelerations and are supported by the connection points on the chassis.

For the sake of clarity, only supports on a single side of the vehicle are shown. These are implemented symmetrically on the right side suspensions. Since this load case is only interesting for the BEV (Battery Electric Vehicle) chassis concept, this free body diagram only visualises the final version of the BEV chassis.

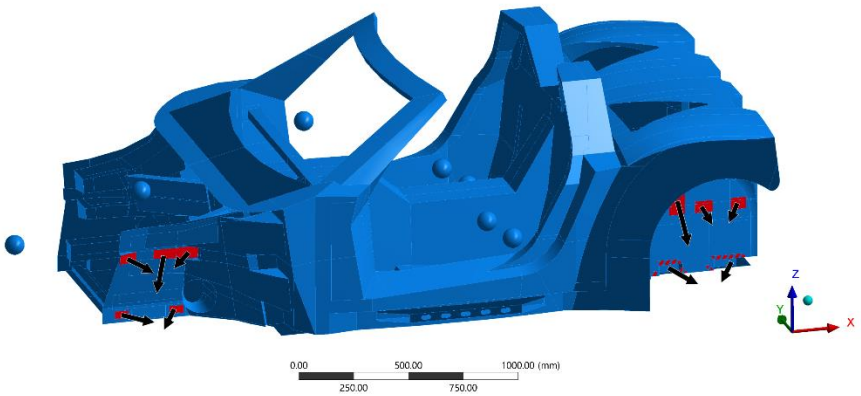

Figure 6.1 Free body diagram for extreme driving, supports in red, direction of fixed deformation in black (symmetric supports are applied to the right-hand side)

6.1.2 Frontal Collision

The load case for a frontal collision is derived from the regulations as explained in Section 3.2. This load case is based on ECE R94, where the vehicle drives into a crash barrier 56km/h with 40% overlap. To analyse a collision statically, the method of inertia relief will be used as described in Section 5.3. External loads should be calculated to apply this method. In order to do this, the system is divided into two sections. The crash barrier and crash attenuator as energy dissipating structures on the one hand, on the other hand the rest of the chassis is assumed to be "rigid". In Figure 6.2 one can see four longitudinal aluminium profiles on the front of the vehicle which act as crash attenuator. By deforming under a constant load, these profiles can absorb energy, which will afterwards look like as the folded profile in Figure 6.3.

Figure 6.2 Roding Roadster chassis including sub-frames, courtesy of RA

Figure 6.3 Crash attenuator profile after energy absorption

For a static analysis only the "rigid" part of the chassis can be analysed. To define the force acting on this "rigid" part a load is calculated, which defines the minimal force required to bring the car to a standstill within the energy absorbing length of the crash attenuator. This will be compared with an allowed upper limit for the injury criteria to evaluate human occupant injury as discussed in Section 5.2.2.

Load Determination

At first the kinetic energy is calculated, based on the mass of the ICE Roding Roadster and the collision velocity of 56km/h. The kinetic energy before the collision can be calculated at 141kJ. For the mass, the prescribed unladen kerb mass including the two 50th percentile crash test dummies is used. This has a total value of 1162kg, with the crash test dummies weighing 77.7kg each. [1, 44]

The work kinetic energy theorem can be used to calculate the energy absorption capacity of the crash barrier. This theorem states that the performed work is equal to the change in kinetic energy. [35] Therefore, by using the frontal area, displacement and crush strength, the absorbed energy can be calculated. The assumption is made that the crush force will be constant throughout the entire depth of the barrier. Since the barrier is higher than the hood of the vehicle, only overlapping areas will absorb energy. For the collision barrier, consisting out of two sections, the main barrier block is assumed to overlap by 65%, and the bumper element by 75%, of the total barrier surface. This is based on the overlap between the barrier and the energy absorbing section of the vehicle. This overlap was estimated using the CAD master part, in combination with the current vehicle exterior. An additional energy absorption efficiency of 85% is used, which is based on an earlier analysis. This gives an energy absorption of 55kJ for the main block and 32kJ for the bumper elements, giving a total energy absorption of the crash barrier of 88kJ. This value is a more conservative value than the 105kJ, which is absorbed according to an earlier analysis, because this means that more energy must be absorbed by the vehicle. For safety reasons it is chosen to use the more conservative value in this research, which is rounded to 90kJ. This value is assumed to be the maximum energy absorption for the barrier in combination with the overlap of the Roding Roaster, independent of other parameters.

When 90kJ is absorbed by the barrier, the remaining 51kJ kinetic energy must be dissipated by the crash attenuators. Over a length of 0.5m the work kinetic energy theorem gives an average force. For the 1162kg vehicle this is calculated to be 101kN. This means that the crash attenuators will be designed on the basis of this specific collision test. To check if this load does not exceed a HIC (Head Injury

Criterion) of 1,000, this force should be compared to the maximum the allowable acceleration in x-direction. In Section 5.2.2 this was determined at 230m/s^2. For a vehicle of 1162kg this results in an allowed force of 267kN, which is higher than the required 101kN to bring the vehicle to a standstill.

When a collision analysis with a rigid barrier should be performed (such as the Euro NCAP – Full width frontal impact [45]), it can be assumed that the total kinetic energy should be absorbed by the vehicle. When this means that the energy absorbing capacity of the crash attenuators will not suffice, a different methods must be used.

Since the 267kN force is defined as a maximum allowed 50ms average, this value does not directly define the maximum force. Peak loads might occur when the crash attenuator cannot absorb the required amount of energy within the available distance. In this case, the chassis is forced to absorb the remaining kinetic energy instantaneously. However, such situation should not occur, since in this case the 101kN is defined to be sufficient to perform the required work. For this reason no peak should occur when the crash attenuator is designed accordingly. When it is assumed that the duration of the collision is longer than 50ms, this means the 101kN value will directly be the maximum 50ms average. Based on literature this is expected to be a valid assumption. [46, 47]

Description of Final Loads

For the use of inertia relief, it was discussed an additional factor of 1.25 must be applied to cover the dynamic overshoot. For the calculated load this will result in a force of 126kN. This force is divided by both crash attenuators in the front, which can be seen in Figure 6.2. It is assumed that the load ratio between both attenuators is a constant parameter. In the current Roding Roadster the ratio between these loads was designed at 75% at the upper attenuator and 25% of the load at the lower attenuator. This ratio is kept similar for simplification. This results in a force of 95kN at the top attenuator and 32kN at the lower one. In Figure 6.4 the supports for these loads are shown in a free body diagram. Due to the use of the inertia relief function no supports are present. As in the extreme driving load case, the spheres represent the point masses for all component weights included in the model. It is assumed that only masses in the rigid part of the vehicle can be accelerated by the inertia relief function to cancel out forces. For example, in this phase of a frontal collision, the headlights and the radiator do not move with respect to the impact barrier. Therefore in a frontal collision these masses were eliminated from the model. For the side collision no such components are available since there is no separate designated crumple zone.

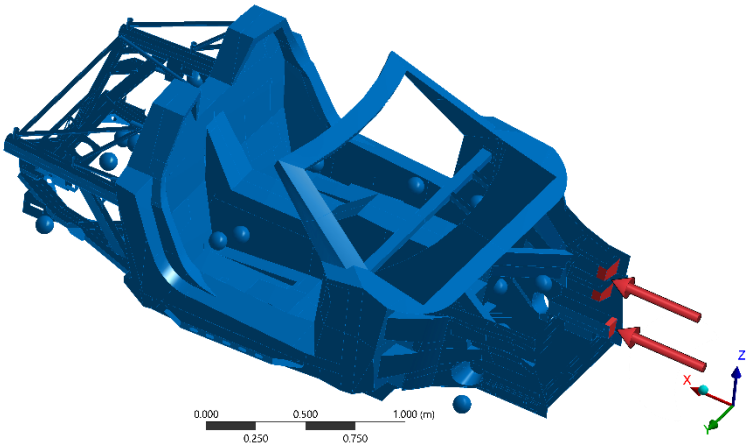

Figure 6.4 Free body diagram for frontal collision, showing supports and loads in red

It must be noted that in practice there is a connection between the left and right attenuators (seen in Figure 6.2), however in this model the conservative assumption is made that all loads are transferred through only the left attenuators.

For verification of the model analysing the frontal collision results will be compared with an available analysis on an earlier version of the chassis. This earlier version has slight geometrical changes, but has an identical lay-up as the current version. This analysis is however not an analysis of the ECE R94 collision test, but the Euro NCAP frontal collision. The standards set by Euro NCAP are often applied by major car manufacturers to receive a rating for the safety of their vehicles. However, since application of this standard is not mandatory for approval and since it does not result in requirements or restrictions, the test described in ECE R94 will be used for analysing the chassis in this research. For the frontal Euro NCAP collision however the same test as ECE R94 is conducted at a different velocity (64km/h

instead of 56km/h for ECE R94). [48] For verification the forces on the chassis are calculated in a similar fashion with only increased velocity. This results in 176kN on the upper attenuator and 59kN on the lower one.

Later on, this analysis will also be adapted for analysis of the BEV. For the kerb weight of 1424kg, which will be determined in Section 7.1, this results in a force of 190kN for the upper attenuator and 63kN for the lower one.

6.1.3 Lateral Collision

For type approval in the EU the ECE R95 describes a 950kg crash barrier colliding with the side of the vehicle at 50km/h. For this collision the same method is used to create a static load case to be applied using the inertia relief method.

Load Determination

Since there are no particular energy absorbing structures in the vehicle, for a lateral collision only the barrier is assumed to dissipate energy. This means that the entire chassis is seen as the “rigid” part of the chassis to protect the occupants. During the crushing of the barrier, this barrier itself decelerates and the vehicle accelerates up to the point where they have the same relative velocity. The energy absorbed by the chassis is therefore neglected. This assumption is conservative since energy absorption of the chassis would result in less severe loading.

ECE R95 describes a total energy dissipation of the barrier of 45kJ over a distance of crush 330mm. It also describes the force-deflection curves for the crush structure which shows a maximum force of 255.5kN. This value holds for the upper limit of the crush structure. [1] It is assumed that after crushing the barrier, the vehicle and barrier travel at the same velocity. For this reason the force of 255.5kN is assumed to be the maximum force during the collision.

This assumption is valid, when the work performed by the barrier is higher than the change in kinetic energy of the vehicle, according to the work kinetic energy theorem. [35] The work performed by the barrier is assumed to be 75% of the maximum defined 45kJ. [1] The 75% efficiency is based on earlier analyses at Roding Automobile GmbH.

When no energy is absorbed elsewhere, the remaining kinetic energy after the collision 58kJ, based on an initial kinetic energy of 92kJ. Using the same vehicle weight as for the frontal collision, this means total velocity of the vehicle and test vehicle after impact is approximately 7m/s. This means for the vehicle only 32kJ kinetic energy is present. At a force of 255.5kN, this kinetic energy can be transferred within 12cm work (based on the work kinetic energy theorem). A larger displacement would mean a lower force. For this reason 12cm seems to be conservative, based on displacements during several collisions test, and is therefore used. [49, 50, 51, 52]

In Figure 6.5 the supports for these loads are shown in a free body diagram. This surface is extracted from the projection of the barrier shown in Figure 5.3. This neglects the effect of load introduction via the door. In practice this will result in high local loads on the hinge and latch. Local reinforcement of these points should be analysed during the detailed design phase.

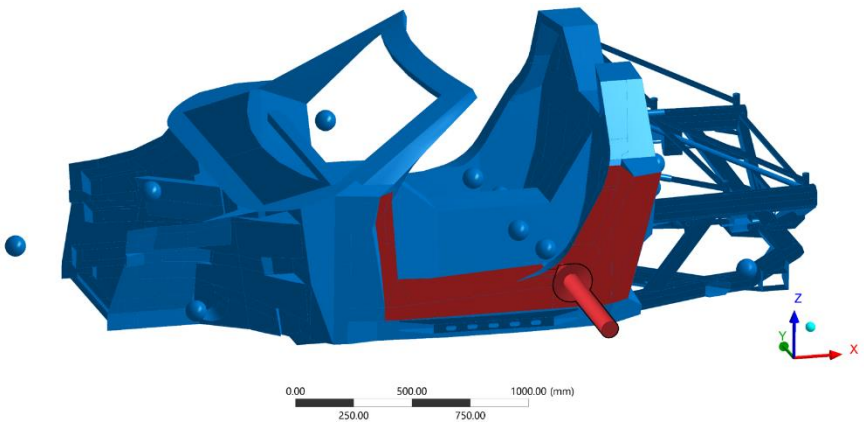

Figure 6.5 Free body diagram for lateral collision load, showing supports and load in red

For the load on the highlighted surface a remote force is modelled to act on the centre of gravity of the barrier. [1] This load assumes a virtual deformable body connecting the supported nodes with the loads to include all moments. This will make the analysis more realistic, since the centroid of the force does not align with the centroid of the supports. For all version of the Roding Roadster in this research, this means that the force is applied further to the rear than the CG is positioned. Since the centroid of the load cannot be estimated as accurate for the frontal collision, here additional moments were not included.

The additional point mass in comparison to Figure 6.4 represents the weight of the front section of the vehicle. This weight was excluded from the rigid part of the chassis for the frontal collision as explained before.

Injury Criterion Verification

For the original Roding Roadster weight, the allowed 50ms average force for this HIC is only 200kN according to the acceleration in Section 5.2.2. This force is less than the set 255.5kN. This means that for the relatively light Roding Roadster, the deceleration would be too large when a crash would have a duration of 50ms. Since this is approximately the case based on literature, the acceleration for the light Roding Roadster higher than allowed. For this reason research must be done on the increase of energy absorption or occupant protection during impact on the ICE Roding Roadster, with for example airbags. In this method additional occupant protection would result in higher reference values when calculating the ASI (Acceleration Severity Index), defined in Section 5.2.2. Since the set 255.5kN is a conservative value independent of vehicle weight, this load should be verified as well when the original Roding Roadster is analysed using this method.

However, for the heavier BEV the acceleration will be lower than the allowed 172m/s^2, which means a HIC of 1,000 is not exceeded. For this reason, a force of 255.5kN will be used to analyse the load distribution during a lateral collision in this research. It must be noted that this value is independent of vehicle weight as long as the HIC value is not exceeded. However due to inertia relief method, the weight distribution does influence the load distribution in the vehicle. In this case the 1.25 factor to include dynamic overshoot should be added as well. This results in a force of 319.4kN for a lateral collision according to ECE R95. Although the accelerations on the ICE Roding Roadster do not fall within the set conservative limits, this force will be analysed as a reference for the load distribution in the BEV.

6.1.4 Rear-end Collision

For type approval, ECE R34 dictates an additional test consisting of a collision from the rear of the tested vehicle. This test is specifically set up to prove prevention of fire risk is ICE vehicles. Since the implications of this regulation are not clear for BEVs, it is assumed that prevention of fire will be the same criterion for this regulation in BEVs. From this assumption is extrapolated that during this test, the goal will be to keep the REESS intact. For safety of the passenger also the passenger compartment must protect the occupants during this collision, which means this section should remain intact as well.

ECE R34 defines a collision with a 1,100 kg rigid barrier at 50km/h, which is visualised in Figure 5.3. In most vehicles there is less space for a crumple zone in the rear, with respect to the front crash attenuator. In the ICE Roding Roadster no independent rear crash structure is present, since the rear substructure will absorb the energy in the event of a rear collision as much as possible. Since in the BEV this area will probably contain high voltage electronics, a rear crash attenuator is desirable. This splits an energy absorbing structure form the stiff rear substructure.

A shorter attenuator in combination with the rigid barrier results in a significantly lower energy absorption with respect to the frontal and lateral collision. This means that the assumption that all energy will be converted in the deformation phase of the crash attenuator is not valid here. For this reason this phase will not be the critical load on the chassis during this collision. After the crushing of the rear crash attenuator, the remaining energy will create a peak load on the chassis. The height of this peak is however depending on the stiffness of the frame. Since this is very difficult to estimate, the forces in this phase of the collision will be taken over from another vehicle analysis by Roding Automobile GmbH. Based on this analysis the load peak of 30g is taken over. This is used to give a first impression of the loads involved in a rear collision.

The model for rear end collision will also be solved using the inertial relief function. For this reason also here the load must be increased with 25% to include dynamic overshoot. For the BEV this load results in a force of 58kN, based on the kerb weight of 1424kg (Section 7.1) in combination with two 77.7kg

occupants. This load is applied to the connecting points of the crash attenuator, which is visualised in Figure 6.6 for the BEV concept. This load is introduced on the connection points of the rear crash attenuator, which will be constructed later.

This load case is not analysed for the current Roding Roadster chassis, since this would mainly depend on the behaviour of the rear substructure. Since this substructure is designed around the combustion engine, this is not relevant. This load case is only a rough estimation, further analysis of this vehicle for type approval is required.

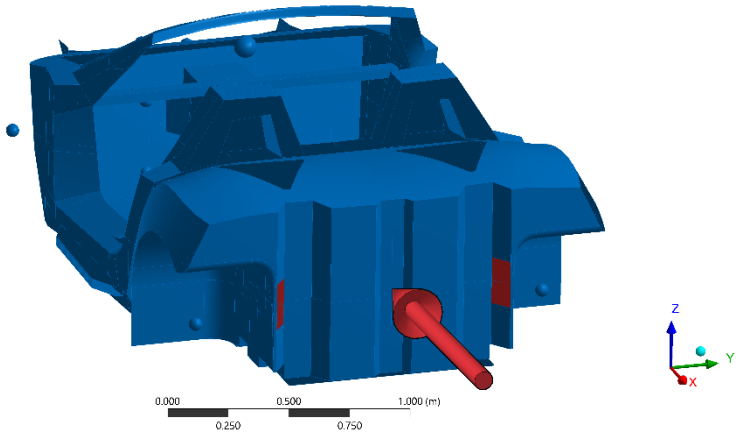

Figure 6.6 Free body diagram for rear-end collision load, showing supports and load in red

6.1.5 Seats and Safety Belts

The loading on the seat anchorages and safety belts are based on the requirements in the regulation ECE R17 and ECE R14. For seat mounted safety belts the loads in ECE R14 should be applied simultaneously with the loads of ECE R17. For this reason both regulations will be combined in a single load case.

The seat anchorage test load is defined as a 20g acceleration of the seat in the longitudinal direction. [1] With a seat weight of 15kg, this force is set equal to 2943N forward. [22] The centre of gravity of the seat is assumed to be at the SRP. Table 6.3 gives a total overview of all loads used in this load case. Table 6.1 presents the coordinates which were assumed to calculate these loads.

Table 6.1 SRP and safety belt coordinates

	SRP_{driver}	Point A	Point B	Point C	Point D	Point E	Point F
	[mm]	[mm]	[mm]	[mm]	[mm]	[mm]	[mm]
X	1540	1635	1580	1920	1840	1480	1635
Y	-378	-120	-378	-555	-550	-378	-636
Z	-22	-120	316.9	550	-65	75	-120

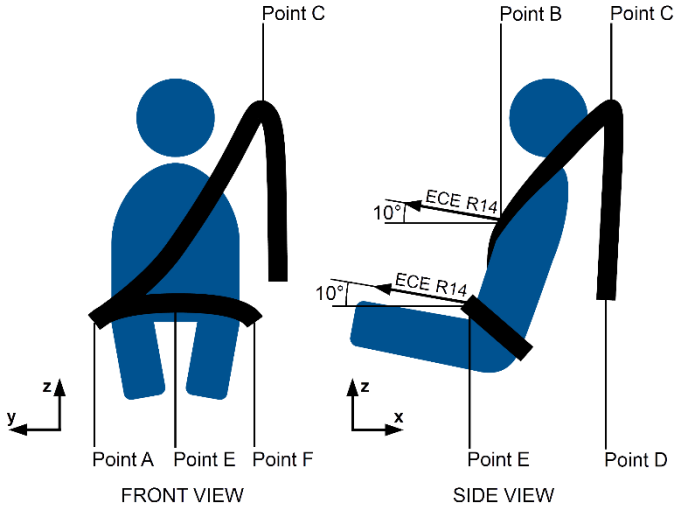

Figure 6.7 Point definitions for safety belts

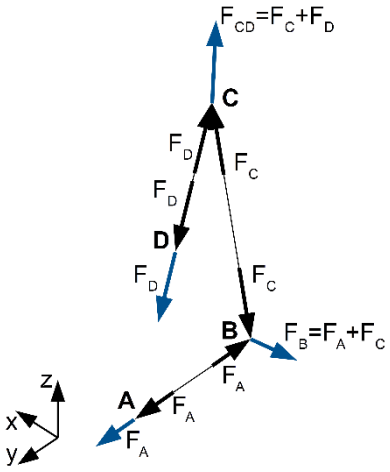

Figure 6.8 Torso strap free-body diagram

For the safety belt section of this load case, it is assumed that as in the ICE Roding Roadster a conventional three-point safety belt with retractor is used. The lower two anchorage points are mounted onto the seat. It is defined that the anchorage points of such belt should be designed to withstand a force of 13500N on the torso strap and the hip strap simultaneously. These forces are assumed to act in point B for the torso strap and Point E for the hip strap as shown in Table 6.1 and Figure 6.7. These coordinates are based on the CAD master part, for the most rear driver position of the 95th percentile male driver. This is chosen due to the fact that this results in larger moment arms, which makes this is the most adverse position. [1] For the passenger position, the coordinates and loads can be mirrored over the xz-plane. These loads are modelled simultaneously, since for type approval all seating positions will be tested at the same time.

To divide the safety belts loads into loads on the seat anchorage points and the cassis mounted safety belt anchorage points, the hip and torso strap are detached in the force equilibrium. This means that the sliding of the safety belt in point A is not incorporated. This makes it easier to distribute the load on the torso strap into a load acting on the seat, a load on the loop point and a load on the retractor.

The force on the hip strap acts entirely on the seat anchorage points. That is why this can be modelled as a remote force, which assumes a virtual body connecting the anchorage points with the point where the force engages to include all moments.

For the torso strap a force equilibrium is used to divide the applied force into three chassis forces. Namely at the anchorage point to the seat (point A), a loop point at the pillar (point C) and an anchorage at the retractor (point D), as seen in Figure 6.7. The force in point A will be applied similarly to the force in the hip strap (as a remote fore on the seat anchorage pints). The forces in point C and point D are applied directly to the mounting position on the chassis. By assuming the loop in point C to be frictionless, the forces can be calculated statically as a truss structure where F_C is equal to F_D. This is visualised in the free-body diagram (FBD) in Figure 6.8. Here the blue forces represent the external loads on the torso strap. The black forces represent the tensile internal loads on the independent members. The calculated forces within this FBD are given in Table 6.2, to display the equilibrium for the replaced original force (F_B) stated in the regulations. In this FBD the blue forces represent the external forces on the safety belt. It must be noted that the external force in point C is a resultant force derived from F_C and F_D, called F_{CD}. Table 6.3 gives an overview of the combination of forces which must be applied to the chassis model to analyse both ECE R17 and ECE R14.

Table 6.2 Forces of torso strap on the chassis for safety belt regulations

	F_A	F_C	F_{CD}	F_D	$F_B = \sum F_A, F_{CD}, F_D$
	[N]	[N]	[N]	[N]	[N]
X	-1328	11967	-14004	2037	-13295
Y	-6230	-6230	6357	-127	0
Z	10549	8205	-23863	15658	2344
Total	12323	15790	28389	15790	13500

Table 6.3 External forces for the seats and safety belts load case (driver only)

	F_{seat} (in SRP)	$F_{hip\ strap}$ (in point E)	F_A	F_{CD}	F_D
	[N]	[N]	[N]	[N]	[N]
X	-2943	-13295	-1328	-14004	2037
Y	0	0	-6230	6357	-127
Z	0	2344	10549	-23863	15658
Total	2943	13500	12323	28389	15790

6.1.6 REESS Compartment Load Cases

For BEVs subjected to ECE R100, a set of structural requirements must be fulfilled besides electronics related requirements, as explained in Section 3.2. [1] For the mechanical shock, the defined accelerations are simultaneously 28g longitudinal and 15g lateral for the component based test. In this research ECE R94 and ECE R95 will be modelled separately from the REESS. For this reason, this load case can be used to design the REESS housing. During the approval process, these collision tests can be used to replace this component based tests for mechanical shock.

The same holds for the crush test, where a force of 100 to 105kN is applied using a 600mm by 600mm crush plate in the y-direction at a position which is determined together with the approval authority. In this crush test the applied force may be reduced, when analyses show that the contact force on the REESS will not exceed this new value in a collision as described for ECE R94 and ECE R95. This means that an analysis of ECE R94 and ECE R95 can be used to decrease the test loads for a component based crush test. When ECE R94 and ECE R95 are executed in practice these can replace the component based crush test completely.

6.2 Analysis of Roding Roadster Chassis

With the load cases defined in the previous section, an FE (Finite Element) model is created to evaluate the performance of the current chassis. To do this, first the validity of the inertia relief method must be checked. This is done by analysing the natural frequency of the current chassis in Section 6.2.2. When this method is found to be valid, the vehicle will analysed using the weight distribution of the ICE Roding Roadster in the Euro NCAP frontal collision, to verify the model by comparing it to an earlier model.

After verification this analysis can be used to define better where the current chassis might require alterations or what sections perform very well. This will mainly be done for the frontal collision (ECE R94) and the lateral collision (ECE R95), since these are expected to have a global impact on the chassis and knowledge is limited. However the extreme driving load case also has global influence, more experience due to numerous test drives is available here. For this reason, this load case is expected to be stiffness dominated. Since no strict requirements can be added without thorough analysis of vehicle dynamics, no modification will come forward form this load case. For that reason the extreme driving load case will only be analysed for the final design. With the current vehicle analysis as reference, the model can be modified for the weight distribution of the BEV Roding Roadster, in Section 7.2.

6.2.1 Establishment of the Finite Element Model

Since the inertia relief function is used, the mass distribution must be accurate to result in a correct load path. That is why for the components from the mass distribution in the ICE Roding Roadster were inserted as point masses. The mass distributions will be further discussed in Section 7.1. As a check the global centre of gravity from the model was compared to the measured centre of gravity in the Roding Roadster. These two were found to have an offset of less than 15mm in all three principle directions. The offset in the centre of gravity comes from the fact that the chassis components weights in the model are calculated from the material distribution instead of the values used in the weight distribution. This small offset is assumed to be negligible. It must be noted that the not-modelled weight components of the chassis, were modelled as a 73kg additional weight in the centre of gravity. This weight is based on the difference between the modelled chassis weight and the measured chassis weight.

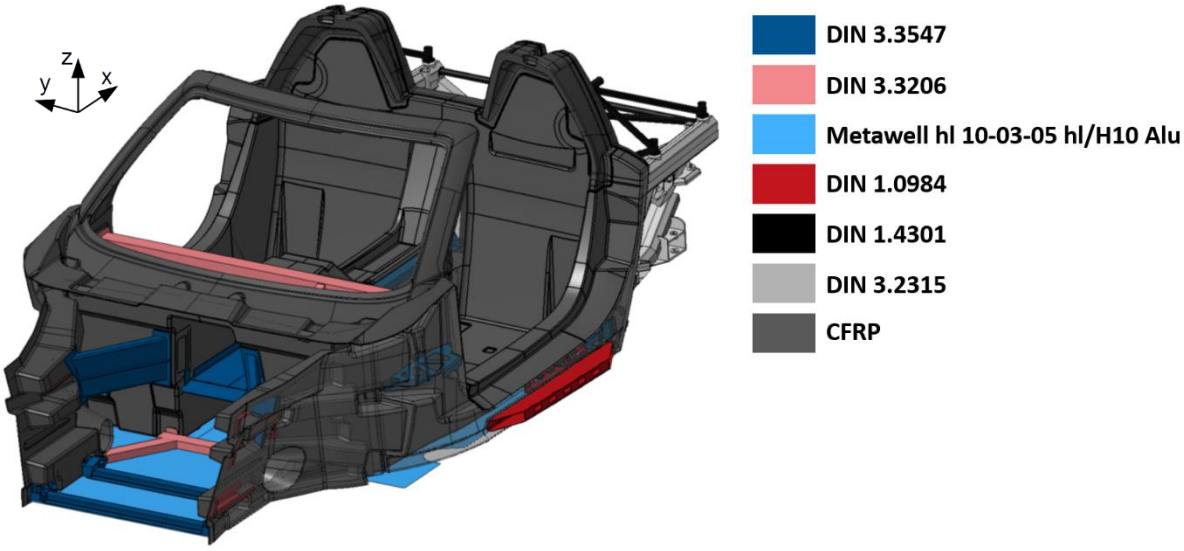

Figure 6.9 Overview of the materials in the chassis

The entire FE model was analysed using a thin walled approach to eliminate complexity. For this analysis a simplified CAD model was created, to exclude complex curvatures and not loadbearing features. In Figure 6.9 one can see the materials in the chassis assigned to all subcomponents by colour according to DIN standards. These materials are used as input for the model in combination with the

correct lay-up according to the lay-up plots used for the CFRP (Carbon Fibre Reinforced Plastic) parts. [31, 32, 53] This results in the thicknesses shown in Figure 6.10 for the simplified geometry. An overview of the used material properties can be found in Appendix B. For the CFRP parts, an intermediate CFRP-material from the ANSYS Material Database was used for both unidirectional and woven materials. The material closest to the used material for the original chassis was chosen. This is done because there is no complete dataset available for the used material.

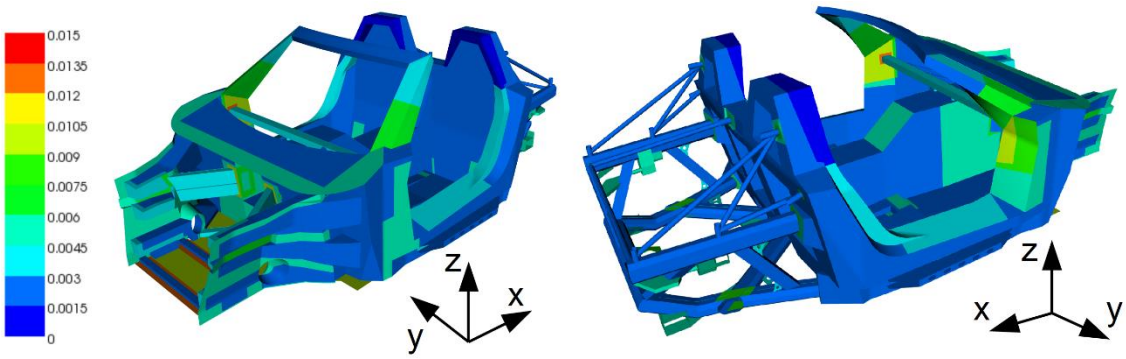

Figure 6.10 Thickness in simplified chassis

6.2.2 Natural Frequency Analysis

As explained in Section 6.1.2, the natural frequency of the chassis must be found first, to compare the period of this natural frequency with the period of the impact. This will be done to check if the method using inertial relief, is valid for this vehicle. From typical analysis and earlier analysis for the Roding Roadster it can be seen that the compared frontal collision has a duration of more than 0.15 seconds. [16, 46] This period is approximately similar to the duration of a lateral crash. To fall within the 25% margin stated in Section 6.1.2, the lowest natural frequency may occur at a frequency higher than $2.2 * \frac{1}{0.15}$Hz = 14.5Hz. [16]

The lowest natural frequency of the modelled ICE vehicle, is found to be at 18.9Hz, which makes the method of inertia relief valid for this model. This is analysed by supporting the model equally as described in Section 6.1.1. This way no additional stiffness is added by limiting rotation or in-plane translation for every suspension point. In Figure 6.11 the mode of this frequency is visualised with an amplified deformation. Since it is difficult to perform a similar modal analysis including a realistic REESS behaviour, it is assumed that the use of the inertia relief function is also valid for the BEV concept.

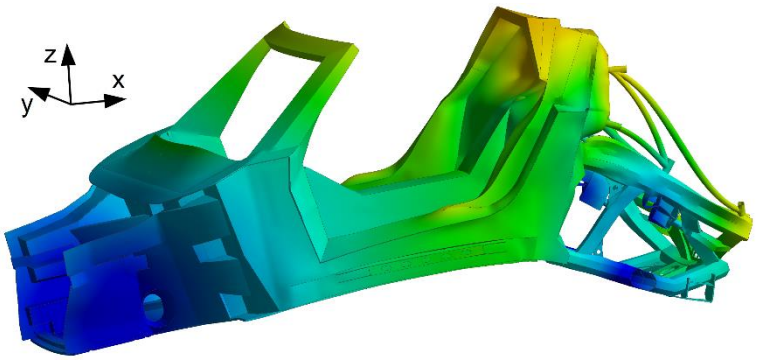

Figure 6.11 Lowest natural frequency mode (18.9Hz) visualised with amplified deformation for the ICE Roding Roaster chassis and weight distribution

6.2.3 Model Verification

The frontal collision is analysed first for verification using the Euro NCAP velocity on the ICE Roding Roadster. This is done since for this situation a comparable analysis is available. In Figure 6.12 and Figure 6.13 one of the outputs of this existing analysis of the Roding Roadster chassis are shown for verification. Since the reference analysis is a dynamic model, results change throughout time. For the comparison, the most critical point in time during the crumpling of the crash attenuator is shown.

The shown FE results, which will be used for verification, were modelled different from the developed model. That is why slightly different results are expected, although behaviour and order of magnitude should be similar. The main difference is that the created model is based on a static analysis, where the

analysis in Figure 6.12 and Figure 6.13 is modelled dynamically. Therefore in this analysis the chassis is assumed as an isotropic material, to eliminate the complexity of non-linear composites modelling. To analyse similar load paths, in the static model the influence of supports is eliminated by using the inertia relief function, as explained before. Another difference is that for the inertia relief the mass distribution was modelled using separately supported point masses for all major components in their centre of gravity. The remainder of mass was distributed over the major mounting surfaces. In the dynamic model the vehicle weight was not modelled as separate components, but only the total weight and centre of gravity were regarded. This means that there are more positions counteracting loads due to inertia are introduced into the chassis in the new static model. It is expected that this will give a more realistic overview. In the output this will also result in higher local loads at points where components with a large mass are supported, such as the engine for the ICE Roding Roadster.

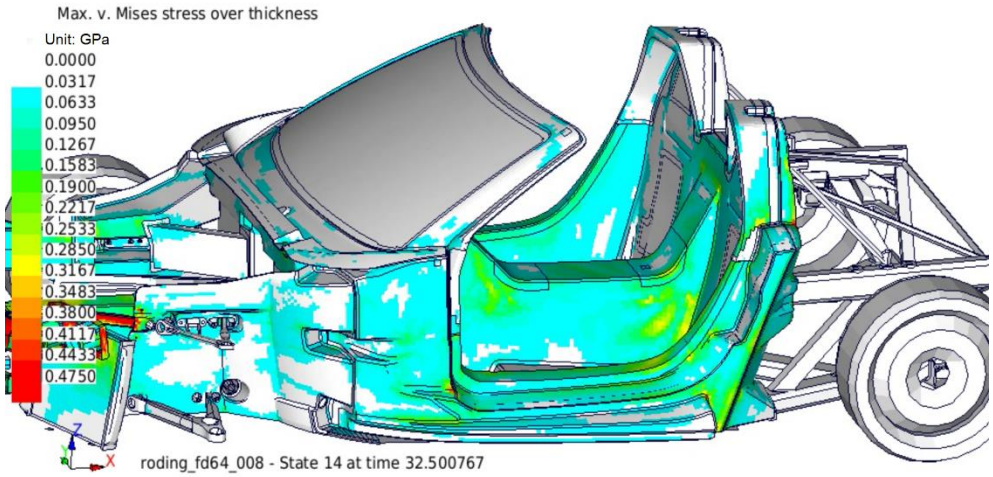

Figure 6.12 Von Mises stress in reference Euro NCAP analysis of Roding Roadster chassis, view 1

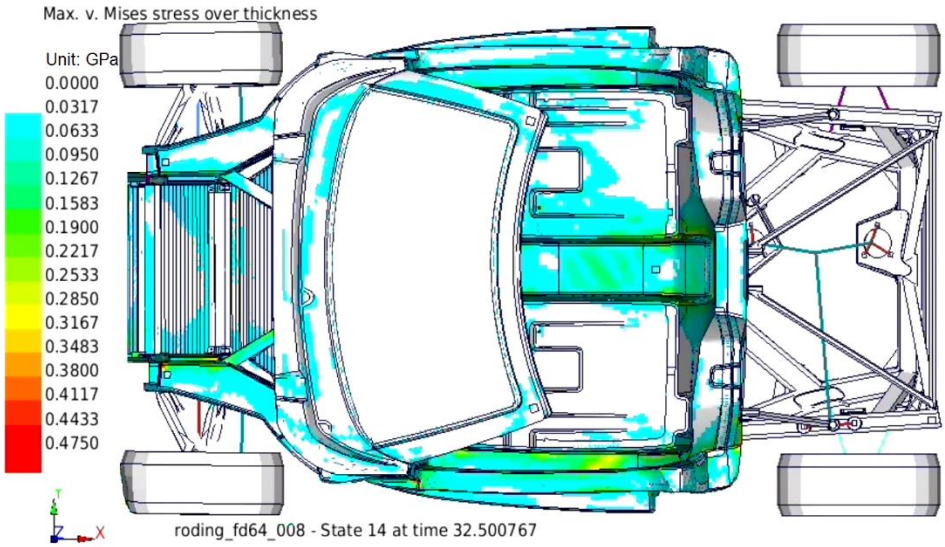

Figure 6.13 Von Mises stress in reference Euro NCAP analysis of Roding Roadster chassis, view 2

To compare the models qualitatively, the behaviour of both models can be compared. However for a quantitatively comparison, it is difficult to compare common composite failure criteria to the given isotropic von Mises stresses. This is the case since for fibre reinforced materials, stresses are not identical in every layer. The layers which contain fibres in the direction of the load path, will show higher stresses than the layers with fibres in different directions. For the isotropic materials, the loads can be distributed over the entire thickness since there is no preference in load direction, resulting in lower stresses. For this reason, it would not be fair to compare principle stresses in critical layers with the von Mises stresses. To make a fair comparison, a von Mises plot is created from the fibre reinforced model. This is an unconventional output, but gives an absolute stress for the entire lay-up independent of its direction. This result can then be compared with the reference model easily. For the created model, the von Mises stress is visualised in Figure 6.14 and Figure 6.15.

When comparing both models, one can see roughly the same behaviour and order of magnitude for both models. One can see that the magnitude of the stress in point A (Figure 6.14) is approximately similar to the values shown in the reference analysis, which ranges up to around 350MPa. At point C (Figure 6.15), equivalent values can be found in both models as well (Figure 6.15), since both models show values around 100MPa at the outer face of the beam and values up to 350MPa on the inner face. In point B (Figure 6.14) a relatively big difference can be seen. Where this difference originates is difficult to isolate, since the exact structure of the reference model is unknown. It is expected that the weight distribution for the reference model supports a major part of the weight at the rear substructure, since the weights were not modelled as separate components. This might result in higher loads at point B, since the middle tunnel is a critical point connecting the rear substructure to the rest of the vehicle. This is in line with the expected differences between both models. Based on this comparison the model is assumed to show results which are reliable enough to estimate the performance of the structure during a collision.

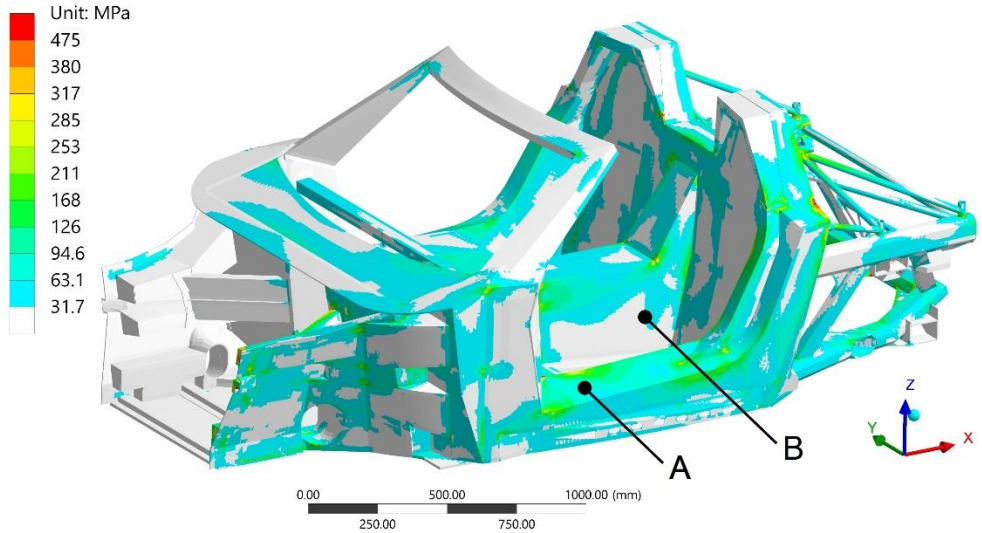

Figure 6.14 Von Mises stress in Euro NCAP analysis of Roding Roadster chassis, view 1

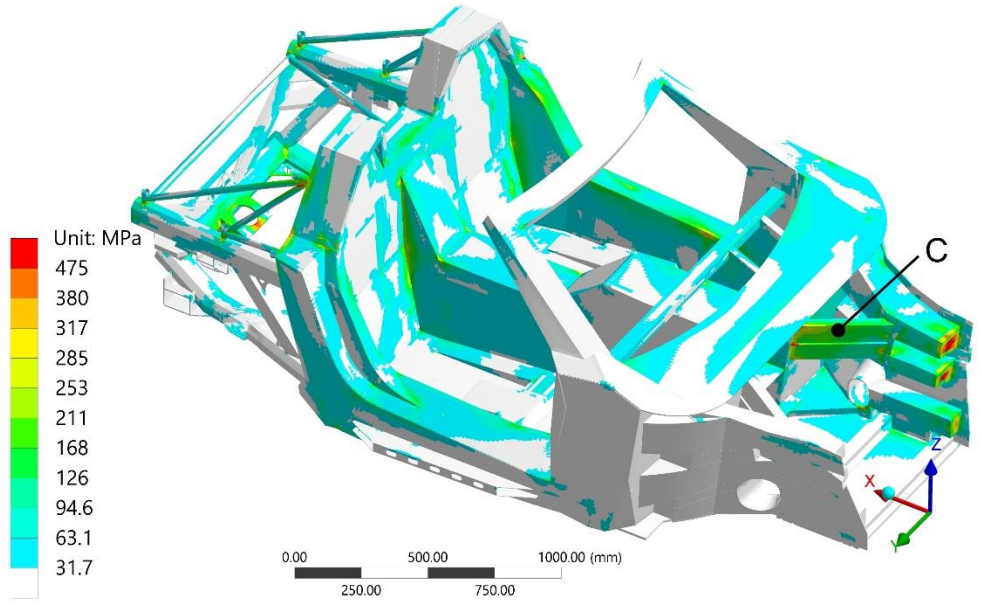

Figure 6.15 Von Mises stress in Euro NCAP analysis of Roding Roadster chassis, view 2

6.2.4 Collision Analyses of Conventional Roding Roadster

To show relevant results for the generated model, the inverse reserve factor is plotted along with the total deformation. The inverse reserve factor shows that a composite material layer has failed at a value of “1” or higher. This is done to give an easy overview of how critical an element is loaded. For isotropic materials, such as the metal components, this is done by issuing a value of “1” when the von Mises is equal to the yield stress. For composite materials the maximum strain, maximum stress, Tsai-Hill and

Tsai-Wu failure criteria are used. [54] The inverse reserve factor is plotted all results for the most critical layer per element. No safety factors are yet involved besides the 1.25 factor covering the dynamic overshoot to ratify inertia relief and the conservative approach in the load case determination.

For comparison, the total deformation of the verified analysis of the Euro NCAP frontal collision is visualised in Figure 6.16. The inverse reserve factor is plotted for the most critical layer in Figure 6.17 and Figure 6.18. Now the model is verified, the loads are changed into the loads which describe the ECE R94 frontal collision. In Figure 6.19 the total deformation is plotted, where Figure 6.20 and Figure 6.21 show the inverse reserve factor. In this model the load case for the lateral collision is added. Figure 6.22, Figure 6.23 and Figure 6.24 show the results for this lateral collision analysis according to ECE R95 in the ICE Roding Roadster. It must be noted, that for this vehicle weight, vehicle accelerations were calculated to exceed the allowable HIC.

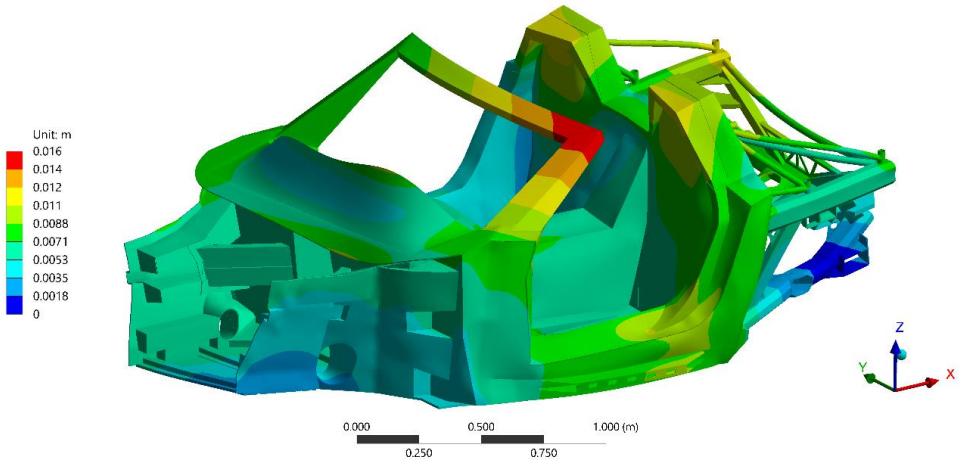

Figure 6.16 Total deformation for Euro NCAP frontal collision of the ICE Roding Roadster (amplified visualisation)

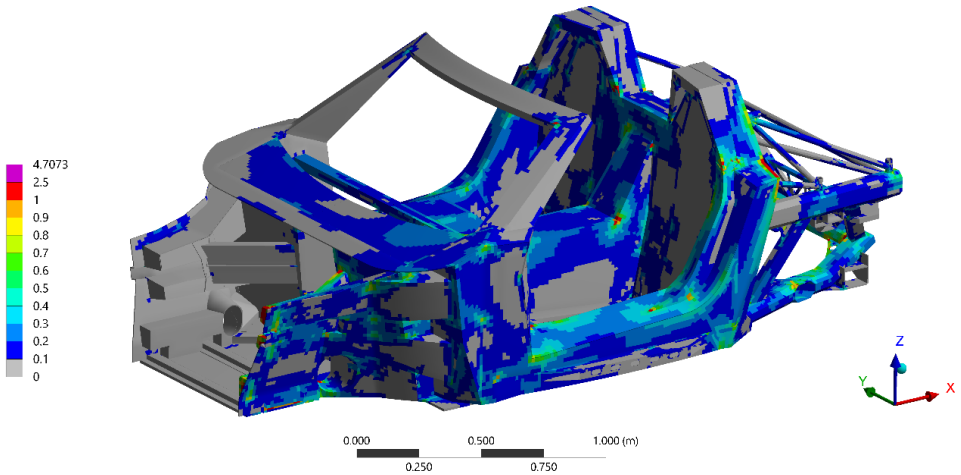

Figure 6.17 Inverse reserve factor for Euro NCAP frontal collision of the ICE Roding Roadster, view 1

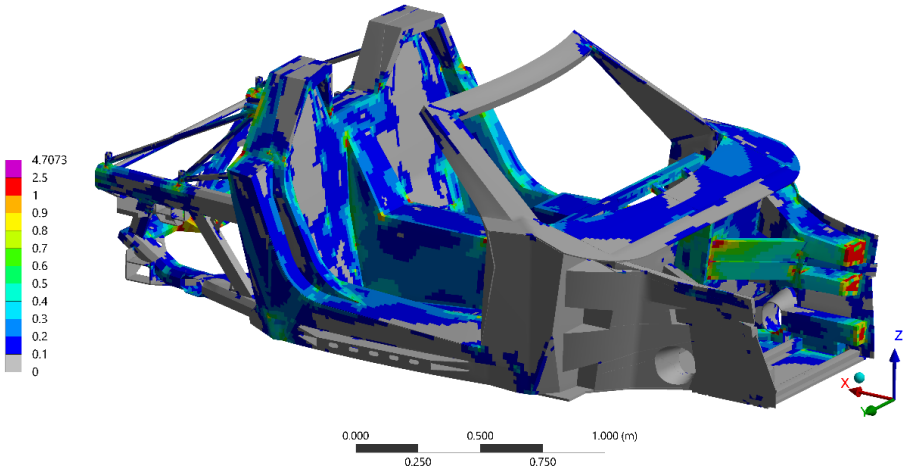

Figure 6.18 Inverse reserve factor for Euro NCAP frontal collision of the ICE Roding Roadster, view 2

It can be seen that for the frontal collision in Figure 6.21, the surface around the crash attenuators shows some failure. Due to the lower load in the ECE R94 test, this failure decreases with respect to the Euro NCAP test in in Figure 6.18. In reality this part will be stiffened by the attenuator flange itself, which will make this section less critical. The same happens in the rear substructure, at the points where the engine is suspended. This makes sense, since the engine represents the largest mass. Large deformation in the water shield at the bottom of the windshield are probably less critical in reality, since this section in reality has more geometrical stiffness and is supported by the windshield as well.

Further it can be seen that the sharp edges result in local single elements with high peak loads. This can be the result of the simplification in geometry, where the sharp edges can cause an overshoot. The severity of these stresses should be analysed more thoroughly in the detailed design phase, where a more accurate geometry must be analysed to calculate local loads properly. It is expected that stress concentrations will occur at these positions, but decrease in terms of intensity when increasing fillet radius, based on the available distance for a good redirection of loads.

It is assumed that the extremely high maximum values of the models are the result of model simplifications. For the front crash this value occurs at a single element in the seam between two tube sections of the rear substructure. In Figure 6.20 this position is highlighted with an arrow. All elements adjacent to this element show a value below an inverse reserve factor of 1.5. This indicates an overshoot of this single node, which occurs due to a complex joint between different components.

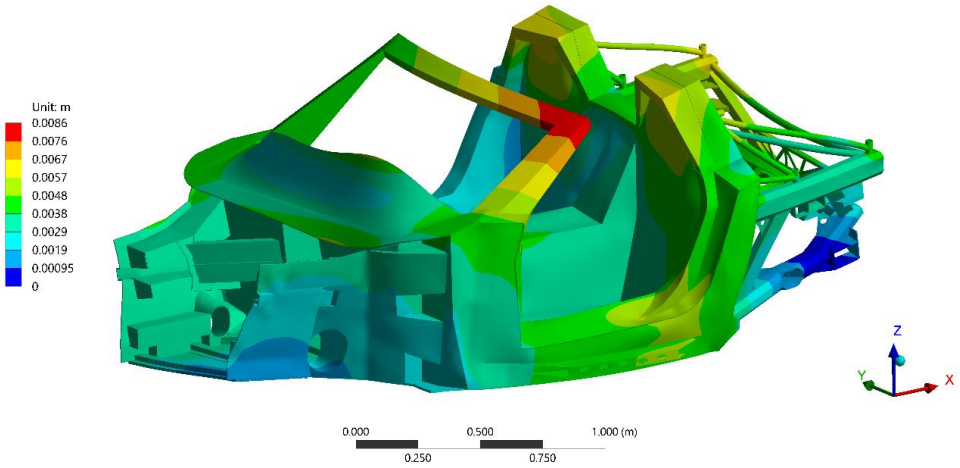

Figure 6.19 Total deformation for ECE R94 frontal collision of the ICE Roding Roadster (amplified visualisation)

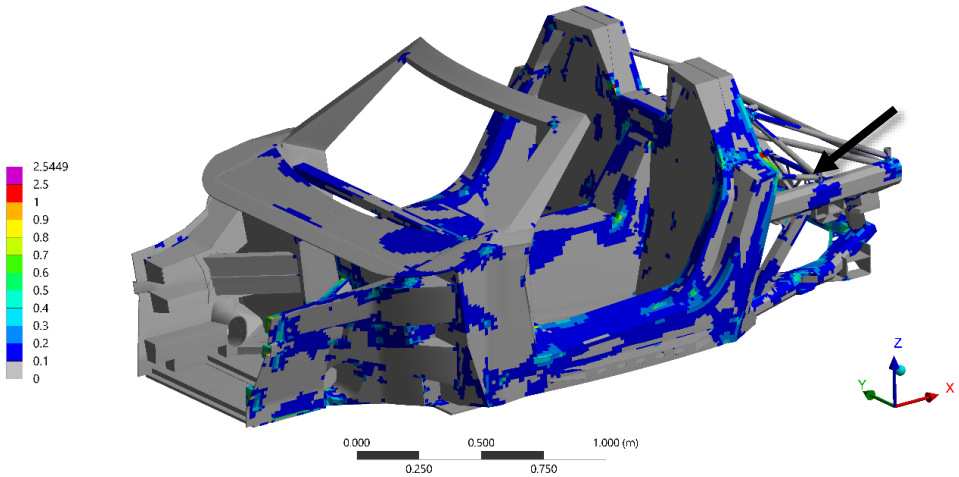

Figure 6.20 Inverse reserve factor for ECE R94 frontal collision of the ICE Roding Roadster, view 1

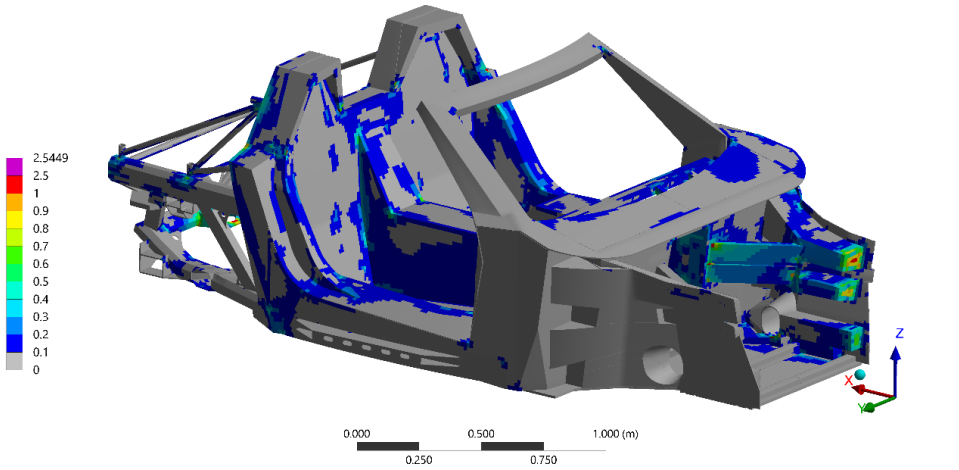

Figure 6.21 Inverse reserve factor for ECE R94 frontal collision of the ICE Roding Roadster, view 2

For the lateral collision very high Tsai-Wu criterion values occur in the “B” pillar. This happens because in x-direction the middle of the barrier is positioned at the hip point of the driver. The results show that the load introduction in the “B” pillar is not sufficient. Another load concentration can be found at the connection between the “A” pillar and the sill (the structural section below the door). This expected to be caused by the stiffening effect of the “A” pillar. For the analysis of the BEV this position should be reviewed in more detail. The connection of the rear substructure and passenger compartment show critical failure values as well. These critical point are taken along in the concept development and will be addressed in the design of the new chassis.

A single extreme peak value, similar to the peak in the frontal collision, occurs for the lateral collision. In Figure 6.23 this position is highlighted with an arrow. This peak value occurs at a complex point where several components join. Adjacent elements drop extremely in value for the inverse reserve factor. The local inaccuracy of the model at this location is supported by the fact that under loads which do not effect this region, unrealistic inverse reserve factors still occur at this location. Besides that, a shell based model is not able to determine the loads in a joint very accurately, so accurate load transfer between different components and layers should be analysed in more detail in the detailed design with a more accurate model. It can also be concluded that the failing section is part of one of the U-shaped covers (better distinguishable in Figure 4.5 on page 19). Because this component is not designed to transfer the principle loads during an impact, it is assumed that the presence of failure at this position is not detrimental. For this reason this position will not be the main point of attention. The critical adjacent load bearing components and other extremely critical positions do require more attention in the design of the chassis for the BEV and during the detailed design.

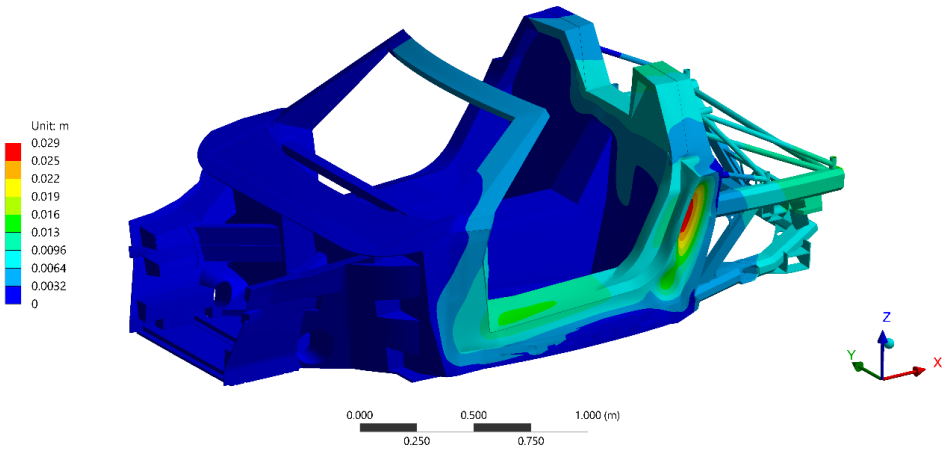

Figure 6.22 Total deformation for ECE R95 lateral collision of the ICE Roding Roadster (amplified visualisation)

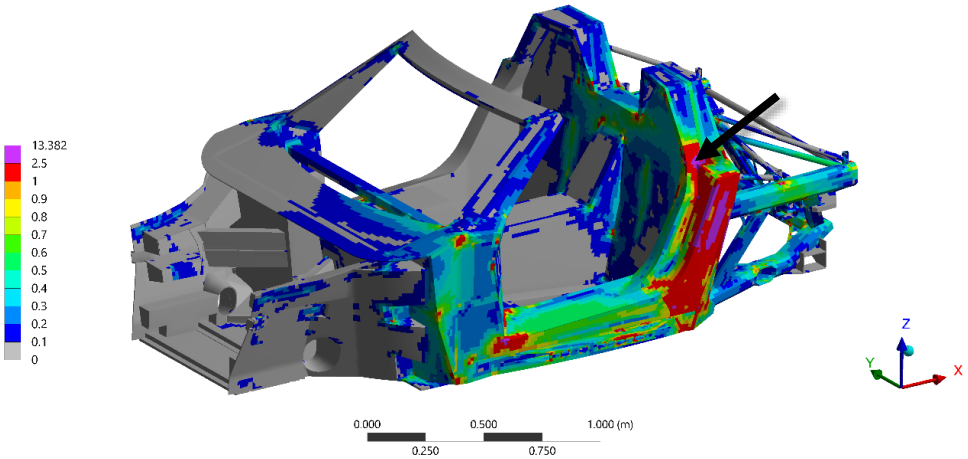

Figure 6.23 Inverse reserve factor for ECE R95 lateral collision of the ICE Roding Roadster, view 1

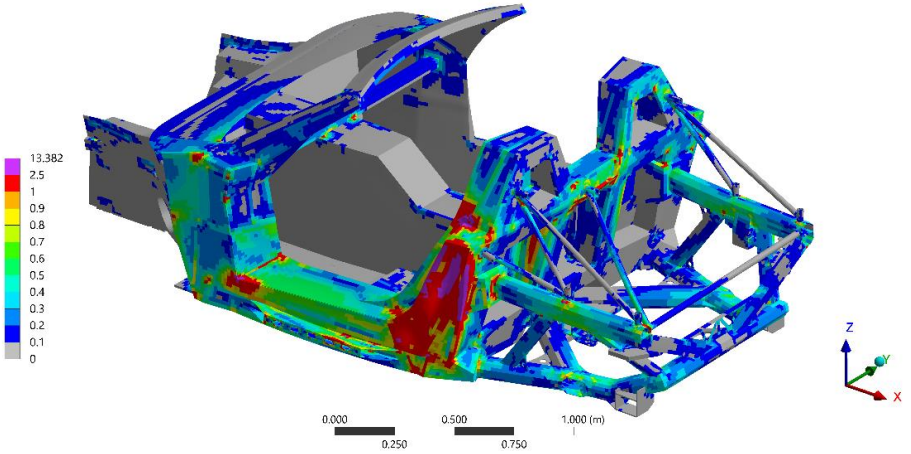

Figure 6.24 Inverse reserve factor for ECE R95 lateral collision of the ICE Roding Roadster, view 2

With these results, a reference was created for the most important load cases from Section 6.1. The next step in the structural analysis will be the analysis of the original chassis in combination with the weight distribution of the electric version of the Roding Roadster. To be able to do this, the best powertrain and its weight distribution will be selected in Section 7.1. The modified analysis, including this weight distribution can be found in Section 7.2. The results from this analysis will be used to create a starting point for the revised chassis, which will be analysed in Section 8.3.

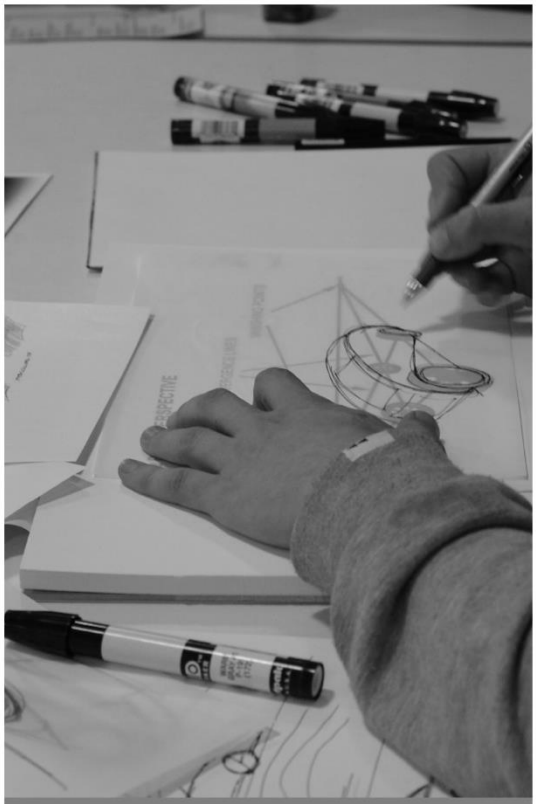

Concept Development

7

Now that it is defined what regulations and requirements the chassis must fulfil and how the chassis performance will be evaluated, it is possible to develop concepts which comply with the set boundaries.

Before creating structural chassis concepts, the powertrain will be chosen using a trade-off. In the first section of this chapter different powertrain concepts will be developed according to state of the art component options. These concepts will be compared by their weight distribution and its effect on the characteristics of the vehicle. From this comparison the best powertrain concept will be chosen.

Using a fixed powertrain, different concepts are developed and evaluated for the structural concept of the vehicle. In the last part of this chapter a trade-off will be made between these concepts. This trade-off is based on the estimated weight, the costs per vehicle and an additional rating for each concept.

7.1 Powertrain Selection

In this research, the powertrain concept determination is split from the chassis concept. This is done because the chassis is seen as a very adaptable component, which would result in too many variables. Roding Automobile GmbH depends on suppliers for the electric powertrain, which is a relative small market. For this reason it is also seen as a better method to pick the best solution for the powertrain and use this as input for chassis concepts. The validity of this assumption will later be verified by checking the influence of the new chassis on this decision.

The possible powertrain options will be assessed by mainly two factors, namely cost and weight. In terms of costs, lower costs are desired. In case of the weight, a lower weight will result in lower roll resistance, but also in higher accelerations. Besides the total weight, the distribution of weight also has a major influence on the vehicle performance. The position of the centre of gravity (CG) and the mass moment of inertia both influence the acceleration, braking and cornering performances considerably. Performance is a very important factor for sports cars. For this reason a trade-off is made between different powertrain configurations based on the weight, weight distribution and costs.

7.1.1 Powertrain Configuration Options

Before analysing, the different options for a powertrain are set [11]:

1. A concept combining the motor with a fixed gear to drive a differential. This differential divides the power between two axles connected to the wheels, allowing different rotational velocities. Since during a market analysis (Appendix C) no individual motors were found to suit the power requirements, this concept is equipped with two motors driving a single shaft. This is visualised in Figure 7.1, where “M” stand for motor, “G” for fixed gearbox and “D” for differential.
2. Two separate drivetrains, powering both rear wheels separately, can be an option to eliminate mechanical components (Figure 7.2). In this case the differential can be replaced with software which makes sure the power is distributed correctly. This is called an “electronic differential”.
3. This option is based on in-wheel motors, visualised in Figure 7.3. Since this configuration limits the motor volume due to the surrounding rim, in-wheel motors with high power outputs are scarce. For this reason this layout will require four motors to deliver the required power, since two would not deliver the required amount of power.
4. A second four wheel drive option is considered to investigate possible advantages in powertrain layout. This concept uses one motor in the rear and one in the front, as seen in Figure 7.4. Splitting the powertrain might be an option, to create a better weight distribution without adding weight, since all concepts already require multiple motors. This concept can be combined with a gear and differential driving four drive shafts. This concept is considered to check its positive influence on the longitudinal weight distribution. The concept can also be equipped with four motors to drive all wheels independently. However since this is not desired from the stated requirements, this concept would add unnecessary components at a higher weight than the third option.

The previous powertrain concept numbering will be used throughout this research. The decision for one of the concepts above can be made based on the difference in power distribution. Separated propulsion enables for example torque vectoring, which uses active control for the power distribution across the wheels. This increases the grip and performances when cornering, but increases complexity. To utilise the opportunities posted by the different options, decisions beyond the scope of this research must be made. This is mainly dependent on incentive to invest in the development of technologies supporting these concepts. Since this choice is relatively subjective, these differences are neglected when the cost and weight trade-off shows an evident preference for one concept. For the same reason, development costs differences between the different options are not taken into consideration. It is expected that for the assumed production numbers, these differences in development costs result in a negligible cost difference per vehicle.

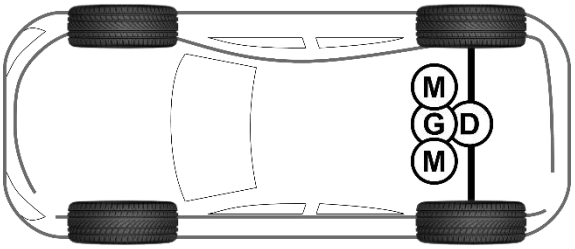

Figure 7.1 Schematic overview Concept 1

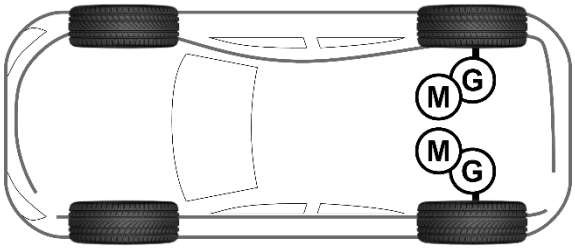

Figure 7.2 Schematic overview Concept 2

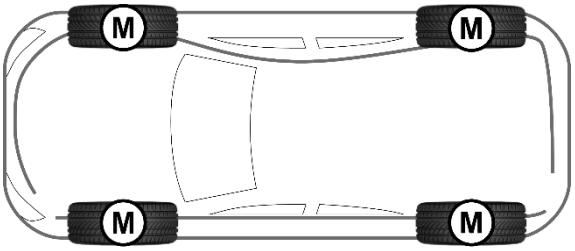

Figure 7.3 Schematic overview Concept 3

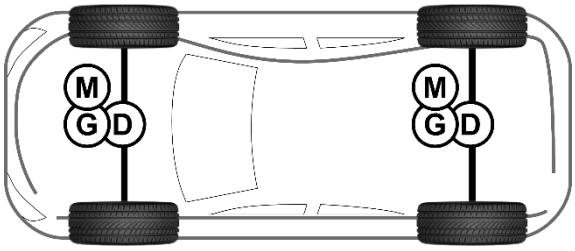

Figure 7.4 Schematic overview Concept 4

Assumptions

The Roding Roadster was taken as a starting point, excluding the powertrain components, to act as basis vehicle for the electric version. The original weight distribution is based on the measured centre of gravity in the Roding Roadster and the known distributed weights. [32] It is assumed that component weights and distribution of the rest of the vehicle will not change considerably when the chassis is designed for an electric powertrain. As stated before, the sensitivity of the decision model for changes to the chassis will be checked later.

For the four different options, the weights and costs are estimated. These are based on off-the-shelf components, excluding the gearbox. Gearboxes can be developed and produced as desired in-house at lower costs by Roding Automobile GmbH. The cost and weight of the in-house developed gearboxes are based on the gearbox currently in development. [32] For the HV (High Voltage) components the assumption is made that the system would operate at a bus voltage of 400V because this is the voltage used in the major section of the industry. This is the case since this current is well balanced between power losses and isolation requirements. [11] Appendix C is created to give an objective overview of state of the art powertrain components for electric vehicles. The components which are reported in this overview are used to base the powertrain concepts parameters on, which will be used in this section.

Powertrain Concept Components

As an input, the REESS (Rechargeable Energy Storage System) was required to have a capacity of 70kWh. Appendix C also gives an overview of the state of the art options for battery modules. Based on these options, the assumption is made that the required REESS capacity can be achieved with a total weight of 500kg and 400L. This includes subsystems such as battery management systems and wiring. These parameters are independent of the other powertrain components in total size and weight. The REESS along with the other component weights can be found in Table 7.1, based on Appendix C.

Table 7.1 Component weights for different powertrain options

	Concept 1	Concept 2	Concept 3	Concept 4
Name	**Component weight [kg]**			
Basis vehicle (driver excl.)	749	749	729	749
REESS	500	500	500	500
Charger	12	12	12	12
DC/DC	3	3	3	3
Auxiliaries	30	30	30	30
Wiring	10	10	10	10
Motor	2x 49 = 98	148	4x 36 = 144	2x 49 = 98
Gear	40		n/a	2x 30 = 60
Inverters	2x 11 = 22	2x 11 = 22	within motor	2x 11 = 22
Drive shafts	2x 4.5 = 9	2x 4.5 = 9	n/a	4x 4.5 = 18
Kerb weight [kg]	1473	1483	1424	1502

7.1.2 Powertrain Weight Distribution

In this section the weight distribution for the different concepts will be evaluated. At first, imported vehicle parameters will be extracted from the weight distribution. Next possible positions for the REESS will be discussed and loading diagrams will be plotted.

Using these determined vehicle components in combination with the distributed weights of the Roding Roadster (excluding powertrain), a spreadsheet is created to calculate the CG for all concepts. For a realistic interpretation of the weight distribution, luggage and occupants are taken along in the determination of the CG.

For the CG position in the x-direction components are distributed in weight fractions per 50mm increments. In the other two principle directions the position is entered as point load, since for these directions only the global CG position is relevant. Using these positions and weights, the CG of the vehicle can be calculated. This is done by calculating the moment of every weight increment around the origin. When this total moment is divided by the total weight, a representative arm will result in the x-position of the CG. The same can be done for the y and z-direction, to calculate all three components of the CG-position. This spreadsheet will be used to create a trade-off between the concepts in combination with the accompanying costs. For this trade-off, parameters which can be evaluated independently (such as mass and cost) are weighted. Other parameters are weighted by evaluating their offset from the most ideal value.

Along with CG, for every increment the mass moment of inertia is determined along the z-axis in the centre of gravity (I_{ZZ}). This is done by multiplying the mass of every element by the squared distance between its centre of gravity and the axis of interest, as shown in Formula 7.1. This moment of inertia can be used to assess the agility of the car, since a higher mass moment of inertia results in a higher resistance against accelerations. In this case a higher I_{ZZ} will result in in a lower angular acceleration when cornering, as seen in Formula 7.2. This is the case since the torque (T) is limited by the maximum force on the wheels due to limited grip. Therefore with a limited torque, the moment of inertia defines the angular acceleration (α), which should be as high as possible for an agile sports car.

$$I = \sum_i r_i{}^2 m_i \qquad \text{7.1 [35]}$$

$$T = I * \alpha \qquad \text{7.2 [55]}$$

Using the CG-position along the x-direction in combination with the position of the wheels in x-direction, the mass distribution between the front and rear wheels can be calculated using a moment equilibrium. According to literature less than 60% of the weight should be loaded on the rear wheels. In the case of rear wheel drive (RWD) vehicles the weight distribution should be above 50% on the rear suspension. In rear wheel powered vehicles this value should be around best between 53% and 55% on the driven axle. [8] For the evaluation of the concepts the mean value (54%) will be used as ideal position for rear wheel drive vehicles. This balance between traction and cornering performance and is in line with the experiences at Roding Automobile GmbH. In the ICE (Internal Combustion Engine) Roding Roadster the value is around 55.5/56.5% depending on the engine version. This is experienced as sufficient but would be preferred to travel slightly forward, which is in line with the values found in literature. [8] This means a slightly translating the CG forwards would be beneficial.

For all-wheel-drive (AWD) vehicles the ideal weight would be less depending on traction of the rear wheels. On the other hand there is no reason to prefer a higher load on the front wheels. For this reason the all-wheel drive concepts will be valued with respect to the 54% and 50% target value. This method will be reviewed when from both extremes of this range a different concept comes forward.

Without altering the suspension the CG height will influence the following parameters:

- *„Anti"-features:* The „anti"-features describe the longitudinal to vertical force coupling in the suspension. In a double wishbone suspension this represents the distribution of forces between the wishbones and the shock absorber when accelerating or braking. This results in a change in pitch angle of the vehicle during accelerating and braking. These parameters are defined by the geometry of the wishbones with respect to the CG height. For accelerating this feature is called anti-squat and for braking anti-dive and are described as a percentages. A value of 100% would mean that the entire force is carried by the wishbones, which makes a very shaky ride. A lower value would cause the vehicle to pitch. This has a positive influence on the wheel pressure during braking and acceleration at the cost of energy absorption in the shock breaker.

  In race cars higher wishbone forces are desired to decrease energy loss, but may cause the suspension to lock due to increase in friction. For this reason, anti-dive should be designed below 30% and is typically between 20 and 25% according to Trzesniowski and Smit. [8, 56] This 30% limit only holds for relatively heavy race cars, since this will result in higher suspension forces. In passenger cars brake forces are lower, which means a less strict limit is applied in industry (14 to 48% front and 40 to 120% rear [8]). The ICE Roding Roadster has a value of 31% front and 27% rear anti-dive. Since the weight of the electric vehicle will be higher with respect to the conventional Roding Roadster an increase in anti-dive is undesired.

  Anti-squat should not be higher than 40% and is currently 20%. This value was improved in the last Roding Roadster upgrade (where it had a negative value before) and showed to have a positive effect on the vehicle behaviour. Since anti-squat is evaluated in the driven wheels, the front suspension must also be checked for AWD concepts. The anti-squat in the front is currently 1% (assumed the power distribution front/rear is 50/50). This value is relatively low and might be tweaked when an AWD concept is chosen.
- *Roll resistance:* A change of CG height also influences the roll resistance of the vehicle. This resistance is defined by the moment around an instantaneous centre around which the vehicle rolls. This centre is called the roll centre and is defined by the suspension geometry. Both front and rear suspension have an independent roll centre. For the trade-off, the height of the line between both roll centres (roll axis) at the centre gravity is evaluated. With a constant suspension the CG height and x-position can be used to calculate the change in roll resistance for all concepts. Although this change in moment can be compensated using stiffer or weaker springs, this influences the ride comfort and the cornering capability due to different wheel loads. This means that the change in roll centre should be as small as possible, since the current balance between comfort and roll stiffness is favourable.

From both features it can be seen that a vertical change in CG unbalances the suspension characteristics. By setting the roll resistance in the current vehicle equal to 1, the change will be addressed as a ratio in the trade-off. For anti-dive and anti-squat the values are calculated as well. For the assessment of the concepts, it is assumed the suspension is fixed. This means only the change in CG height influences anti-dive, anti-squat and roll resistance. For that reason the vertical translation should be minimised to keep the parameters balanced for all parameters. [8] For this reason only a single parameter, roll resistance ratio, will be evaluated in the trade-off. How bigger the offset in roll-resistance, the more negative it will be valued to represent all three features.

A second limit for the CG height is the "slip-before-roll" condition. This means that in lateral acceleration the car would reach the maximum grip limit of the tires before it would roll over. With a maximum lateral acceleration of 1.4g, the lateral force would let the car tip over when the CG would lay more than 337mm above the origin. [32, 56] For this value it is assumed that the CG would lay on the xz-plane. When this is not the case the CG height for "slip-before-roll" will not be equal for turning in both direction. In Table 7.2 it can be seen that the current concepts do not come close to this value.

REESS Positioning

The available design envelope for the new drivetrain must be define. At first, the combustion engine and other parts of the powertrain are taken out of the Roding Roadster. When this is done, space for a new drivetrain exists mainly in three different locations:

- Behind the passenger compartment, where the combustion engine is normally placed.
- In the luggage compartment, in the front of the car.
- In the middle tunnel between both passengers. This middle tunnel is highlighted in Figure 7.5. For ergonomic considerations it is expected that this section cannot be designed larger than its current size.

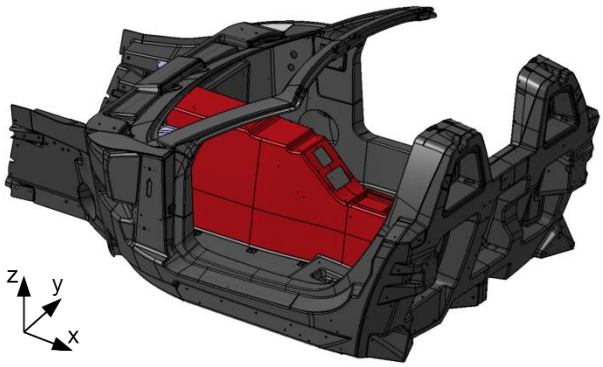

Figure 7.5 Middle tunnel in the Roding Roadster chassis accented in red

Figure 7.6 shows a global overview of the design envelope for the new powertrain in red. This envelope is based on the current suspension and interior. Since the Roding Roadster is a relative small vehicle, it is not possible to create other major design spaces without changing the vehicle layout by changing the entire concept. This is due to the fact that the spaces not included in the design envelope are either occupied by the occupants or the suspensions, or must be kept clear to prevent obstruction of the view of the driver.

Since in the end, this vehicle will be produced in small series, the REESS will probably be approved using component based tests to save costs using small series type approval. For this reason the REESS is limited to a position between 420 mm from the front and 300 mm from the rear of the vehicle. [1] The blue transparent section in the front is located between these limits but lies in the crumple zone of the ICE Roding Roadster. Therefore no REESS components will be placed here for regulatory and safety purposes.

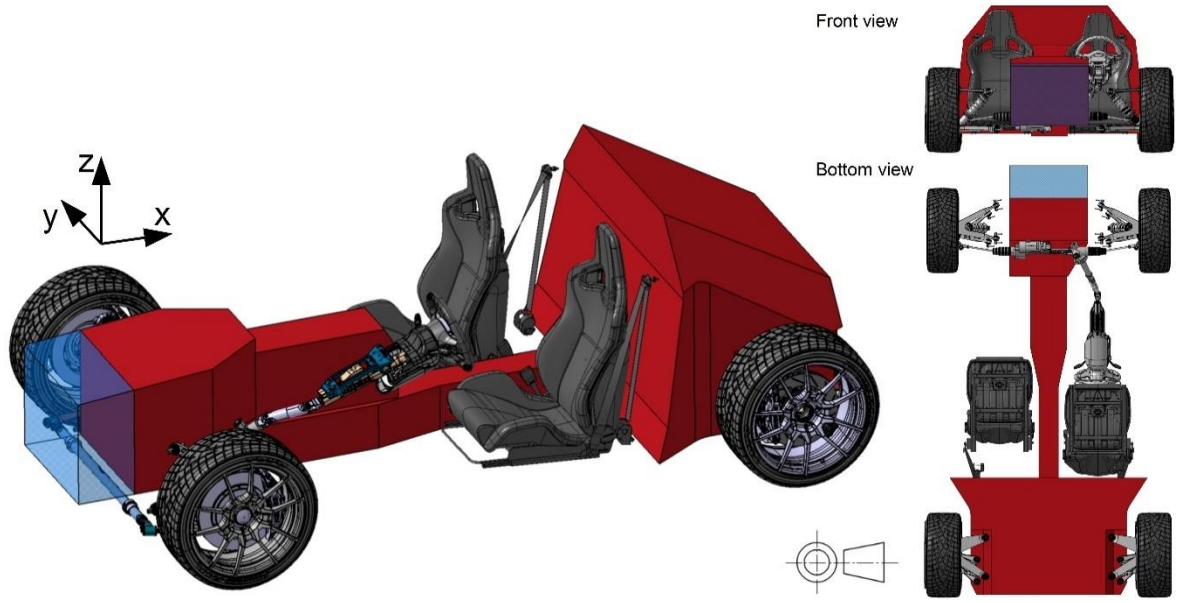

Figure 7.6 Design envelope for electric powertrain in red

To calculate the weight distribution, the motor is located around the driven axle. Since power losses should be as low as possible, the inverters are always positioned relatively close to the motors. This is done since these components use the largest amount of energy. It would make sense to place the REESS in the rear where the engine was placed, since electric motors do not take up all available space. For this set-up the CG was positioned too far aft, which would place between 59 and 62% of the weight on the rear wheels for the different concepts. These values were extracted from the weight distributions spreadsheet. The next section will show an overview of the results. The bottom half of the middle tunnel normally houses the petrol tank. Conservatively measured, this design envelope holds about 75L,

however to create a more ideal weight distribution, the entire middle tunnel is assumed to be filled with REESS cells (approximately 110L). This would result in a maximum of approximately 137kg REESS in the middle tunnel. Since this volume can never be used to the full extent, for this reason the design space in the middle tunnel is assumed to be 130kg. This leaves 370kg to package elsewhere. Where packaging is a term for the process of component placement.

To make the REESS not too complicated, it was chosen not to place REESS cells in the front of the vehicle. This decision was made since the remaining 370kg, when placed in the front, would bring too much load on the front wheels. Splitting the REESS between the middle tunnel, rear and the front part of the vehicle is judged to create a too scattered REESS system. Therefore, this solution is not being considered. Only battery modules in the rear and front, without using the middle tunnel would be possible for the weight distribution. The downside of this layout is that no space is left for an accessible luggage compartment, which should be included. Another downside is that the mass moment of inertia increases with approximately 15% as well, so this option would not be suitable. This value is derived using the method described for the weight distribution spreadsheet using Formula 7.1. The elimination of this option also means that for all concepts the luggage compartment will remain in the front, as seen in Figure 7.7. As stated before is the entire central tunnel filled with battery modules, so this part of the luggage compartment will not be available in the electric version anymore.

Figure 7.7 Luggage compartment in ICE Roding Roadster, courtesy of RA

Loading Diagrams

Figure 7.8 shows the mass distribution for the concepts including luggage and occupants, which can be seen as a single distributed load. In a free-body diagram this would result in Figure 7.9. This example makes use of the distributed load of the ICE Roding Roadster. Repositioning minor carry over parts from the ICE Roding (such as the wiper fluid reservoir) was not shown to present any advantages form one concept with respect to the others. For this reason the basis vehicle weight distribution will be left unchanged when evaluating the concepts. Besides the REESS, the other components were iterated with respect to their position to produce the most beneficial parameters possible. This was done within the boundary values described before to produce the mass distributions. Design space was roughly accounted for using the design envelope in Figure 7.6.

Using these mass distributions in combination with the calculated wheel loads, the internal load diagrams along the length of the vehicle can be plotted (Figure 7.10). This plot shows the total internal loads in the yz-plane at every certain x-coordinate. Since the suspension weight does not influence static internal chassis loads, these weights are not included in the internal force and moment analyses. This weight is called sprung mass and is defined as the mass of the car supported by the suspension only. For the weight distribution percentage, unsprung masses are of influence. For this reason, the unsprung masses are include in calculation this value using a moment equilibrium. These diagrams can be used to compare internal loads along the chassis as if the chassis would be a beam. As a reference the conventional Roding Roadster is plotted along and a reference concept is created. In this reference concept the REESS is positioned below the driver, as is relatively common in BEVs (Battery Electric Vehicles). However as explained before, this is not possible without changing the general concept of the vehicle intensively. For the other components in this concept, the powertrain of Concept 1 is copied.

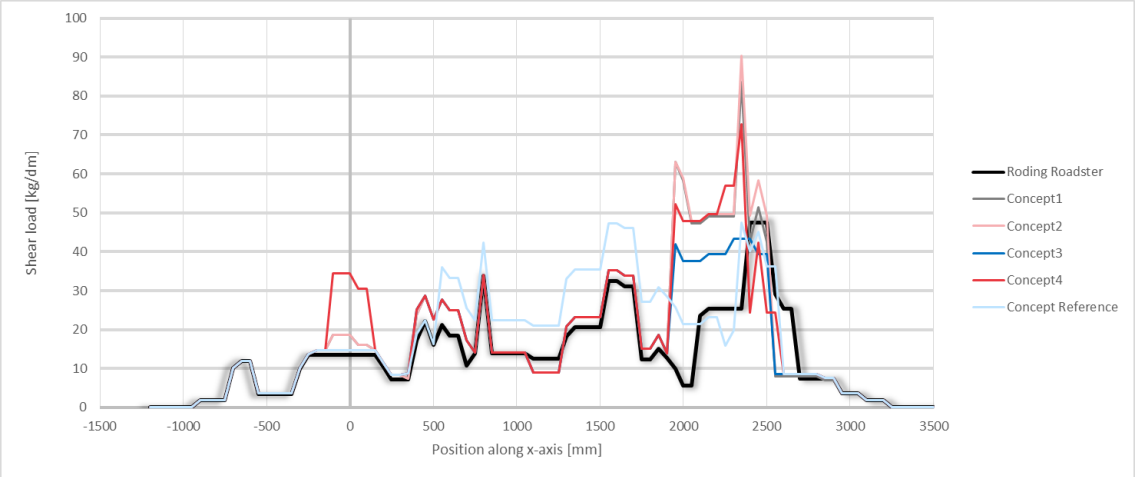

Figure 7.8 Distributed load for all powertrain concepts (sprung weights only)

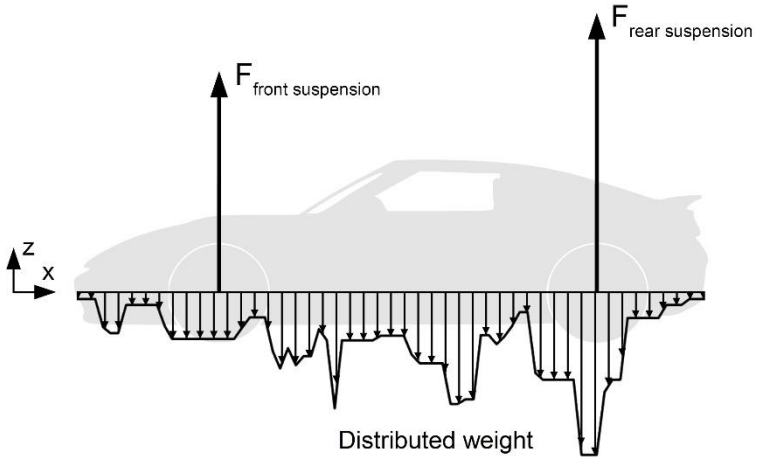

Figure 7.9 Simplified free-body diagram of ICE Roding Roadster

When an internal shear force diagram is integrated, the internal bending moment diagram is shown, as can be seen in Figure 7.11. For example one can see that the hypothetical reference concept is beneficial with respect to the weight distribution, but creates high bending moments in the chassis in between the wheels, as seen in Figure 7.11. Further it can be seen that all concepts have higher internal loads, which seems logical due to higher total weights.

The internal shear force and bending moment model was verified with a similar model in literature and showed less than 1.5% error for the maximum value, when the same input is used. [57] This error occurs since the created model uses a finite number of increments for the calculation. The internal moment diagram is created by integrating the internal shear force diagram. Therefore this error builds up to this 1.5%, which also causes last position to be not exactly zero but the same error of less than 1.5% of the maximum value. Since these graphs are only used to compare concepts qualitatively, this error does not result in any problems for the analysis.

It can be seen that the internal moments for all concepts are higher with respect to the conventional Roding Roadster. This is due to the fact that for the required REESS capacity the vehicle will be significantly heavier. This will result in higher internal loads as in the ICE Roding Roadster which goes along with a heavier chassis (when both are correctly optimised). However with respect to the reference concept, the increase in internal loads is only about half. The largest distinction between the concepts can be seen with respect to concept 3, since in this concept a large part of the powertrain is not mounted to the chassis, decreasing internal loads.

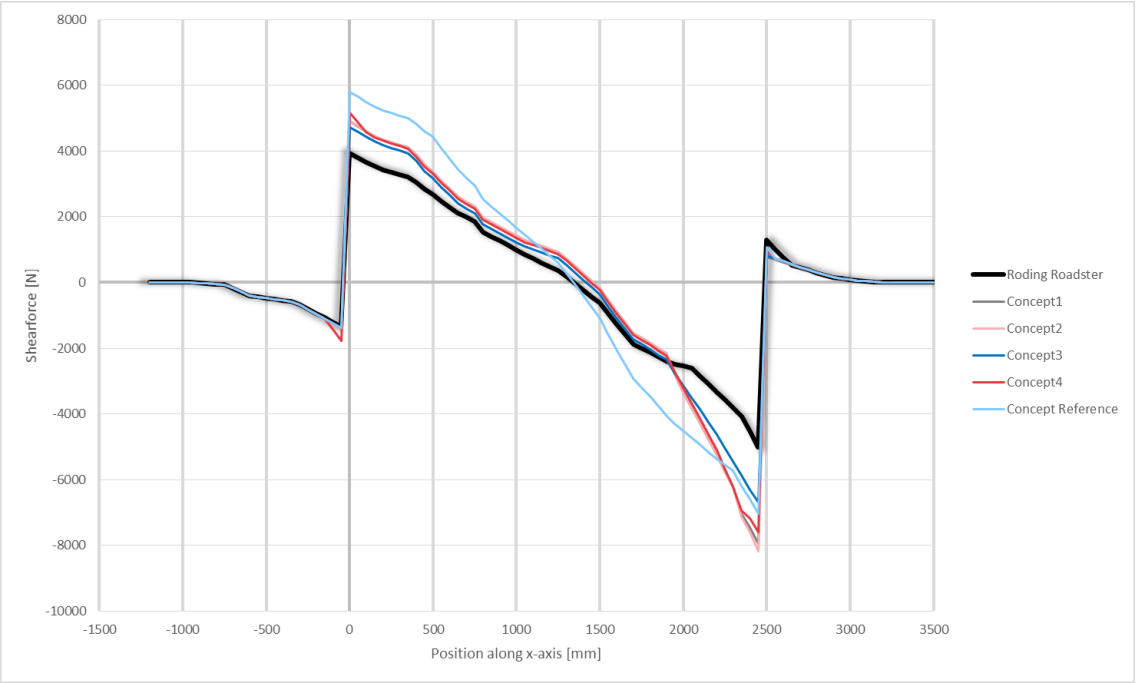

Figure 7.10 Internal shear force diagram powertrain concepts

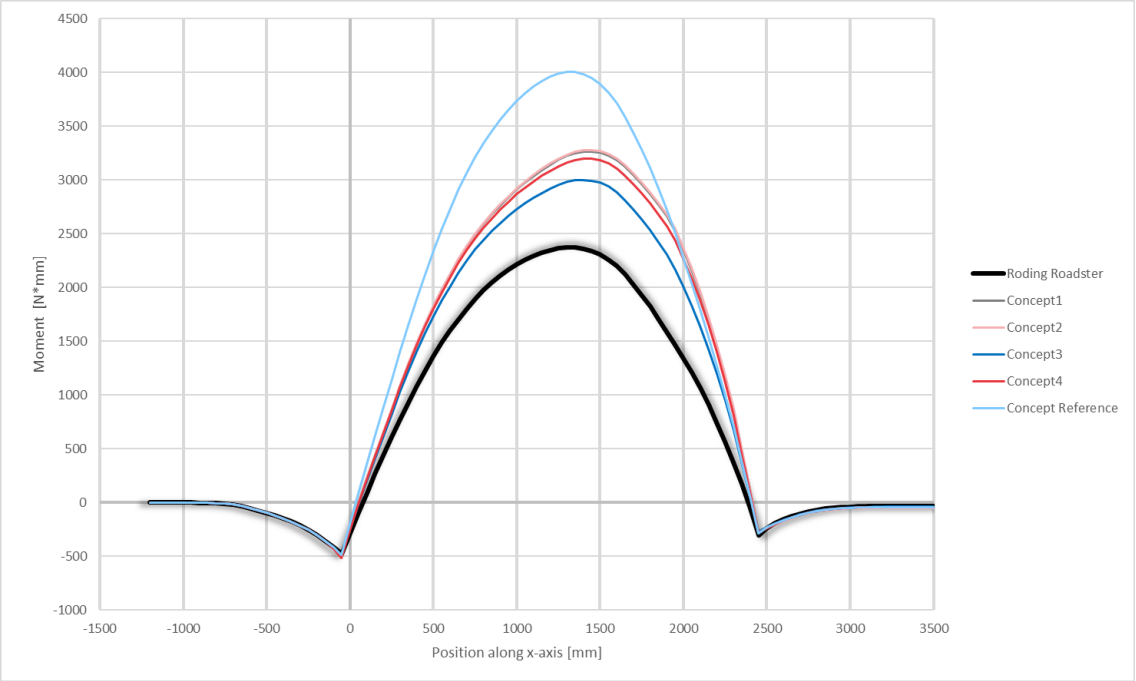

Figure 7.11 Internal bending moment diagram powertrain concepts

7.1.3 Powertrain Concepts Trade-off

Table 7.2 shows the main results of the powertrain concept analysis. This is converted towards a weighted trade-off matrix in Table 7.3 which shows normalised values for the trade-off criteria. In this table values ranging from “-5” to “+5” are awarded for the parameters which are most relevant. Together with Roding Automobile GmbH the weights were awarded to the different parameters, setting mass and cost as major criteria to be in line with the company objective. A reference quantity is used to define the deviation from the target value or average value at which the maximum score is reached (“-5” or “+5”). The reference quantity in Table 7.3 is defined as the value difference between a score of “-5” and “+5”. Earlier in this section, the target values for the mass distribution and roll-resistance were defined. These target values are set equal to the maximum score of “+5” (see Table 7.3). For the total mass, the mass moment of inertia and the costs no target value can be defined. For this reason, the average value is used to set the zero-score value.

It can be seen that with the chosen values, a weight increase of 1kg can be compensated for by cost reduction of €100, and vice versa. This is considered as a fair value for sports cars, based on the average commercial price of €200/kg for optional weight reductions in the Roding Roadster. [58]
It must be noted that for Concept 3, the mass distribution according to the 50% target value shows a value below -5. This is not compensated for by adapting the reference values since this was seen as a worst case target value.

Table 7.2 Main results powertrain concept comparison

	Kerb weight	I_{zz}	Mass dis.	CG_{total} (x,y,z)	Anti-dive		Anti-squat	Roll res.
	[kg]	[m2*kg]	[%rear]	[mm]	[%front]	[%rear]	[%]	[-]
ICE Roding Roadster	1104	1395	55.3	(1381, -3, 102)	31	27	20	1.00
Concept 1	1473	1593	58.0	(1448, -1, 169)	26.8	23.5	17.4	0.85
Concept 2	1483	1602	58.3	(1453, -1, 169)	26.8	23.6	17.4	0.85
Concept 3	1424	1655	55.1	(1375, -1, 111)	30.4	26.7	9.9	0.98
Concept 4	1502	1715	54.5	(1361, 0, 128)	29.2	25.6	9.5	0.93
Concept Ref.	1473	1451	53.6	(1336, -1, 2)	40.5	35.5	26.2	1.38

Further subjective notes with respect to every concept can be made:

Concept 1:

This concept is relatively difficult to package, since the motor, gearbox and REESS are all positioned in the rear part of the vehicle. Since the powertrain based mechanical principles, it does not create major challenges for the control interface. However more mechanical components can be seen as more wear and thus an increase of maintenance costs.

Concept 2:

Besides gear difference, this concept is mostly similar to Concept 1. Control of this concept will require more programming, since the drivetrains are not mechanically connected. This enables active torque vectoring, which might be an added benefit, but also adds complexity.

Concept 3:

In this concept motors or inverters do not take up space within the chassis, since these are positioned within the wheels. This results in a concept which is relatively easy to package. The downside of this concept is that the suspension cannot be taken directly from the current Roding Roadster, since it must be adapted to leave space for the motor. The reason to adapt the original suspension was mainly to have a fixed input. Therefore, to make this concept feasible, redesign of the suspension is not seen as a major drawback.

Another downside of the use of in-wheel motors is the increase of the unsprung mass. There is a lot of discussion on the negative influence of this mass on the vehicle performance. Although there is negative influence, physical tests show that this influence is relatively small. [59, 60] No further analysis of the suspension is planned, since the scope of this research is limited to the vehicle chassis. For this research it will be assumed that this suspension alteration is feasible and development costs are negligible with regard to the estimated production numbers. On the control part the same distinction as in concept 2 can be made.

Concept 4:

The components in this concept are very similar to Concept 1, but the power is divided into two separate drivetrains. The advantage is a better weight distribution, but the overall weight is relatively high. The luggage compartment will be jeopardised in this concept as well. On the control part the same distinction as in concept 2 can be made for the power distribution between the front and the rear.

From Table 7.3 one can see that the best concept would be Concept 3, which makes use of four in-wheel motors. The range shown in the weighted average of Concept 3 and 4 is due to the fact that for the AWD concepts no ideal mass distribution is known. It can be seen that for both extreme values of this range Concept 3 would be the best choice. For this reason the rest of this research will be limited to the development of the BEV Roding Roaster using four in-wheel motors.

Although for this concept the suspension requires alterations, in the rest of the report the original suspension will be used for concept development. This is done since the alterations are only expected to have influence on the wheel side of the suspension. For better perception of the wheel positions, the conventional braking system will also remain in the visualisations throughout the rest of the report, as seen in the CAD master part.

Table 7.3 Normalised Trade-off matrix powertrain concepts

	Mass	I_{zz}	Mass distribution	Roll resistance	Costs	Weighted score
Weight factor	10	2	5	5	20	-
Ref. quantity	200 kg	500 m^2*kg	10%	20%	€40000	-
Target value	-	-	54% (50% for AWD)	100%	-	-
Concept 1	-0.1	0.9	-3.1	-2.7	2.3	0.4
Concept 2	-0.5	0.8	-3.5	-2.7	-2.9	-2.2
Concept 3	**2.5**	**-0.3**	**-5.2 to 2.8**	**3.8**	**0.9**	**0.8 to 1.8**
Concept 4	-1.4	-1.4	-4.1 to 3.9	1.6	-0.3	-0.9 to 0.1
Concept Ref.	0.1	3.8	4.1	-14.0	2.3	0.1

As stated before, the sensitivity of the trade-off should be evaluated to know the influence of changes to the basis vehicle. These changes can later in the process be inflicted for example higher or lower loads. Based on Figure 7.10 and Figure 7.11 the conclusion can be drawn that internal loads will not differ massively. For this reason, change in weight of the rear substructure of 25% with respect to the other concepts would be immense. However such change in weight would only change a weighted average in Table 7.3 with 0.2. This change would not influence the concept choice. For this reason it is concluded to be valid, to assume the basis vehicle is similar for all concepts in this powertrain trade-off. Based on the preformed trade-off, a powertrain based on four in-wheel motors (Concept 3) will be used throughout the rest of this research.

7.2 Structural Analysis Incorporating the Electric Powertrain

To get initial insight in the performance of the chassis using the BEV configuration, the BEV weight distribution is analysed in combination with the original chassis. The determination of this distribution was addressed in Section 7.1. The chosen powertrain will replace the point masses for the original powertrain within the verified model. The results are shown in Figure 7.12, Figure 7.13 and Figure 7.14 for the frontal collision.

7.2.1 Frontal Collision Analysis

In comparison to the results for the ICE vehicle, it can be seen that loads for the BEV are significantly higher. A major point of failure became the connection point of the crash attenuator. It is however assumed that this section is stiffened by the crash attenuator itself. Since in both the model and the actual vehicle the overlap of the crash attenuator surpasses the failing section this assumption is valid.

It can be seen that the diagonal beam, supporting the frontal substructure, became critical on the inner facing. The same holds for the sheet metal part supporting this profile on the inner side of this profile (not visible in these figures). It is expected that this failure might be solved with an increase of material thickness, which is a relatively simple solution. Further it can be seen that stresses in the monocoque section of the chassis become higher, but at most positions are still not critical. Another critical position is the connection to the rear-substructure, which should be addressed accordingly in the redesign.

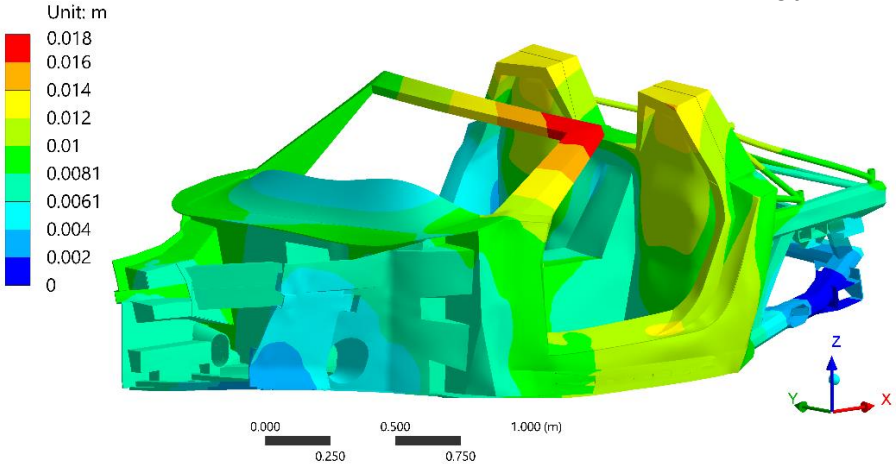

Figure 7.12 Total deformation for ECE R94 frontal collision of the BEV Roding Roadster (amplified visualisation)

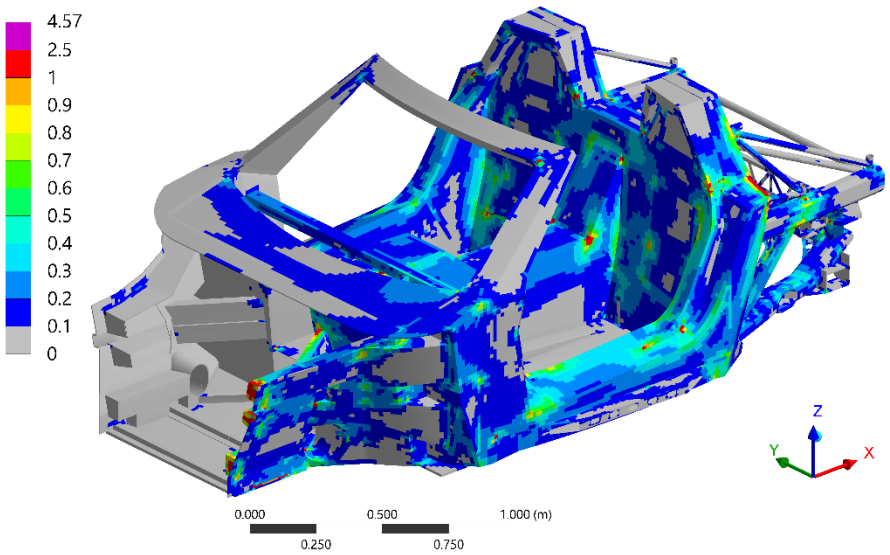

Figure 7.13 Inverse reserve factor for ECE R94 frontal collision of the BEV Roding Roadster weight distribution on the ICE Roding Roadster chassis, view 1

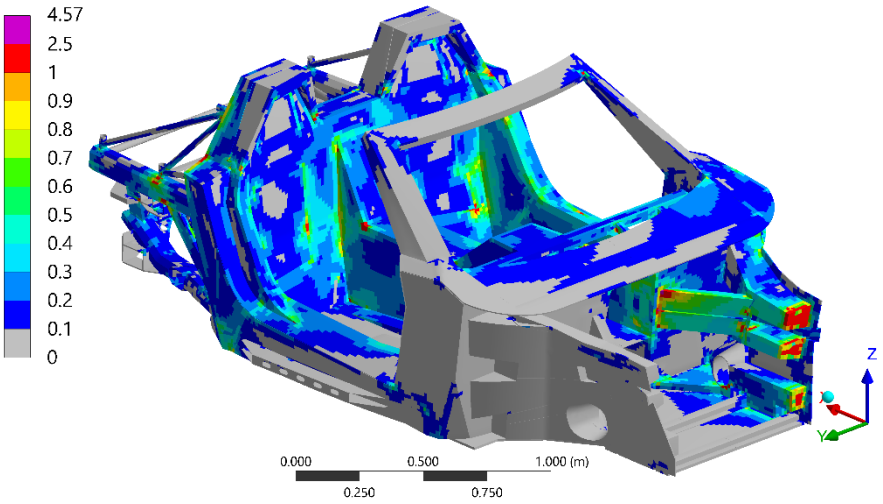

Figure 7.14 Inverse reserve factor for ECE R94 frontal collision of the BEV Roding Roadster weight distribution on the ICE Roding Roadster chassis, view 2

7.2.2 Lateral Collision Analysis

The lateral collision is not shown for the BEV weight distribution since no significant differences can be seen here, with respect to the original weight distribution. This is as expected since the load for the lateral collision is not depending on the weight of the vehicle. Besides that, it was tried to keep the CG as close to its original position as possible, which results in a similar load distribution. The only difference might be in the supports of the large masses of the vehicle. In this case the REESS was virtually connected to the bottom plate and the rear substructure. Since this is comparable to the replaced combustion engine and fuel tank, this creates no significant changes. When the BEV chassis is analysed, differences at the mass supports might occur since then the correct connection points are available and the structure can be adapted accordingly. It must be noted that the accelerations in the original vehicle were too high for the defined HIC (Head Injury Criterion). However stresses are comparable for this weight distribution, because the total weight of the BEV is higher, which results in a lower and acceptable vehicle accelerations. For this reason it is possible to have similar structural performance while resulting in different injury criteria.

As seen in Section 6.2 the lateral collision mainly shows severe failure in the “B” pillar. Since in the current design no measures were taken to comply with ECE R95, this failure should be addressed accordingly in the redesign. Another high load occurs at the front of the sill, as seen in Figure 6.24. The severity of this position should be analysed later since it will be influenced by the structural performance of the door and more accurate curvature of this section.

To comply with the regulations on ECE R94 and ECE R95, minor changes on the chassis are mandatory. However for redesigning the chassis, to accommodate the selected powertrain, mainly the redesign of the rear substructure is required. When the changes to comply with regulations can be solved locally, the frontal substructure and driver compartment might be adopted from the ICE chassis.

To be able to do this, the failure in the frontal substructure support is expected to be solved by an increase of material thickness. The failure in the rear substructure interface is neglected, since this can be redesigned accordingly in combination with the new rear substructure. For the lateral crash, steps must be taken to establish a better load introduction. For this reason the “B” pillar should be reinforced. This high load introduction is however independent of the chassis concept and does therefore not contradict the use of the current passenger compartment. It is expected that using additional inner strengthening panels and/or changing lay-ups locally might solve this critical problem. Other minor critical positions should readdressed when the chassis is adapted for the electric powertrain.

By adopting the frontal substructure and driver compartment, the knowledge on the current chassis can be used to its full extent for the development of the BEV. When the passenger compartment of the original vehicle is adopted, it is not required analyse the ergonomics. As explained in Section 5.1, the absence of hazardous obstacles for the occupants must be checked. This is confirmed using the head freedom envelope and the SAE mannequins and will therefore not be analysed further. Another advantage might be that a prototype could be produced at low costs. This would save a lot in development costs. Therefore, the focus during the development of the BEV chassis will be on the rear substructure and REESS housing in combination with the existing passenger compartment and frontal substructure. When this research is followed by a detailed design, it is up to Roding Automobile GmbH to decide if it is justified to redesign the monocoque and frontal substructure or that a change of material usage will suffice.

7.3 Concept Development of Chassis Structure

In Section 7.17.2 the best powertrain concept was chosen to use four in-wheel motors in combination with a REESS in the middle tunnel and rear section of the vehicle. From Section 7.2 it was concluded that there are no crucial reasons to adjust the frontal substructure and driver compartment of the current chassis. By combining the knowledge of the current chassis, the chosen powertrain, design envelopes and load cases, different concepts will be developed in this section. The rear substructure in the ICE Roding Roadster, as seen in Figure 4.4 (page 19), is mainly constructed around the combustion engine. For the incorporation of the electric powertrain, this section will mainly house the REESS. Therefore this vehicle section is influenced most by the transition towards an electric vehicle and will therefore be the focal point in the concepts. In this section three different concepts are explained. This is used to pick the chassis concept, using a trade-off, which can be found in Section 7.4.

7.3.1 Concept Determination

One of the selling points of the Roding Roadster is the low weight. To keep this weight as low as possible it is tried to create concepts in which as less weight as possible is required to create a stiff and strong chassis. In this rear section three main components can be used to do this, being the REESS itself, the REESS housing and the chassis. Developing these components separately would result in a heavy combination since these components might be able to support each other and create a stiff and strong structure when they are assembled cleverly.

Using this philosophy, a first concept (Concept A) will directly combine these functions as much as possible. This means that the chassis structure can directly be used as housing for the REESS compartment. A sealed REESS compartment will be achieved by closing all access points with lids. This seal is required to keep water out of the REESS, since this can create large problems. Closing all openings is difficult to achieve using an aluminium frame. For this reason this chassis will consist of a composite rear substructure. The disadvantage of this concept is that the REESS cannot be removed as one single component. Therefore it must be possible to exchange modules via the openings in the chassis during maintenance.

A second concept (Concept B) would use a similar composite rear substructure. A removable closed REESS will be mounted to the chassis, to decrease problems with sealing multiple points within the chassis.

When the REESS in Concept B is a separate housing, there is no need to create it out of fibre reinforced materials from geometry perspective. A third concept would therefore use a similar removable REESS

which is mounted in a metal rear substructure (Concept C). This concept would be closest to the configuration as it is for the combustion engine. Figure 7.15 gives a quick impression of all three concepts. The REESS is drawn in red. Sections 7.3.3 to 7.3.5 explain these three concepts in more detail. In the design of the chassis concepts, the two characteristic arches at the rear were not taken into consideration (which can be seen in Figure 4.2). This was done to leave more space for a change in the exterior design. Before elaborating on the chassis concepts, first a structural concept for the REESS will be discussed in Section 7.3.2.

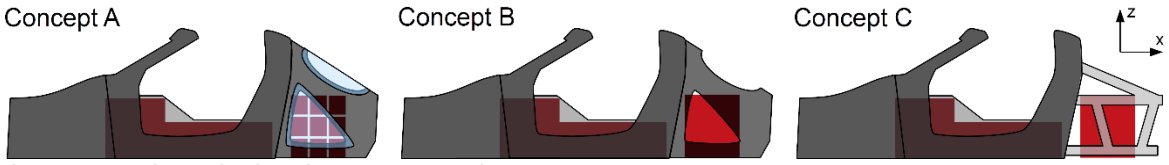

Figure 7.15 Schematic chassis concept overview

7.3.2 REESS Concept

As stated before, the structure of the concepts would be used more efficiently when the internal structure of the REESS will directly add strength and stiffness to the chassis. Since this influences the chassis design significantly, this is researched first.

The main functions of the REESS housing are fixing the battery modules and protecting the modules from the elements. Figure 7.16 shows the difference between a triple structure and an integral version of the chassis, REESS structure and REESS housing. In electric vehicles developed by Roding Automobile GmbH up to now, the REESS had relatively small height. Therefore these vehicles mainly consisted out of a single height modules mounted onto only a structural bottom plate. This decreased the possible advantages of an integral REESS structure. Since for the required REESS capacity, a higher REESS must be constructed the weight disadvantage of decoupled structure would increase significantly. For this research a versatile, simple, cheap and sizable REESS system was developed using the structural efficiency as focal point. The first impression of this concept can be seen in Figure 7.17.

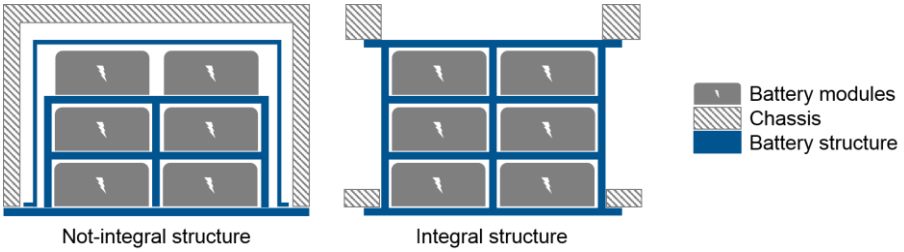

Figure 7.16 Difference between an individual and an integral REESS structure

This concept makes use of plates to which the modules and subsystems can be pre-assembled. These modules can than easily be stacked into a box using parallel profiles. Inbetween stacking of the layers it would only be required to connect cables and optional coolant hoses connecting the subsequent layers, to finish the electrical system. In this research the parallel profiles will be assumed to be vertical for simplicity. Placing these profiles parallel but at an angle, in combination with horizontal layers, is possible but takes up more space and increases complexity. In practice this might make the system feasible for difficult geometries.

For vertical support I-profiles are used. These profiles will be mounted onto the plates before installation. These profiles will also be used to mount connections to the parallel profiles. These connectors also have a constant cross-section and can therefore be produced as low cost extruded aluminium profiles. For the I-profiles this can either be done by aluminium extrusion or carbon fibre, to possibly save weight. Aluminium extrusion is assumed for its simplicity. In Figure 7.17 the connection is visualised in more detail on the right. Not all side panels are shown for better visualisation. One advantage of this concept is that this system would be very adaptable. This means it can be either worked out for Concept A, where the mounting profiles are chassis mounted, as for Concept B and Concept C to create a separate REESS. In Concept B and C the connection between the box and chassis is very important to have a chassis benefitting of the stiff and strong REESS design. Besides the application for this researched vehicle, this adaptable modular concept might also be applicable for other BEV's developed by Roding.

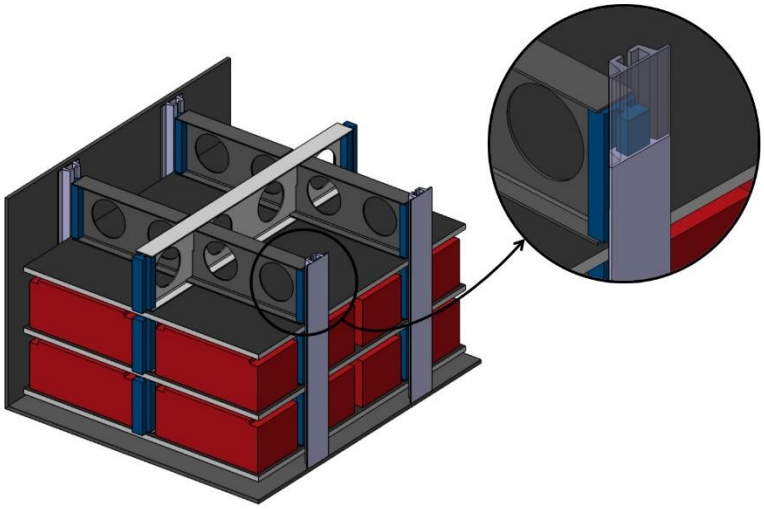

Figure 7.17 REESS housing concept

Creating a separate REESS can be done relatively cheap, since it can be made out of simple stiff panels, which are assumed to be CFRP (Carbon Fibre Reinforced Plastic) sandwich panels. The advantage of this system is that it can be redesigned for different vehicles or other battery modules at low costs. Cables and optional cooling circuits can be mounted to the I-profile its web plates. A cut-out in the layers might be required to enable the cables going from one to the other layer.

Production of the panels is cheap since flat panels are relatively labour efficient. The sandwich panels can be either produced using vacuum infusion, which limits the core material to foam. Another production method is hand-lay-up. This can either be cured in a vacuum bag in the autoclave or heated in a press as a possibly cheap solution. In this case the material is not placed in the autoclave but cured under a distributed pressure from a hydraulic press, with heating elements embedded. This can be best seen as combination of hand lay-up and compression moulding. The advantage is that this process excludes the costs of vacuum materials and labour costs involved with applying them. Roding Automobile GmbH is already familiar with this process, which decreases development costs. In Section 8.2.2 the manufacturing of this concept will be worked out in more detail.

In this concept a method should be found to fix the blue connections in Figure 7.17 to the parallel profile, since otherwise al vertical loads would all be carried by the bottom plate. Bolts from the outside would create a lot of additional points of failure for the sealing. However on the inner side it is difficult to create a connection, since the space between the modules and the side walls is preferably as small as possible. A solution might be to split the connecter into two separate parts which can be tightened within a small space using an open-ended spanner. This is visualised in Figure 7.18, where only a parallel profile section, the I-profiles and connector are shown. The advantage in this concept is that the required bolts and nuts will already be installed when stacking a layer. After placing the plate into the REESS compartment the nuts need to be tightened only.

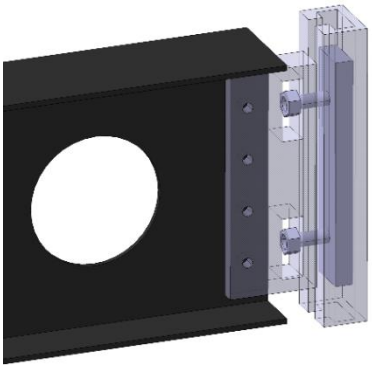

Figure 7.18 Vertical mounting concept detail

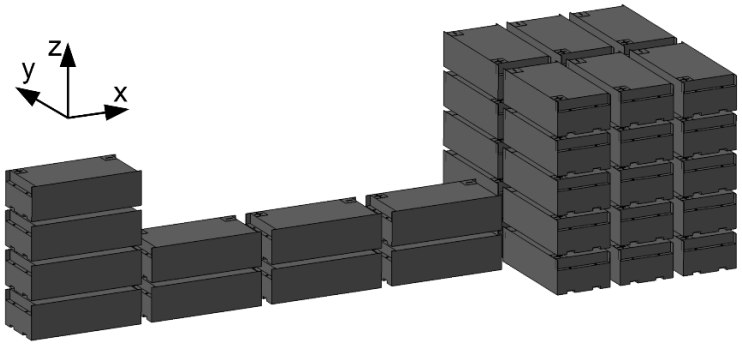

Figure 7.19 Assumed battery module layout

Up to now no specific module was chosen. For consistency throughout this report modules will be assumed to be equal to be battery modules used earlier by Roding Automobile GmbH. [32] The layout of the modules can be seen in Figure 7.19.

7.3.3 Concept A

The advantage of the first concept is that there is no double structure. When designed optimal this can save weight. This however comes at the cost of a more difficult installation of the battery modules.

Concept A1

This chassis concept in combination with the REESS concept from Section 7.3.2 is named Concept A1. For Concept A1 to work, a hatch larger than the REESS horizontal cross-section should be available. This hatch should form a durable sealed closure, which is more reliable at the top of the substructure since this avoids problems with impact and dirt from the road. This REESS concept cannot easily be applied to the REESS in the middle tunnel, since it is would be difficult to mount the REESS layers here. For this section a separate box can be created using the same modular system. This box can be mounted to the passenger compartment from below. A schematic overview of the assembly sequence can be seen in Figure 7.20. It can be seen that the rear substructure will be produced separately to maintain the modular chassis which can be used for other Roding Automobile GmbH projects.

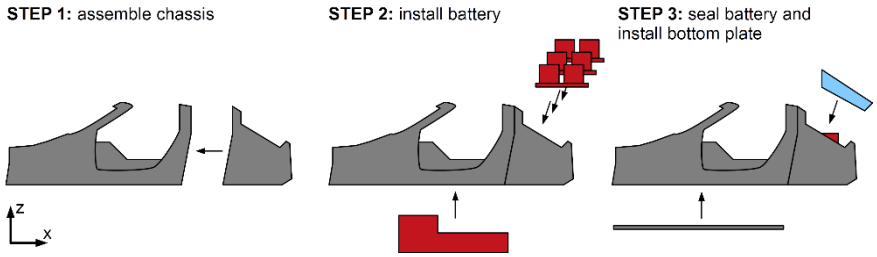

Figure 7.20 Assembly sequence Concept A1

The downside of this concept is that it is difficult to mount the REESS guiding/mounting profiles vertically to the chassis. This is a major limitation in this concept. In Figure 7.21 and Figure 7.22 the concept is roughly visualised. It must be noted that the assumed module layout from Figure 7.19 is not yet applied in these impressions. The passenger compartment in Figure 7.21 was not changed with respect to the current Roding Roadster chassis. However, the rear cover (seen in red in Figure 4.5 on page 19) is omitted in this design. Depending on the geometry of the passenger compartment, the rear surface can be used to mount the guiding profiles. This defines the surface to be flat and vertical and eliminates the possibility of a structural flange on the top of this section, since this would interfere with the stacking system. This blocks the possibility to construct an integrated structural member here. Since currently the rear of the passenger compartment is nor vertical and flat, a connecting structure is required, which results in additional parts. The resulting space in between the REESS can however be used for other high voltage components. In detailed design the accurate positioning of these components should be verified with to have negative influence on the centre of gravity position.

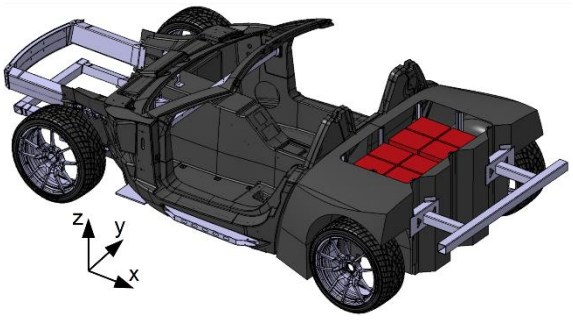

Figure 7.21 Concept A1 with ICE Roding Roadster passenger compartment and frontal substructure

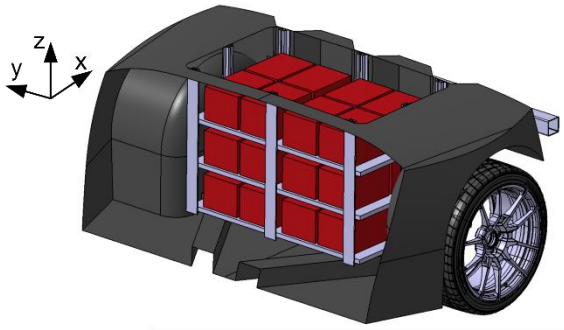

Figure 7.22 Concept A1 rear substructure

The surface to which the suspension is mounted can also be design such that it has a vertical section which can be used as a mounting surface for the guiding profiles at the sides of the REESS. To create a proper construction an additional plate can be used to mount a profile to which supports the rear of the REESS. Another solution is to design the chassis up to this point and construct the rear part of the vehicle from non-load bearing body parts. This would make it possible to design a geometrically stiff geometry for the rear and leave room for the energy absorbing structure (Figure 7.21). The crash attenuator is this figure is roughly sized around an aluminium rear crash structure developed by Roding Automobile GmbH for a different vehicle. [32] After a small impact from the rear, this gives the opportunity of repairing the vehicle by replacing a simple component. The mounting bracket is this first

design is prone to puncture by the crash attenuator. For this reason this structure concept will be altered in the detailed design, but is visualised here to give a global perception of the concept.

Concept A2

A second option (Concept A2) is to install “shelves” into the rear substructure before mounting it to the passenger compartment. This can be seen in Figure 7.23. This decreases the required hatch size, since only battery modules have to go through, instead of entire REESS layers. The disadvantage of this concept is that modules need to be mounted to the structure and connected with a limited space.
In Figure 7.24 the installation of an arbitrary sized battery module was visualised. It must be noted that this substructure is attached to the passenger compartment at the moment of installation. This is assumed since it is unfeasible that for REESS maintenance the chassis including all other systems must be disconnected at this connection interface.

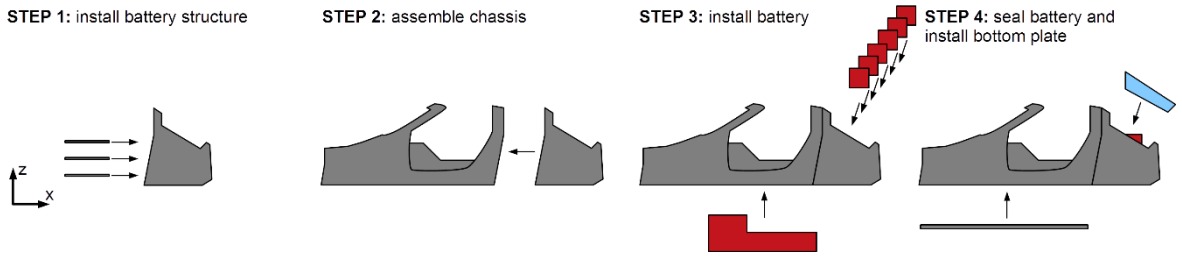

Figure 7.23 Assembly sequence Concept A2

The method in Figure 7.24 makes use of horizontal panels with cut-outs for accessibility. When the modules are lowered into the correct location they can be rotated so that the modules are mounted across these cut-outs. Figure 7.24 shows that this makes installation very difficult when space is limited. Besides mounting, another downside is that all modules must still be connected within this small space. In addition to the use of more access points, partially building up the shelving structure along with the REESS might be a solution for more accessibility. In practice this will still be very time consuming and impractical. For this reason Concept A2 is eliminated since it is seen as an unfeasible concept for series production. For this reason Concept A1 is referred to as Concept A in the rest of this document.

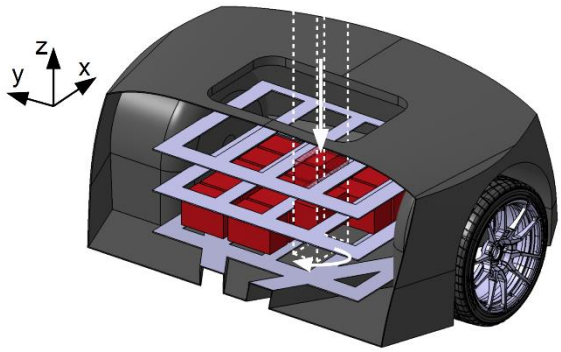

Figure 7.24 Rear substructure Concept A2, visualisation of battery module installation

Figure 7.25 Carbon fibre preform for RTM production [61]

Producibility of the Rear Substructure

The design of the rear substructure is constructed from relatively large sections. These sections of the rear substructure are relatively flat and can therefore be deformed at relatively low loads. A solution for this is to create the rear substructure from thick sandwich material, to stiffen the structure. When this is done using aluminium honeycomb, this can directly be used for grounding the housing as explained in Section 5.3.

Since the rear substructure is a complex part with negative draft sections, this part should either be produced in multiple sections, or a multiple section mould must be used. For production processes with single sided moulds, the mould face of the outer shell can best be on the outside of the product to create a neat product. On the inside high accuracy is only required locally where critical parts are attached, this can for example be done using extra removable pressure plates.

Low pressure RTM is a production process which can be very beneficial for small series production. An advantage is that material costs are lower, since dry fibres and resin can be 40% cheaper than prepreg. [32] However, depending on the product, initial costs can be very high. For simple products plies can be

cut and placed into the mould relatively easily. The resin flow in the mould can for simple products be controlled without major problems as well. This however means the rear substructure must be divided into multiple, relatively simple geometries.

At production rates of 500-1000 vehicles a year, this means each part must be produced 2-3 times a day. Since low pressure RTM typically has cycle times in the range of a several hours, this production process will require double mould sets and a large number of hydraulic presses. These moulds are relatively expensive, since expensive metal moulds must be milled for both sides of the product. To cure the mould, heated liquid is pumped through cavities milled into the mould, increasing mould costs even more. Another downside is that the hydraulic presses for two sets of moulds and the multiple parts would cost approximately €2mln (assumed at least 10 presses of €200k each). [62] This assumption only includes the hydraulic presses required for the resin infusion process. When preforms are required to create these components, this might double these initial investment costs, only covering the hydraulic presses. Preforming is a process in which a different set of moulds is used to form dry lay-ups in the required shape. The use of accurate preforms will result in a smaller deviation of production quality and therefore lower the amount of rejects with respect to manual lay-ups used in RTM. An example of what such a preform looks like can be seen in Figure 7.25. A binder is used to hold the lay-ups together, which is most often a powder which can be part of the bulk carbon material. In simple geometries, lay-ups do not have a complex shape, excluding the need for preforms. The downside of preform production is the need for additional moulds and presses which are either filled manually or robotically.

After manufacturing, the components need to be assembled. This can already be classified as a labour intensive process without reviewing the arising sealing issues. Another downside of this method is that manual lay-up of dry fibres cannot be done as accurate as with prepreg material. This will therefore result in more rejects.

It is also possible to create the substructure constructed out of less parts using RTM, which increases component complexity. Care must be taken with dry fibres lay-ups, since these cannot be placed in complex moulds directly. In large series, preforms must be used to make more difficult geometries feasible for RTM. As explained before, this increases initial investment costs massively. More complex shapes also result in higher development costs, since besides preforms, the resin flow during infusion of the fibres must be controlled.

For this reason it will be unfavourable to produce the rear substructure of the chassis as a single part using RTM. For relatively simple parts RTM will be a suitable solution. However, at production rates of 500-1000 vehicles a year, it is not expected to break even to invest in expensive machinery and long development time to save on material costs. Another downside of the RTM process is that it will also cancel out the possibility of grounding via the aluminium honeycomb. However it is theoretically possible to produce sandwich materials using a foam core in the RTM process, this will involve high development costs. Another important note is that additional costs are involved for appropriate grounding.

For vacuum infusion and hand-lay-up, a positive mould can be milled from which multiple composite, single sided moulds can be drawn at relatively low costs. For hand lay-up this can best be made out of carbon fibre, to prevent problems with different coefficients of expansion during autoclave curing of the prepreg. Autoclaves are relatively expensive, but are more flexible in use, since they are not set up for a specific mould. For the daily production of 2-3 rear substructures, a single autoclave can be sized to suit the requirements. This can best be streamlined with the production of the entire chassis. Autoclaves are assumed to range in the same price range as a single hydraulic press.

Although the external structure is relatively complex, it is possible to produce the outer shell of the structure as a single part. Dividing the structure into multiple parts might decrease production costs of the separate parts, but results in higher costs for assembly and in decrease of accuracy. For this phase it is assumed that the outer shell of the rear substructure will be produced as a single part. Production of such complex parts means it will probably be produced in two laminating steps to ensure quality. This means that the outer skin will be cured before laminating the entire sandwich. This doubles the autoclave costs and consumable costs. Autoclaves are also seen as a large initial investment. However, as explained before, large autoclaves can be used very versatile. This means that during lay-up of the mould, the autoclave can be used for other parts, in contrast to the hydraulic presses required for the RTM process. This will decrease the initial investment on machinery severely with respect to the RTM process.

For easier production and more parallel manufacturing, the different sections of the mould can be laminated separately in a hand lay-up process, as seen with the Porsche 918 Spyder rear substructure in Figure 7.27 (complete chassis in Figure 7.26). For this vehicle the two halves are combined before curing, to create a single product, as seen in Figure 7.28.

Figure 7.26 Porsche Spyder 918 Chassis [63]

Figure 7.27 Lamination of mould segment of the Porsche 918 Spyder CFRP rear substructure [64]

Figure 7.28 Combining the different mould segments and application of vacuum materials for the Porsche 918 Spyder rear substructure [64]

For vacuum infusion, the mould material depends on the used resin and therefore the curing temperature. Creating the lay-up for vacuum infusion, the same problem arises as with RTM. For simple products this can be done at low cost with a high scatter, where for more complex parts one needs to create preforms as well, which involve high initial costs. An additional problem with vacuum infusion is that it is difficult to create an accurate lay-up of auxiliary materials, which results in a resin flow which is more difficult to control. This creates a risk for dry spots and increases the number of rejects. This risk can be minimised for thick laminates in simple geometries. For this reason this method is often used in ship building. Building neat complex sandwich structures using this method is however not justifiable. It must be noted that for vacuum infusion, similarly to RTM, honeycomb is not suited as a core material. This implies that additional costs would be involved for grounding the chassis using vacuum infusion as well.

It is not expected that a product as complex as the rear substructure can be divided into parts which can be produced without preforms using an RTM process. This means that besides high development costs on the production process of RTM, high development costs for the production of preforms must be accounted for. In combination with the additional assembly costs, these initial development costs and large number of required presses are not expected to be compensated for by the lower costs of materials. For this reason it is decided that the external shell of the concept will be produced using hand lay-up. Alternative production processes for other parts will be investigated later, after the concept trade-off.

For simplicity, the closures in this concept can best be designed as not load-bearing. To eliminate grounding problems in these panels, the panels will be made out of glass fibre reinforced materials to be non-conductive, stiff and light. Since these panels have no difficult geometries, a suitable production method for these panels would be thermoplastic forming. This uses reinforced thermoplastic sheets, which are heated and subsequently pressed between two moulds to consolidate. [65] After pressing, these parts only need to be trimmed by milling or water jet cutting. It is also possible to produce these panels using a process for thermoset resins, however this will probably result in higher labour costs due to a more complicated process. Sealing can be guaranteed using an O-ring placed in a groove, which can be milled in either the lid or chassis side.

Besides the closures, through which the REESS can be installed and maintenance is performed, other mounting points in this concept will create critical sealing points as well. To seal the interface of the passenger compartment and the REESS compartment, the interface can be bonded. With a closed

middle tunnel, this will create a sealed compartment. However mounting points such as suspension points must sealed as well. In the current vehicle, highly loaded point are jointed to the composite chassis using metal plates with locknuts welded to them, for a proper load transfer and tightening with single side access (as seen in Figure 7.29). Around this point a bonded cover or another solution is required to sustain a sealed box. This can for example be done by bonding a cup over this mounting point. Although for all these points a solution can be found, it creates a lot of critical points, where a seal must be guaranteed.

When this concept is chosen and structural analyses show the REESS hatch weakens the chassis a lot, a loadbearing hatch can be constructed. Another method to stiffen this section is to make use of an additional bracing which is more often used in the engine bay of sports cars, as seen in Figure 7.30.

Figure 7.29 Nut plates as used in Roding Roadster

Figure 7.30 Stiffening brace in Dodge Viper -edited- [66]

7.3.4 Concept B

In concept B the REESS is completely assembled before installation into the vehicle. This improves accessibility and shortens lead times, since the REESS assembly can be done concurrently. In this concept there are less critical problems with sealing the REESS housing since it has less additional function, which is another advantage. It is also simpler to create positions to attach the guiding profiles for the REESS layers parallel.

To combine the middle tunnel REESS and the REESS in the rear structure, this REESS can best be installed into the chassis from below. Since the opening can still be designed on the upper side of the REESS this is reliable in this concept. Another advantage is that installation from the bottom is easier done using a standard car lift, available in service stations during maintenance. The assembly sequence for this concept is schematically shown in Figure 7.31. This sequence is similar for Concept C, so no separate figure is inserted for this concept. In this sequence the REESS bottom plates are visualised separately. In practice it would make sense to integrate the REESS housing and bottom plate, to create a stiff but light combination. For this reason, the bottom plate material will be replaced by a CFRP sandwich panel which can be combined with the sandwich REESS housing.

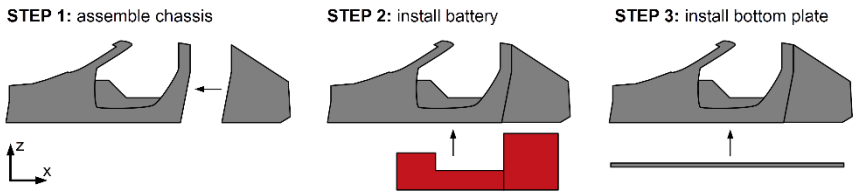

Figure 7.31 Assembly sequence Concept B and C

When reviewing the current chassis, this concept would make it impossible to include the two diagonal braces highlighted in red in Figure 7.32. The main function of these braces is to create a stiff structure under lateral loads. This function can be replaced by the REESS and bottom plate, which can act as shear plate. This should be reviewed when the extreme driving load case is analysed. This also holds for Concept C, where the diagonal braces will be replaced to be able to install a single REESS. In this design the rear cover (seen in red in Figure 4.5 on page 19) is omitted as well. Its structural function will be replaced by the REESS and new rear substructure.

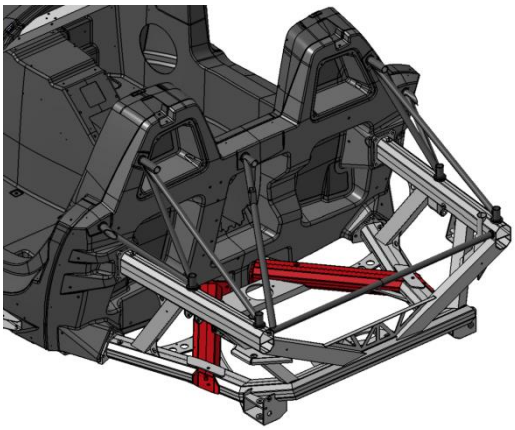

Figure 7.32 Y-brace in Roding Roadster chassis

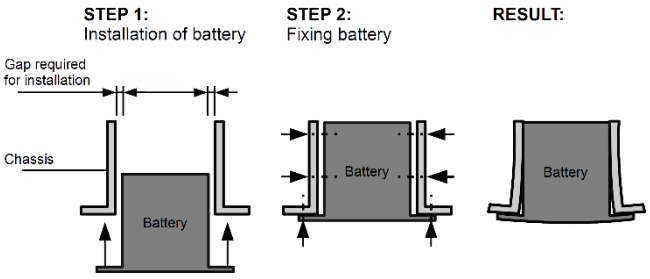

Figure 7.33 Deformation problem with REESS fixation

To create a stiff loadbearing REESS compartment which is installed from below, the mounting points must be laid out strategically in the design. When a REESS is only mounted by fixing the bottom plate, an extremely stiff bottom would be required to keep the REESS from deforming under horizontal accelerations. For this reason additional mounting points are required. On the other hand, installation room and tolerances should be taken into account. For example, to install the REESS, it cannot be designed based on a tight fit between two parallel mounts. When a tight fit is required for a good connection this can cause problems since it forces the geometries to deform, as seen in Figure 7.33. This can be solved by designing the system with members that can deform without problems in the desired direction. This however often decreases the structural performance. Another option is to mount distinct positions in different planes. This transforms out-of-plane offset into in-plane translations, which makes sure the required tolerances fall within tolerances for a borehole, instead of forcing an offset to close. Larger offsets can be accounted for by using slotted holes. Using this philosophy the REESS housing and bottom plate are designed as seen in Figure 7.34. It must be noted that this philosophy is mainly important when mounting two large parts together, such as the REESS housing and the rest of the chassis.

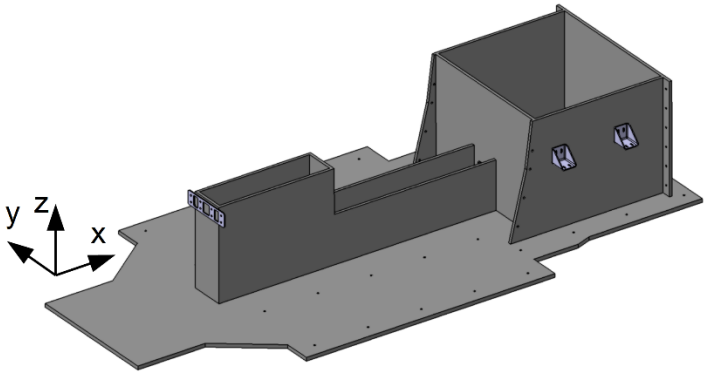

Figure 7.34 Bottom plate and REESS housing Concept B

This REESS housing is installed when all systems are fully assembled. This means that the REESS production can be done independent from the rest of the vehicle, to shorten the production process. The main advantage of this concept is that this construction can be built out of plates. These can be made out of carbon fibre reinforced facing with an aluminium honeycomb core. This core can directly be used to ground the REESS according to ECE R100, as discussed in Section 5.3. Since it cannot be guaranteed that the connections between the plates will have a low resistance, it is best to connect all panels with a separate grounding point. This can be done from the inside of the REESS to have the rivnut in a dry environment to decrease the risk for galvanic corrosion. When reviewing the panel dimensions for adequate grounding, it can be seen that a plate may reach lengths up to more than 17 meters (assuming the same lay-up and panel width). For this reason a single rivnut per panel is assumed to suffice without estimating each panel independently.

This REESS compartment is designed to solely use plate elements, which means the production time is cut significantly and expensive and complicated mould is required for none of the sections. For the lids, a load bearing stiff plate can be used or a light watertight panel might be a solution. The choice between these two solutions can be made later in the detailed design, when the structure is analysed

accurately. At this point it is assumed that lightweight covers will be used. These can be produced using thermoplastic forming, as was proposed for Concept A.

To fix the REESS not only by mounting the bottom plate to the bottom of the chassis, the rear plate is designed to be a bit wider than the module compartment. This way the REESS can be bolted to the chassis without adding sealing complexity. The same was done in a different plane with the side walls of this REESS section. These walls can be mounted to brackets on the rear of the passenger compartment, to create a stiff combination. This directly facilitates a position to work around tight tolerances. It must be noted that at both sidewalls two mounts are placed in a parallel direction, which demands higher accuracy. Since both mounting points are in the same component, errors are relatively small, and can be further decreased by using a CNC-mill or jig to position the required mounting points.

Using an additional bracket, the front of the REESS compartment can be mounted to the front of the passenger compartment to improve the efficiency of an integral system. The same can be done in the middle of the middle tunnel, which can easily be covered by interior electronics. This additional bracket is not yet accounted for, but might be added when detailed design shows the added benefit. The brackets on the side of the main REESS compartment (Figure 7.34) can be installed after raising the REESS into the vehicle, to stiffen the chassis under lateral suspension loads. These brackets can be placed strategically with respect to the suspension mounts and the internal REESS structure to add maximum stiffness. By use of slotted holes, positioning of these brackets can be done using relatively large tolerance. To mount these brackets to the REESS, blind threaded holes can best be used to eliminate the risks of a malfunctioning sealing at this point. This can for example be done using solid inserts. Inserts at Roding Automobile GmbH are commonly made of aluminium. To prevent galvanic corrosion these inserts are isolated using a cataphoretic coating, which is a common corrosion coating in the automotive industry. [67, 68] This method proved to be effective in similar applications at Roding Automobile GmbH and will therefore be applied to all aluminium components in the vehicle. A threaded bushing is inserted into the threaded holes to create more durable connection points with respect to soft aluminium.

The space between the diagonal rear of the passenger compartment and the REESS can be used to mount small vehicle systems. Since these can be mounted to the REESS housing, this can be best taken as an advantage to pre-assemble and connect HV components here.

In combination with a composite rear substructure this REESS concept will result in Concept B as seen in Figure 7.35. The outer geometry is relatively similar to the one in Concept A, with the major difference that the REESS is installed from below instead of from the top. Another advantage of this concept is that not all cut-outs need to be sealed, since the rear substructure does not serve as REESS housing. For manufacturing the same reasoning holds as for Concept A, which results in the assumption that the external shell of the rear substructure will be produced using hand lay-up.

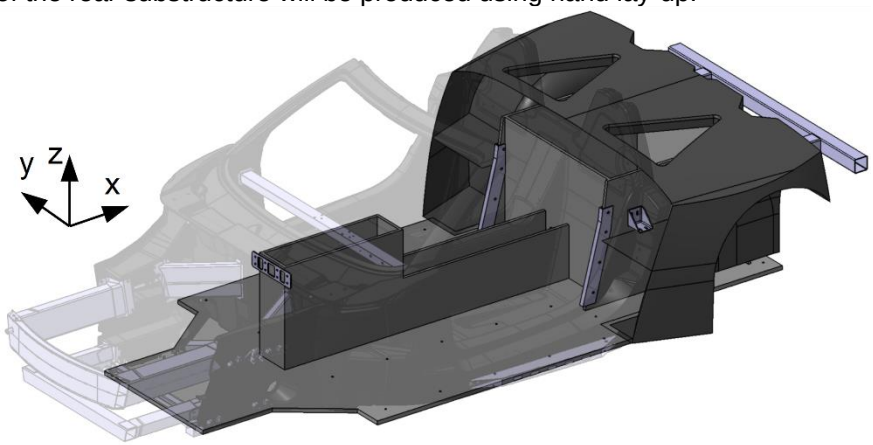

Figure 7.35 Concept B visualisation, passenger compartment and frontal substructure semi-transparent

In Figure 7.36 one can see the mounting points in more detail. The side brackets are mounted onto a horizontal plate, which is designed to connect the “B” pillar (the rear roof support), REESS structure, suspension points, rear crash structure and the rest of the chassis. This way all elements will strengthen and stiffen the overall structure when assembled. These brackets will be installed through the cut-out in the top, since these brackets make the REESS compartment wider than the available width to lift the REESS through. The fasteners to fix the rear plate can be tightened externally as seen in Figure 7.37. Using threaded insert this can be done with single side access.

To fix the REESS side panels to the passenger compartment, a cut-out was made in the wheel arch. This access point will be closed off by a cover, which will be installed to protect the load bearing CFRP against dirt and water since for impact.

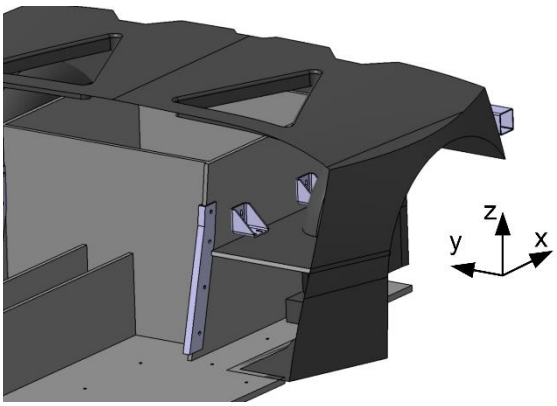

Figure 7.36 Concept B visualisation view 1

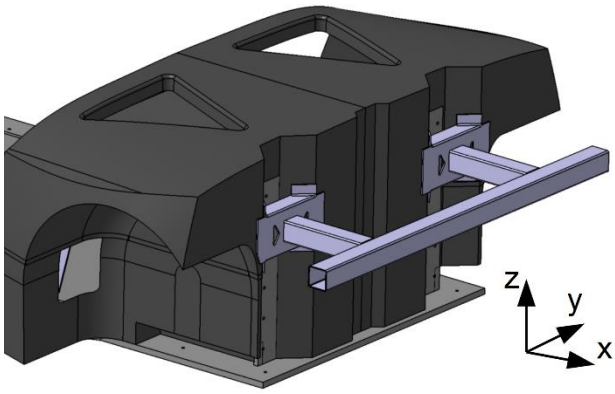

Figure 7.37 Concept B visualisation view 2

7.3.5 Concept C

For the layout of Concept C, the same reasoning for the REESS installation holds as for Concept B. Therefore in this concept, the REESS will also be mounted from below using a similar REESS. With respect to a carbon fibre rear substructure, a frame structure will probably result in more body parts to create the exterior. However this means that mounting components will be much easier since without closed exterior (body) panels. For this reason it will be easier to design additional brackets and mounting points with easy access in this concept. The production of metal comports is less depending on the skills of the production crew, which is another advantage of this concept. This results in easier rework and less rejects, resulting in lower costs.

The rough interpretation of Concept C is based on a rear substructure, developed by Roding Automobile GmbH for the ICE Roding Roadster, as seen in Figure 7.38 and Figure 7.39. This uses a complex milled console to attach the upper wishbone, tie rod and rear connection point of the lower wishbone. This part is also used as a central node to which extruded profiles are welded. A similar component was constructed for the other lower wishbone connection point. These parts are adapted to incorporate a mounting surface for the rear of the REESS. The advantage of these milled parts is that a stiff structure is created with a relatively small number of parts and therefore small number interfaces. This saves a lot of time in assembling the rear substructure by adding complexity to a section which would already require advanced manufacturing techniques. A similar solution can be found in the rear suspension of the BMW i3 (Figure 7.40).

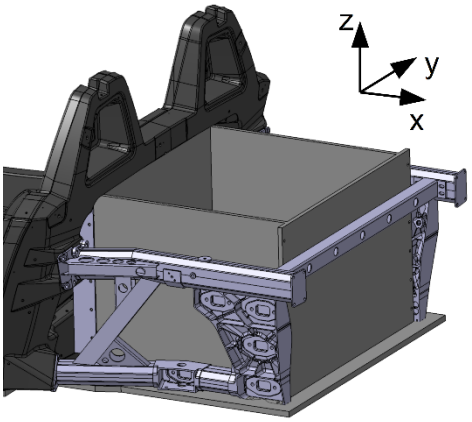

Figure 7.38 Concept C rear substructure view 1

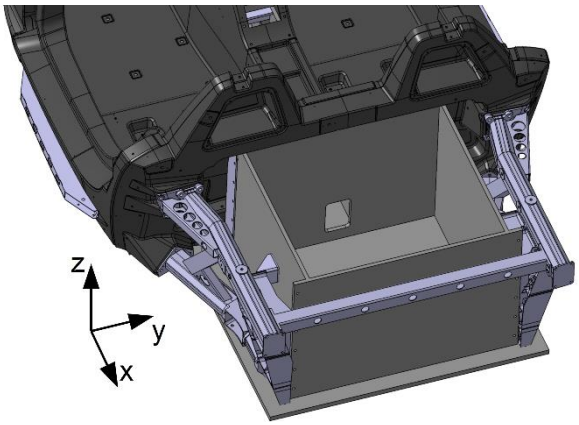

Figure 7.39 Concept C rear substructure view 2

In contrast to Concept A and Concept B, the rear component of the passenger compartment is included in this concept to form the interface for the metal substructure. A similar mount can be made on this substructure to fix the side of the REESS as in Concept B. For the middle tunnel section the same solutions are available in this concept as in Concept B. In Figure 7.39, one can see an additional bracket on the side of the large REESS compartment. This is similar to the additional brackets in Concept B. The lateral profile on the rear can be used to assemble the rear substructure accurately before installing

the REESS. For lateral suspension forces this profile will be supported by the rear plate of the REESS. Furthermore, the bottom plate will be connected to the frame, to create an integral structure. When required, additional connections can be added easily during the detailed design phase. A crash structure can be designed to suit this concept easily.

Since welding heats the structure locally, it is known that the product can deform during cooling down. This means it is difficult to create highly accurate parts using a welded structure. This can be solved by designing the initial components of the frame with a small amount of excess material at critical mounting points. After welding, the entire frame is re-milled to make sure critical points are positioned accurately with respect to each other. This is mainly done for the suspension points, to guarantee the desired performance. Since this additional milling step is required to reach relatively tight tolerances at the suspension connection, it might be interesting to replace the milled consoles by casted parts. This becomes more interesting with rising production numbers. This production process is also used by BMW, for a similar component in the BMW i3, shown in Figure 7.40.

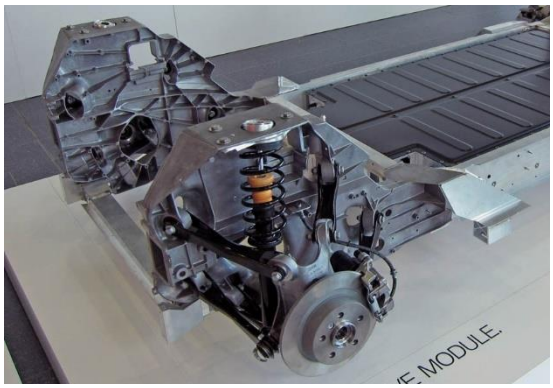

Figure 7.40 Casted console for rear suspension in BMW i3 [69]

7.4 Chassis Concept Trade-off

For the trade-off between the chassis concepts, weight and costs are used as the two main trade-off criteria. Costs can be broken down further, which is done in Section 7.4.2. The weight estimation will be described in Section 7.4.1. Before this is done, the identified strengths and weaknesses for the three concepts will be summed up first in Table 7.4, Table 7.5 and Table 7.6. It must be noted that some of the strengths and weaknesses are more relevant than others. For example in series production it is very time consuming when a lot of seals must be checked to ensure a properly closed REESS box. An automated production process is very unlikely for these production numbers, which means this sealing risk must be addressed independently for every single vehicle. The worse accessibility of Concept A and Concept B with respect to Concept C can however result in a more complicated design, but is a disadvantage which only needs to be addressed once.

Table 7.4 Strengths and weaknesses of Concept A

Positive	Negative
+ No double structure for REESS required	- High risk for malfunctioning sealing
	- Difficult assembly of battery modules (poor accessibility)

Table 7.5 Strengths and weaknesses of Concept B

Positive	Negative
+ REESS completely interchangeable for maintenance	
+ Concurrent assembly of REESS and chassis	

Table 7.6 Strengths and weaknesses of Concept C

Positive	Negative
+ REESS completely interchangeable for maintenance	- Deformations due to welding must be considered
+ Concurrent assembly of REESS and chassis	- More body parts required
+ Good accessibility	
+ Easily adaptable to changes	
+ Less rejects than CFRP components	

7.4.1 Chassis Concept Weight Estimation

Weight estimations for the relevant components in all three chassis concepts will be estimated within this section. Since the concept phase was only regarding the rear section of the chassis, this weight estimation will only be used to address weight differences. Determination of the total vehicle weight will be addressed in Chapter 9.

An estimation is made for the weight of the REESS inner structure. Since the REESS is assumed to have a structural function, the rest of the chassis may have an influence on the material lay-up within the REESS. Despite this fact, it is assumed that the inner structure weight of the REESS structure is constant in all three concepts and will therefore not influence the concept decision. It is expected that the loads described in Section 6.1.6 are relatively high. This is done to guarantee safety and will presumably exceed other load cases, which make these loads design driving for the REESS structure. For this reason the assumption that the REESS inner structure will require the same structural weight for all concepts is reasonable.

Table 7.7 shows the general properties used for the concept weight estimations. Based on the original typical (monolithic) lay-up of 2,5mm in the ICE Roding Roadster, a standard sandwich lay-up is defined for the weight estimation. In this lay-up, the 2,5mm skin is divided into two symmetric skins on both sides of the sandwich panel. When using the same materials as the test panel in Section 5.3, this results in an aerial weight of 4.9kg/m^2. This is based on a lay-up with skins with an aerial fibre weight of 2 layers of 630gsm (V_f=0.62), in combination with a 10mm thick core. This is the lay-up used for the REESS structure. To create a stiffer structure for larger spans, the rear substructure is assumed to have a similar lay-up using the same aluminium honeycomb core with a thickness of 20mm. This lay-up results in an aerial weight of 5.5kg/m^2. [32]

Based on the created CAD model of the REESS layout (Figure 7.19), the required lengths and the weight of the profiles were estimated for the REESS inner structure. This results in 19kg (aluminium) profiles, 15kg sandwich panels (with a 10mm core), 6kg connections and approximately 2kg additional adhesive, brackets, bolts and cable clips. This means that the inner structure of the REESS will weight approximately 42 kg in total.

Table 7.7 Input properties for concept weight estimation

Property/Component	Value
Sandwich panel, 10mm core	4.9kg/m^2
Sandwich panel, 20mm core	5.5kg/m^2
Nominal CFRP density [31]	1600kg/m^3
Nominal aluminium density [31]	2700kg/m^3
Aluminium guiding profile nominal weight (based on 5.5cm^2 cross sectional area)	1.5kg/m
Running meters guiding profile	8m
I-profile nominal weight (based on 0.12m height, 0.05m width and 3mm thickness, 15% deducted for cut-outs)	1.20kg/m
Running meters I-profiles	6m
Connection points between guiding profiles and REESS layers	100g/pc.
Connection points	60pc.
REESS layer plates	3m^2

In Table 7.8, Table 7.9 and Table 7.10 the weights are estimated for the REESS structure and the rear substructure. For easier comparison, the entire bottom plate in every concept is seen as part of the REESS structure. For REESS closures a constant of 5kg is assumed.

In Concept B, the horizontal stiffening panels are included in the rear substructure area. Brackets and screws are estimated at an additional 2kg for both Concept B and Concept C. For Concept A, this value is estimated to be 6kg since the panels to connect the gap between the REESS structure and the rear substructure are not yet included in the surface areas. An additional REESS weight can be found for all concepts in the category “additional weights”, which is equal in all concepts (3kg) and therefore does not influence the outcome of the trade-off. This is included to give a fairer estimation of the real weights.

For the trade-off only the relevant weights are estimated, being the rear substructure, REESS structure and the connection structures. To complete the list of weight differences required for the trade-off, additional weight changes complete the estimation. These additional weight changes include the removal of the passenger compartment rear section for Concept A and B and the additional required body panelling for Concept C. The passenger compartment rear section was estimated at 9kg, including nut plates, using CAD and lay-up data. The additional body panelling in Concept C is estimated at 14kg by weighing uncoated rear fenders, rear-hood support and B-pillar covers. [32] Table 7.11 gives a summarized overview of the weight estimation.

Table 7.8 Properties for weight estimation Concept A

Property/Component	Weight	Surface area
Middle tunnel REESS housing	7kg	1.4m^2
Bottom plate surface area	13kg	2.7m^2
Inner REESS structure	42kg	
REESS housing lid	5kg	
Additional weights (inserts/brackets/miscellaneous)	3kg	
Rear substructure	33kg	6.0 m^2
Connecting structures	6kg	
Replacing passenger compartment rear section [32]	-9kg	

Table 7.9 Properties for weight estimation Concept B

Property/Component	Weight	Surface area
REESS housing (+bottom)	34kg	7.0m^2
Inner REESS structure	42kg	
REESS housing lid	5kg	
Additional weights (inserts/brackets/miscellaneous)	3kg	
Rear substructure	29kg	5.3m^2
Connecting structures	2kg	
Replacing passenger compartment rear section [32]	-9kg	

Table 7.10 Properties for weight estimation Concept C

Property/Component	Weight
REESS structure weight (equal to concept B)	81kg
Additional weights (inserts/brackets/miscellaneous)	3kg
Rear substructure (from CAD)	22kg
Connecting structures	2kg
Additional body panelling [32]	+14kg

Table 7.11 Overview weight estimation

Property/Component	Concept A	Concept B	Concept C
REESS structure weight [kg]	70	84	84
Rear substructure weight [kg]	39	31	24
Further weight changes [kg]	-9	-9	+14
TOTAL [kg]	**100**	**106**	**122**

7.4.2 Chassis Concept Cost Estimation

In the confidential version of the report, a cost estimation is given in this section. Since this contains proprietary information, this section is omitted in this version of the report. In Section 7.4.3 the normalised costs for all concepts will be presented. The remainder of this section will elaborate on the used assumptions to estimate costs.

The cost estimation is based on estimated material usage and manufacturing time. First, material costs are based on the surface areas reported in the weight estimation. The price of the sandwich panel per square meter is based on the bare materials, without consumables and labour. A scrap factor of 30% is included in this price, to cover remnants from cutting. The price of consumables is based on the same surface area with an additional 100% of material, since vacuum bags and foils must always outreach the product. This factor also includes additional costs such as tacky tape and other minor material costs. Later labour is estimated for each concept, based on its complexity.

The costs of the inner REESS structure are similar for all three concepts. For this inner structure no moulds are required, since it consists of only flat panels. Labour hours for the composite rear substructure are based on working hours documented for other complicated components, including steps such as mould preparation, laminating and demoulding.

Milling costs are based on internal quotations, using the mould break-up as shown in Figure 7.41. It is assumed that the front and bottom panel of the mould can be made from sheet metal. Therefore it is assumed these costs are negligible and they are not visualised in this figure. Mould materials are based on 6m^2 product which is assumed to result in 8m^2 mould face, due to margins and flanges in combination with the earlier mentioned 30% scrap, this results in approximately 21m^2 for two mould sets which can be used in parallel to reach the required production capacity.

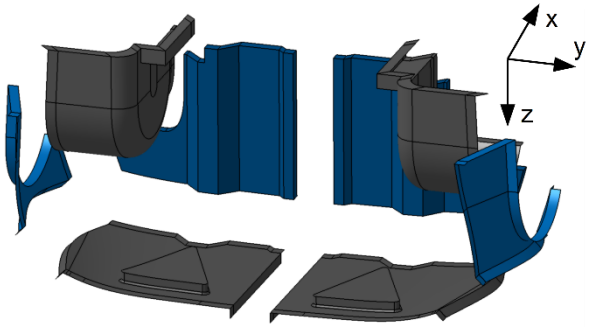

Figure 7.41 Moulds break-up for rear substructure

Further the cost estimation involves an estimation for initial investments in machinery and facilities such as autoclaves and plie cutters. For Concept C the price of the rear substructure is based on external production. This eliminates initial costs such as machinery costs. The total price is based on the price of the rear substructure where the concept was inspired on, in combination with an estimated price reduction of 33% due to scaled-up, optimised production.

7.4.3 Chassis Concept Trade-off

The mass and cost estimations are normalised similarly to the method used in Section 7.1.3. The normalised values can be found in Table 7.12. The mean value for weight and costs is set equal to zero and scores are given between “-5” and “+5”. A reference quantity is set for these extreme values. The origin of weight saving with respect to cost saving is trivial. For that reason, the ratio between the reference quantity for weight and costs is kept equal to the one set in Section 7.1.3.

Changes in the weight distribution are relatively small in between the concepts. Therefore this will not be reviewed for choosing the chassis concept as was done for the powertrain. In Table 7.4, Table 7.5 and Table 7.6 important aspects of the concepts were assigned. These scores are used to grade each concept, resulting in a third trade-off criterion. Concept A scores low (-2), since this concept involves high risks in sealing the REESS compartment. Concept C is however very adaptable, since changes in the milling program can be made easily. It is also very accessible, which makes it easier to assemble. Therefore this concept scores a “1”. The valuation of is increased by to a score of “2”, to include the decrease the amount of rework and rejects in the metal substructure with respect to Concept A and Concept B.

These scores are evaluated with a weight factor of 3. In this case this means the score of “-2” can be compensated for with either 24kg weight difference or €2400 difference in costs. This is assumed to be a fair ratio for the additional complexity of Concept A with respect to a reference score of 0 (or Concept B in this case). From Table 7.12 one can see that based on the three trade-off criteria, Concept B is the best.

Table 7.12 Normalised Trade-off matrix for chassis concepts

	Mass	Costs	Score	Weighted score
Weight factor	1	1	3	-
Ref. quantity	20 kg	€2000	-	-
Concept A	2.3	2.3	-2	-0.3
Concept B	0.8	0.3	0	0.2
Concept C	-3.2	-2.7	2	0.0

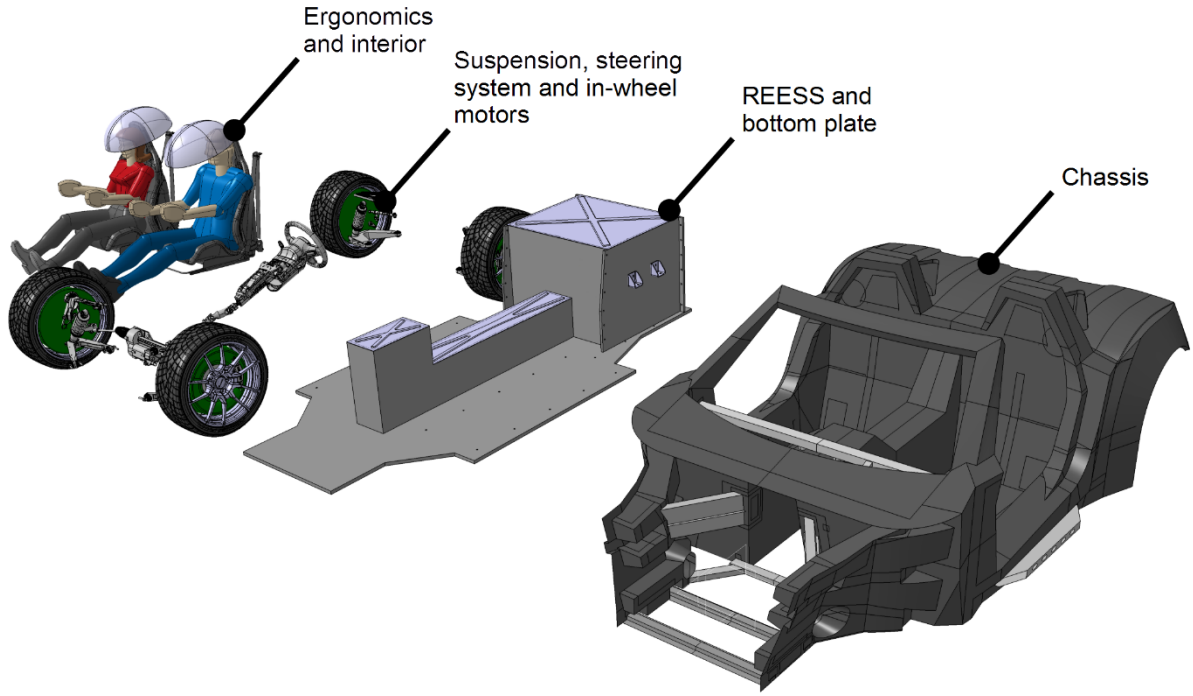

Figure 7.42 Exploded view of the chosen concept components

From Section 7.1, it came forward that a concept using four independent in-wheel motors is the best solution. The main reasons to prefer this concept were the low weight and costs in combination with a more flexible design envelope. This will be combined with a REESS in the middle tunnel and rear section of the vehicle using the developed modular system. The housing of the REESS will be constructed sandwich material for structural performance and grounding.

In the chosen chassis concept (Concept B), this REESS is combined with a composite rear substructure, which replaces the metal substructure in the ICE Roding Roadster. An exploded view of the combined concept can be seen in Figure 7.42. This vehicle concept will be worked out in more detail in the rest of this research.

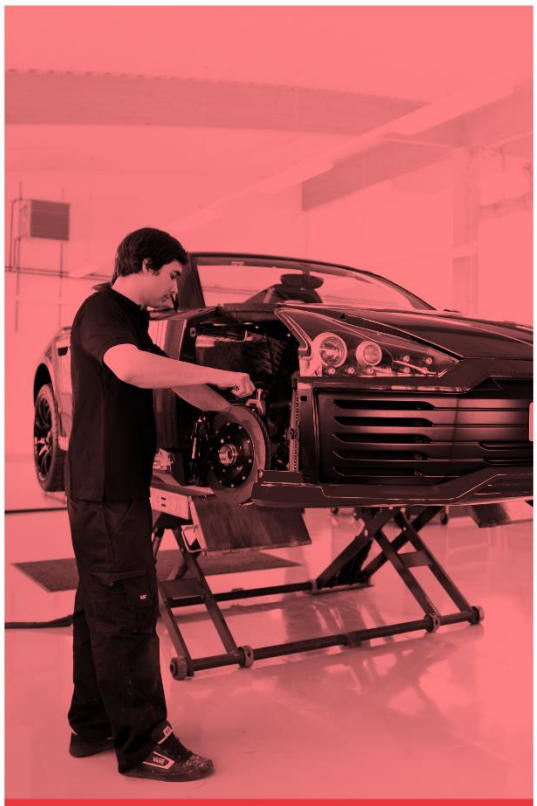

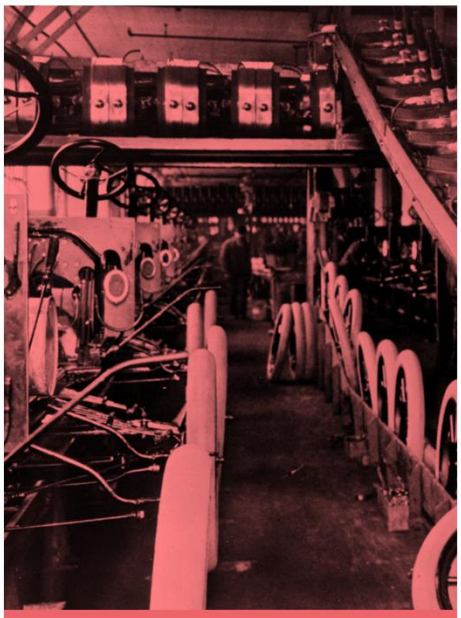

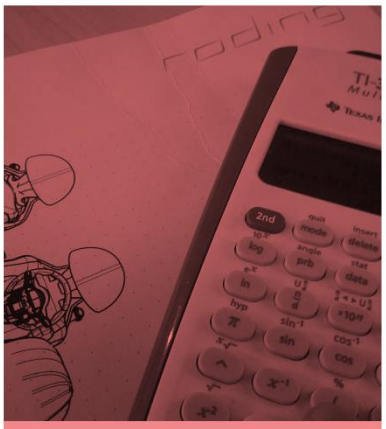

8 Concept Analysis

From Chapter 7 it was concluded that the best concept for the battery electric version of the Roding Roadster uses a powertrain with 4 in-wheel motors. To accommodate the REESS (Rechargeable Energy Storage System), the rear substructure is replaced with a composite substructure which will be attached to the current passenger compartment. This structure will be combined with the separately assembled modular REESS structure to create a stiff and strong combination. An overview of the current state of the concept is given in Figure 7.42 at (page 75).

This chapter will first elaborate on a more detailed layout of this concept. This will be followed by a description of the detailed design of some of the most critical concept features, including solutions on manufacturing and assembly of different components. Focus is is placed on keeping costs and weight low.

With these aspects addressed, the performance of the chassis concept will be estimated under the most important load cases. This wil be done by adapting the FE (Finite Element) model, which was created in Chapter 6.

The findings from this chapter will be used to review to final concept in Chapter 9.

8.1 Component Layout

In Chapter 7 the best concept was chosen. This concept replaces the metal rear substructure of the original Roding Roadster by a composite rear substructure in combination with a modular REESS (Rechargeable Energy Storage System) and bottom plate combination made out of sandwich material. An overview of the concept can be found in Figure 7.42 (page 75). To evaluate this concept more accurate, it is important to fix the layout of the major components. In this section the position of the HV (High Voltage) components will be discussed first, since these will be added to the system with respect to the ICE (Internal Combustion Engine) Roding Roadster. The routing of the coolant and electric circuit will be roughly determined as well. This is significant since passages and mounting sequences might be limited by this routing.

8.1.1 High Voltage Components Layout

Due to the use of in-wheel motors which incorporate the inverters, there are not a lot of HV components which need to be positioned besides the REESS. The only important components left are the charger and DC/DC converter, which require a relatively low amount of space. In comparison to the motors, the DC/DC converter does not use a lot of power. For this reason its cable length does not decrease system efficiency significantly. For the charger the same holds since it is only used when plugged into the power grid. Positioning of these components can therefore be done based on practicality and available space.

Based on the components in Appendix C, the DC/DC converter was found to fit in the wedge between the main REESS compartment and the rear of the monocoque. Opposite to this position there is room left for for example the vehicle control system, which facilitates the communication between all subsystems. It must be noted that components which should be accessed during maintenance regularly should not be positioned here, because the REESS should then be removed. However for mounting reliable components, such as the DC/DC converter, this position is suitable. The charger can be fitted in the front of the vehicle, in front of the luggage compartment. These positions are in line with the assumed positions in the weight distribution calculated in Section 7.1 and are included in Figure 8.1.

8.1.2 Electric Circuit and Coolant Circuit Layout

As already explained in Section 8.1.1, it might be efficient to mount components in the wedge between the main REESS compartment and the rear of the monocoque. It must however be noted that after installation of the REESS this position is difficult to reach. Mounting these components to the monocoque means that connections must be made before shifting the REESS into position. Mounting these components to the REESS means that they must be connected to a wire loom attached to the REESS. This is a good option, since the REESS itself must also be connected to the HV wire loom. This means that besides the REES, a part of the HV system can be installed parallel to the body manufacturing. This increases the benefit of positioning the DC/DC converter in this position, as explained in Section 8.1.1. After installation of the REESS, this only leaves a number of connections to be made to hook up the motors and the charger for example. This can be accessed through the access point in Figure 7.37 for the rear motors. In the front this can easily be accessed before installing the luggage compartment lining. Since the bottom of the middle tunnel is wider than the top, there is enough room besides the vertical sides of REESS to mount this wire loom.

For safe maintenance it must be possible to connect and disconnect the REESS after installation. That can easily be done in this case when the connector of the REESS is positioned at the front of the REESS. This way, this position can be easily accessed by for example removing a small hatch or cover in the luggage compartment lining.

The low voltage wire loom, powering auxiliary components, mainly connects the parts in the passenger compartment. For that reason the LV wiring is best mounted to the monocoque, separately from the HV loom. As explained in Section 3.1, this system is either powered by the auxiliary battery or the DC/DC converter. Since the auxiliary battery is assumed to be positioned in the front of the middle tunnel, a connecting cable for the DC/DC converter should already be connected before installing the REESS.

For the coolant circuit, the same holds as for the high voltage circuit. This can best be mounted to the REESS and connected to the other components after positioning the REESS. Since the REESS itself was assumed to suit different module types, cooling is not yet determined. When REESS cooling will be part of the coolant circuit, a connection on the same panel as the HV connection can be made. The cooling circuit is made out of silicon hose sections and tubes for straight section, which can be made in custom geometries at low costs. This can be done after the exact routing is known.

The radiator, positioned behind the grille, is assumed to be adapted from the ICE Roding Roadster. This section of the cooling circuit might be overdesigned, since a BEV (Battery Electric Vehicle) produces less heat than ICE vehicles. Downscaling these radiators might be an option during the detailed design, when investigating the required cooling capacity.

For the rear wheel motors, the coolant and HV circuit must be routed from the middle tunnel to the side of the REESS. This can be done by passing them through the connecting section of the sidewalls. This section was designed such that during installation the hoses and cables do not collide with the brace on the rear of the passenger compartment. An impression of the cable and coolant circuit is visualised in Figure 8.1.

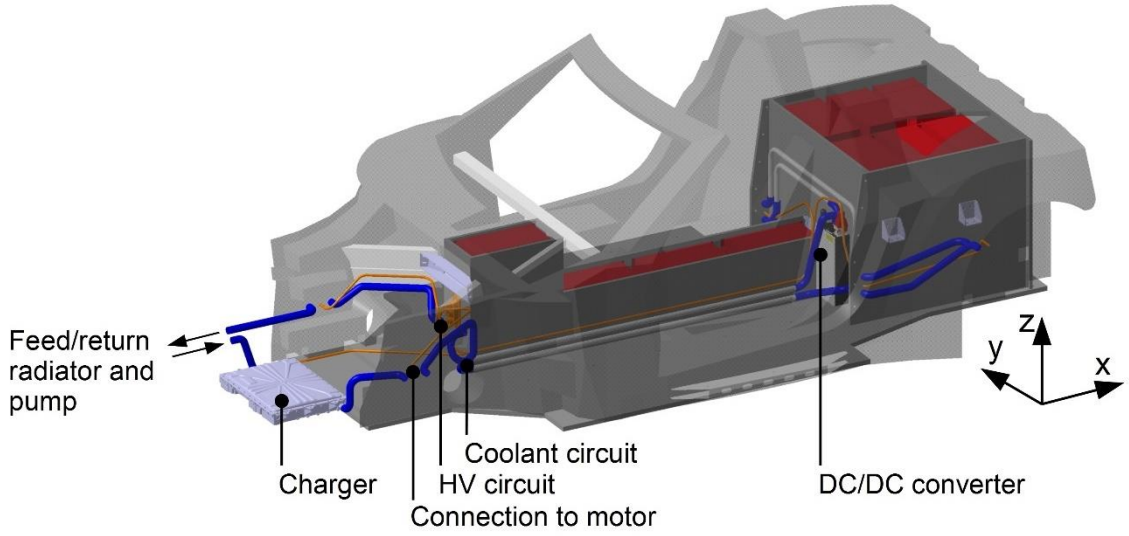

Figure 8.1 HV circuit and coolant circuit concept visualisation

8.2 Manufacturing

To support the feasibility of the chosen concept, some critical points must be addressed. Concepts to solve these points must be developed to create a realistic design while taking its manufacturability into consideration. At first it will be shown how the chassis can be adapted to create a good interface for the suspension. Also the REESS construction will be looked at in more detail.

8.2.1 Suspension Connection

An important section of the new concept is the interface with the suspension. At this interface the geometry is very important for the vehicle dynamics, so for that reason tolerances are relatively small. To still guarantee the vehicle characteristics, this geometry must also be kept under the loads which are present when driving. For this reason, stiffness within this section is an important factor as well.

Figure 8.2 Different types of wishbone joints used by Roding Automobile GmbH

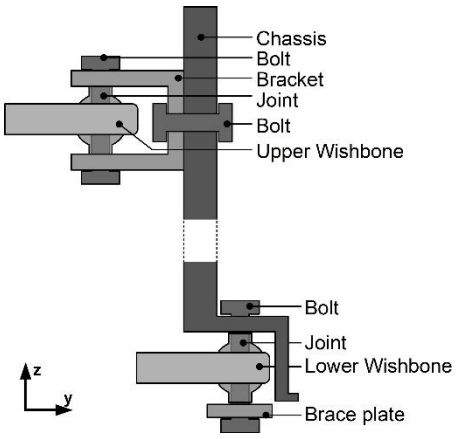

Figure 8.3 Connection concept of rear suspension

The connection of the current wishbones can be made using two interchangeable ball joints, as seen in Figure 8.2. The difference between these joints is only the method of mounting. The joint in the bearing

on the left is mounted into a bracket, where the one on the right is mounted onto a bracket. The selection is only based on the best joint and bracket combination in a specific application.

From the suspension it is seen that the lower wishbone is mounted more inwards, with respect to the upper wishbone and shock breaker. This means that for a similar connection, the chassis should be designed more inwards at the lower wishbones, using a simple bracket which does not add complexity to the CFRP (Carbon Fibre Reinforced Plastic) structure. Another option is to make use of the two different connections. The upper wishbones will be connected using an additional bracket, where the lower wishbones can for example be mounted into a socket which is integrated into the CFRP structure. A first version of this concept is visualised in Figure 8.3. Designing a socket can limit the inward construction at the lower wishbones, since it cancels out the additional space for a bracket similar to the upper wishbones. This additional space is critical for the width of the REESS. To simplify this solution, the upper side of the socket is part of the CFRP chassis, where the lower side of the socket can be closed off with a brace plate, bolted to the chassis on both sides of the wishbones. This plate decreases costs with respect to a milled bracket, since it can be produced using 2D techniques such as laser or water cutting. This can compensate for the additional complexity in the CFRP structure. On the inner side, a nut plate as shown in Figure 7.29 (page 67) can be used.

The concept of a brace plate is a good solution for the front connection point of the suspension. However to create the contact surface behind the rear connection point, a peculiar protrusion is required. This adds unnecessary complexity to the CFRP geometry. For this reason a milled bracket will still be the better solution. In Figure 8.4 this section of the rear substructure is shown, incorporating an impression of the suspension connections as discussed. It must be noted that for the chosen configuration the braking system is already incorporated in the in-wheel motor, however in this figure a conventional braking system is used to visualise the position of the wheel. The socket geometry in the bottom creates a lot of geometrical stiffness, therefore it is assumed that for this section a monolithic lay-up will be a better solution. This also decreases the complexity of this socket.

For the upper wishbones, a socket would increase chassis complexity significantly. For this reason common brackets are used to mount these connection points, as seen in Figure 8.3. For the chassis at this position, core crushing must be prevented due to operational loads and when applying the right amount of pretension to the bolts. For this reason inserts are required, which replace the core material locally with a tougher material. The material of these inserts must be chosen to withstand the local compression loads. When for example solid metal inserts are used at these connection points, it is also possible to tap thread into these inserts to create a blind joint without additional parts. The inserts must be sizes such that loads can be transferred from the insert into the fibre reinforced facings of the chassis and prevent rip out. As explained before, these inserts are mostly made from aluminium with a cataphoretic coating to prevent corrosion. Durability of the threaded hole is achieved by inserting threaded bushings.

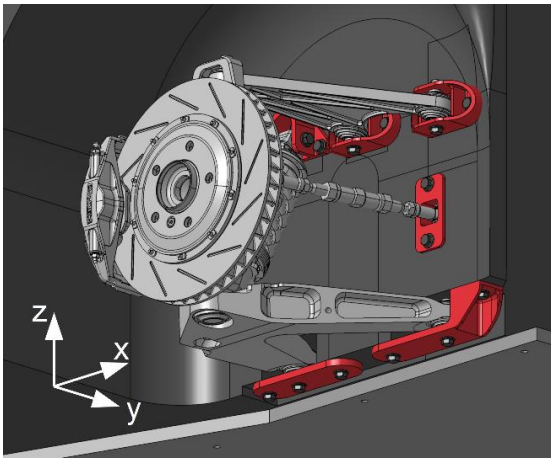

Figure 8.4 Rear suspension including brackets

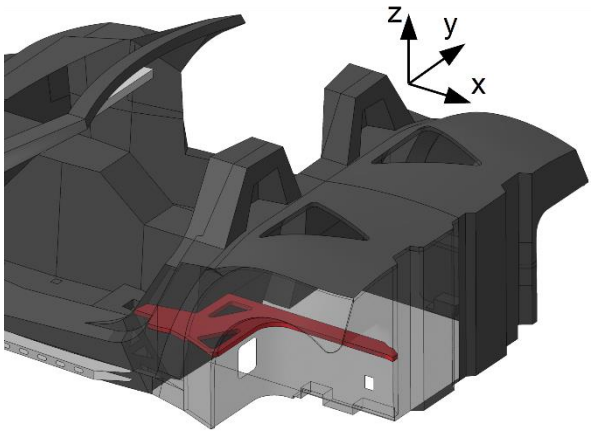

Figure 8.5 Horizontal stiffening and strengthening panel

For better vehicle properties the tie rod (Figure 3.1) of the Roding Roadster suspension is positioned slightly more inwards, with respect to the constructed vertical chassis plane. To limit additional complexity, a milled socket is constructed as part of the bracket. This bracket can be mounted into a

small cut-out in the chassis, which can be milled simultaneously with the other mounting points and trimming the rear substructure.
As explained before, the shock breaker parameters should be adapted to have optimal vehicle performance to suit the BEV weight and weight distribution. Since the shock breaker does not define the geometric path of the moving suspension, and this alteration is required either way, it creates no problem to slightly reposition this shock breaker. Within the lower wishbone, the shock breaker was rotated 12 degrees towards the chassis, to shorten the required bracket length. This causes no collisions with other components and only changes the wheel travel to spring travel ratio slightly. This change must be addressed accordingly during the design of the suspension, but is expected to create no problems within this range.

To create a stiffer and stronger structure, a horizontal plane is installed as explained in Section 7.3.4. In Figure 8.5 the final position and geometry of this panel is shown. This plane has multiple functions:

- Stiffen and strengthen the chassis at the upper wishbone and shock breaker.
- Connecting the REESS to the chassis. This adds strength and stiffness to both the chassis and REESS since the middle REESS sidewalls will be supported as well. To let these brackets contribute the most, they will be aligned with the I-profiles.
- Introducing loads applied by the rear crash attenuator into the rest of the chassis. In the x-direction this plate will add a lot of strength and prevent push through from the crash attenuator. For this reason the crash attenuator will be constructed around the same height. This suits the crash barrier for a rear collision as seen in the CAD master part.
- Adding strength to the “B” pillar, by extending this panel up to the front of the “B” pillar. This will locally strengthen the “B” pillar and transfer loads better into the rest of the chassis.

In the structural analysis of the concept, the behaviour of this plate within the chassis structure will be evaluated.

8.2.2 REESS Housing

This section will elaborate on the more detailed design of the REESS. Critical points will be addressed to check its feasibility, such as the concept for sealing and the manufacturing of the housing.

REESS Sealing

Before the concept trade-off, the concept of a sealed REESS was mentioned. How this sealed housing will be achieved will be discussed in this section. To create a reliable seal it is best to use an O-ring. This elastomeric lace is placed into a groove and compressed by both sides of the joint to create a seal. For this groove a solid section is required, which is not present in the sandwich panel. This will be created by a profile which can be bonded onto the top end of the sandwich panel, as seen in Figure 8.6. Besides a groove for the O-ring this profile also houses threated holes, to which the lid can be screwed. These threated hole is positioned outside the seal, to not jeopardise the seal.

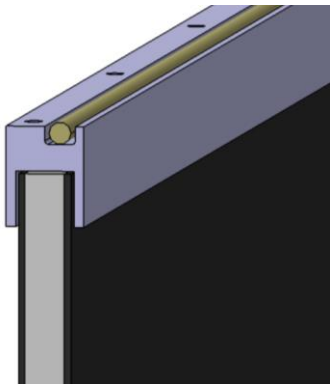

Figure 8.6 Sealing profile

Figure 8.7 Bottom view of sealing profile joint

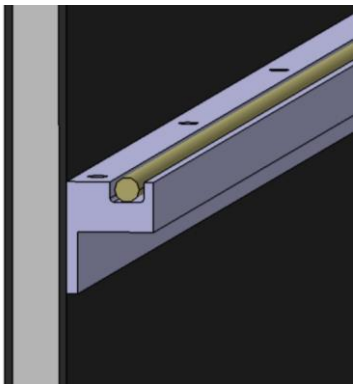

Figure 8.8 Sealing profile edited for assembly in middle tunnel

A different solution might be to make use of a solid core material instead of the bonded profile. The problem with this concept is that it would be difficult to continue the seal in the corner. Another disadvantage of using a solid core insert to house the seal would be that the space to create this seal in would become small when the carbon fibre facings must be avoided.

To create a reliable seal in the corners, the profiles will be mitred. The correct profile lengths can then be assembled using a simple sheet metal brace and a sealing adhesive (Figure 8.7). This results in a

finished frame which can be bonded onto the housing to create a reliable seal. When cutting the panels for the REESS housing, space for this brace can be taken into account. In the lower middle section of the REESS there is no top end to which the profile can be bonded. However here the same profile can be used, mounted to the side of the adjacent sections, as seen in Figure 8.8. One flange can removed, to make it possible to use for example pop rivets to fix the profile during bonding. Another option is to use the corners in combination with adhesive bonding to the adjacent panels, to prevent the additional step of removing a flange.

The sizing of the shown profile is based on the earlier assumed 10mm sandwich in combination with a 4mm O-ring and M4 screws to fix the lid. The groove should therefore be 5.55mm wide and 3.20mm deep. [70] This results in an aluminium profile of 350g/m. To prevent galvanic corrosion, this profile should be isolated by a cataphoretic coating as well. Based on the REESS layout in Figure 7.19, this results in 7 running meters, or 2.45kg. Here a lot of unwanted material is involved to create bulk materials for the threaded holes, which dines the height of the profile (6mm thread + 1.4 mm runout [71]). When the concept is proven it might be interesting to replace the aluminium profile with a lighter material, such as a polymer profile. The durability of the threaded holes can then be guaranteed by the use of threaded bushes.

REESS Panel Manufacturing

The sealing concept assumes that the box to which this sealing frame is mounted is watertight. To achieve this, the box needs to be assembled first. As explained before, this box will be combined out of solely flat panels. Production of these panels can be easily done using prepreg pressing in a heated hydraulic press. Within this production process, it should be taken into account that inserts are required for several joints. This is required to prevent core crushing when tightening a bolted joint and to make it possible to create a blind joint which does not jeopardise the sealed box.

To be able to accurately position inserts, the honeycomb core is stabilised first by curing a single sheet of carbon fibre on both sides. This makes sure the honeycomb material cannot deform as easy anymore. When this is done, cut-outs can be made at the positions where inserts are required. This can be done at low cost using water jet cutting. Now this panel can be used to laminate the total required thickness, during which the cut-outs in the core can be filled with the required insets. When the plate is cured, the finished panels can be cut. For the blind holes a milling step is required. Trimming the panels to its final dimension might be done in this process, or an additional but cheaper waterjet cutter might be used. A financial comparison between both options should be done during the detailed design. An overview of the main steps of this process is given in Figure 8.9.

It must be noted that for the trimming step the positioning of the panel is important, since the insert must be aligned properly. This can for example be done by using two inserts with a small notch rising above the fibre material. These two points can then be used for accurate aligning. This method requires a little cut in the fibre material to let the notch pultrude. During the pressing in the hydraulic press this requires an additional metal sheet with a small hole at the notches, for the reason that pressure would otherwise not be applied to the entire surface. The alignment notches can be positioned at a part of the panel which is outside the product or at a position where a hole will be drilled. This way all signs of its presence will be removed before assembly.

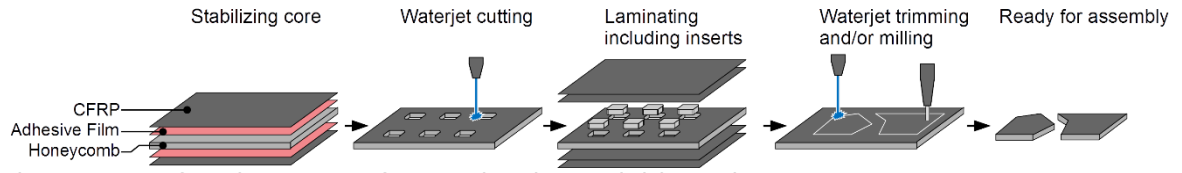

Figure 8.9 Manufacturing process of REESS housing sandwich panels

The exposed composite sandwich bottom plate might not be very durable. This is the case since stone chippings or other causes of small impact might damage the panel. For this reason it is assumed that a thin metal sheet will be bonded to this panel. This panel might protect the REESS from open fire as well, which should be tested for approval of the REESS under ECE R100. Care must be taken to prevent galvanic corrosion between the CFRP and the metal. This additional plate is not taken along in the structural analysis.

REESS Assembly

For the inner layers of the REESS the I-profiles can be bonded to the individual sandwich panels. Inserts in these plates should be designed according to the specific requirements of the used battery modules. Besides mounting the layers to the REESS housing, a connection between the individual layers would increase the stability of the REESS. For this reason blind rivet nuts will be installed in the upper flange of the I-profiles. The next panel can bolted onto this. A more detailed version of a partial stacking system is shown in Figure 8.10, with the actions for mounting a layer highlighted in red. It must be noted that in a narrow module layout, a cut-out in the upper flange might be required to access this fastener. The additional stiffening of the I-profiles using these fasteners might decrease the need of contentious interlocking profiles, as they were constructed at first (see Figure 7.17). The not-interlocking REESS structure is visualised in Figure 8.11. It is chosen to break up the profiles in x-direction, since in this direction no specific external loads are introduced by for example the suspension. Since these upper flanges of the red members in the top layer are not connected via a next layer, these members will not be very effective. It is assumed that sufficient stiffening of this top layer in the x-direction is done by joining this layer with the other layers. It must be noted that the REESS layers cannot be reached from outside the REESS and therefore do not have to be grounded for type approval.

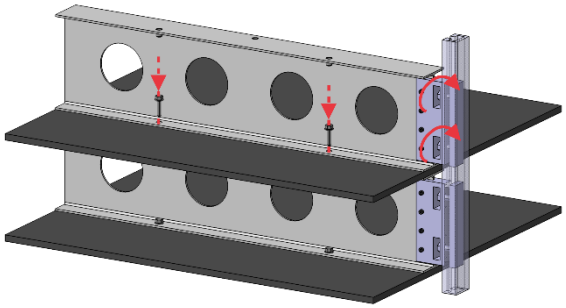

Figure 8.10 Stacking system including fasteners

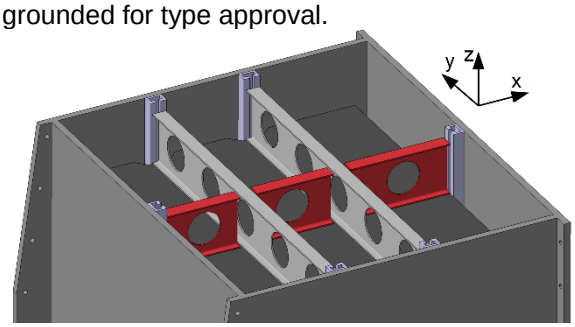

Figure 8.11 Upper REESS structure layer, showing ineffective members in red

To assemble the housing of the REESS, the joints should be designed first. It is assumed that the panels will be joint using finger joints, which is a common joint in woodworking (as seen in Figure 8.12). Using this joining method the panels can be held together with relatively little fixing during assembly. The permanent joining of the panels will be done by adhesive bonding. On the inner side of the joint, this bond will connect the inner facings of the material. However on the outer side, as one can see in Figure 8.12, the core material would be open. As stated before, combining aluminium and carbon fibre in the presence of an electrolyte will result in galvanic corrosion. For this reason these open ends should be covered to protect the panel. The simplest method is to cover these open ends with a bonded profile. For this purpose a light polymer profile can be used, which only acts as a barrier for moist. However it is expected that a load bearing profile connecting the outer skins will add significant strength to the housing. This can be done with for example a CFRP profile which connects the outer facings structurally and prevents galvanic corrosion. This is visualised for both corners and joints within a continuing plate in Figure 8.13. It is recommended that during the further development of this concept these joints are optimised. For a fast assembly, these profiles and the guiding profiles for the REESS layers can be bonded to the panels before joining them together.

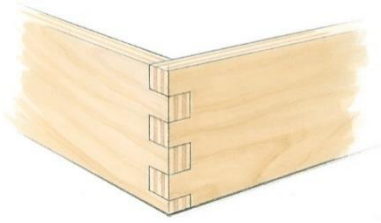

Figure 8.12 Finger joint in a wooden construction [72]

Figure 8.13 Covering profile for either corner joints or in continuing plates

Since the rear substructure will not be produced out of larger panels trimmed to size, open cores can be prevented by using core ramp-down. [54] This can be done by creating a monolithic structure at points where the cut-outs are required later. The loads in the core are transferred into the fibre reinforced skins. This can best be done by tapering the edges of the core to create a transition area as seen in Figure 8.14. [54] This can be done by milling the honeycomb to the correct size. Another, usually cheaper method is to use tapered strips of foam material to create this transition area. At other points, such as the suspension interfaces, a solid insert might be a better solution to reduce complexity.

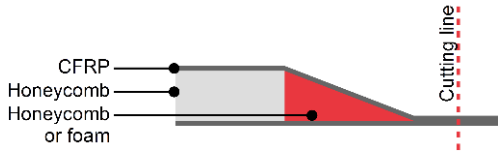

Figure 8.14 Cross section of core ramp-down

For the middle tunnel only a single row of models fits within the chassis, as seen in Figure 7.19 (page 62). For this reason it is relatively difficult to create bidirectional stiffening using the I-profiles as in done for the main REESS section. For a structural purpose this bidirectional stiffening is not required, since spans in this section are relatively short. At the first glance this leaves the two options on the left in Figure 8.15, placing the I-profiles in longitudinal or lateral direction. The benefit of the profiles in the longitudinal direction is that this version is a lot stiffer in the longer x-direction. However, there is little space for positioning these profiles and it makes no sense to stiffen the layers directly besides a stiff REESS housing. A support in the middle of the relatively long span would be beneficial, but is difficult to achieve.

Although stiffness in the y-direction is expected not to be critical, placing the profiles in this direction results in a better mountable REESS layer. Using the same profiles as in the main REESS compartment over such a short span will probably result in an overdesigned REESS structure. An option would be to place these profiles every other module to save weight. However besides withstanding (quasi-)static loads, this might result in problems for the natural frequency of this assembly. This means that if the low frequency vibrations in the driving vehicle come close to the natural frequency of this assembly, the assembly might start to oscillate. To prevent this from happing a small sheet metal bracket is placed between the modules where the profiles were cancelled (most right option in Figure 8.15). This bracket can be mounted to the same guiding profile as the I-profiles. This makes sure that between every battery module there is a support to prevent oscillation at this point, as seen in Figure 8.16. This has a beneficial effect since bisecting the length of a beam quadruples the natural frequency. [73]

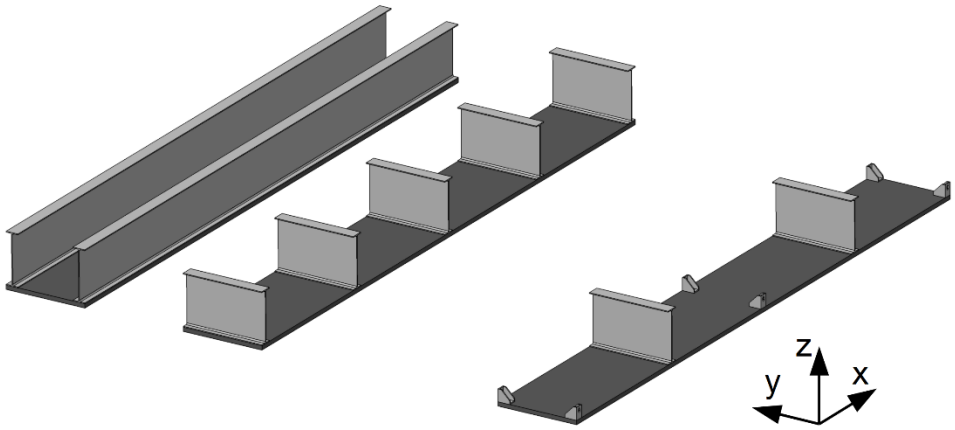

Figure 8.15 Options for REESS layer construction in middle console

Figure 8.16 Natural frequency modes of REESS layer comparing two and three supports

It must also be noted that the modules add a lot of stiffness, which increases the natural frequency and therefore the chance of oscillation. Since the additional brackets fix the thin unsupported and therefore flexible spaces between the modules, this is seen as a good solution. Slotted holes in the new brackets will make sure fixing can be done without requiring tight tolerances. It must be noted that not all I-profiles can be replaced by these brackets since one of the functions of these profiles is to position and support the next layer during installation.

8.3 Structural Performance

In this section the structural performance of the developed chassis will be addressed. This will be done by evaluating the strong and weak points of the chosen concept based on the verified analysis from Section 6.2 and Section 7.2. For the first analysis of the concept, no changes will be made to the frontal substructure and passenger compartment. In Section 8.3.6 an improved version will be used to show

the final results. These results can be used to make alterations and construct recommendations, which will be presented in Chapter 11.

8.3.1 Modifications to the Finite Element Model

It must be noted that in the chosen concept sandwich materials are present. For that reason, additional failure methods must be included in the inverse reserve factor of the analysis, namely core failure and face sheet wrinkling. This is done to check failure of the core material itself and wrinkling due to instability in the fibre reinforced facings.

Since the passenger compartment and the frontal substructure were adopted from the current chassis of the Roding Roadster, only the load cases influencing the new chassis will be reviewed for the new concept. For this reason the “seats and safety belts” load case, which was elaborated on in Section 6.1, is assumed to be conforming regulations. This assumption is based on the current type approval of the ICE Roding Roadster. For the same reason no further analysis of the ECE R12 (protective steering) is performed, which was described in Chapter 3. Besides the structural requirements, ECE R125 will neither be investigated further at this point, since the direct view regulations are not influenced by the replacement of the rear substructure. As seen in literature review, it is known that for direct view regulations minor adjustments are required to comply with the maximum angle of obstruction. [11] It is assumed that this deficiency can be resolved by redesigning the door.

Due to the fact that at this point not all load cases on the chassis are analysed, it is only possible to improve the structure performance of the chassis where it is required for the addressed load cases. Therefore it is not objective to decrease weight by removing material at this moment, since other non-reviewed load cases might be more critical in these regions.

To understand the structural performance of the BEV, it is important to understand the role of the REESS within the chassis. This is however very dependent on the series of connections made in the stacking mechanism. For this reason it is not reliable to include the REESS within the chassis analysis at this moment, except for the bottom plate. Instead of doing that, the two extreme options are investigated to determine the minimum and maximum influence of the REESS on the chassis. This is done by modelling the BEV chassis with only the weight of the REESS. In that case, the REESS does not transfer any loads. A second model is used to run the exact same model, but this time including a rigid REESS. This means a rigid virtual structure is placed between the constructed connection points of the REESS. For the bottom plate, only the section below the REESS models is coupled to this rigid structure.

In detailed design, it is important to verify that the loads transferred though the REESS structure do not result in failure of the REESS structure itself. From both analyses it can be assumed that the performance including a load bearing REESS would lie inbetween the results which are evaluated. It is expected that the version of the model with a rigid REESS will show less critical behaviour around this REESS. Depending on the position of the most critical positions this can be beneficial for the structural behaviour.

At first the different collision load cases will be analysed. The extreme driving load case is analysed to review the influence of the REESS on the chassis stiffness as well. The proposed alterations derived from these analyses will be combined in an improved version of the chassis in Section 8.3.6. After that, the structural performance of the REESS structure is analysed independently.

8.3.2 Frontal Collision Analysis

At first the frontal collision for the concept chassis is analysed. In Figure 8.17, Figure 8.19 and Figure 8.21 an overview is given of the results including a deformable REESS. To set the other boundary for the results incorporating the structural performance, Figure 8.18, Figure 8.20 and Figure 8.22 show the analysis using a rigid REESS. For the most critical features, alterations are suggested. Results including all alterations will be shown in Section 8.3.5.

For the frontal collision it can be seen that the diagonal profile in the frontal substructure is failing in both versions of the analysis. This will be solved by increasing the material thickness of this profile from 3 to 5mm thickness. On the inside of the passenger compartment there is another sheet metal component of which the material thickness will be increased from 1.5 to 3mm as well, to withstand a frontal collision. This alteration adds approximately 2.2kg in weight. The critical interface in the analysis of the conventional chassis between the rear substructure and the driver compartment is eliminated. Therefore no alterations are required here.

Further it can be seen that in the middle tunnel, some peak loads occur for the analysis with a deformable REESS. As seen in the rigid REESS analysis, loads decrease due to the REESS mount on the front of the passenger compartment. Besides that, it is expected that the intensity of these peaks decrease when fillets are added as described before. For this reason, in the design no measures are taken to prevent these local failure peaks at this point.

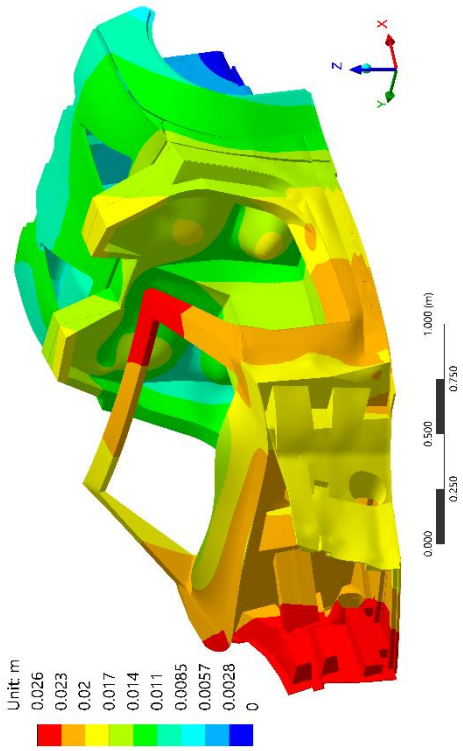

Figure 8.17 Total deformation for ECE R94 frontal collision, deformable REESS (amplified visualisation)

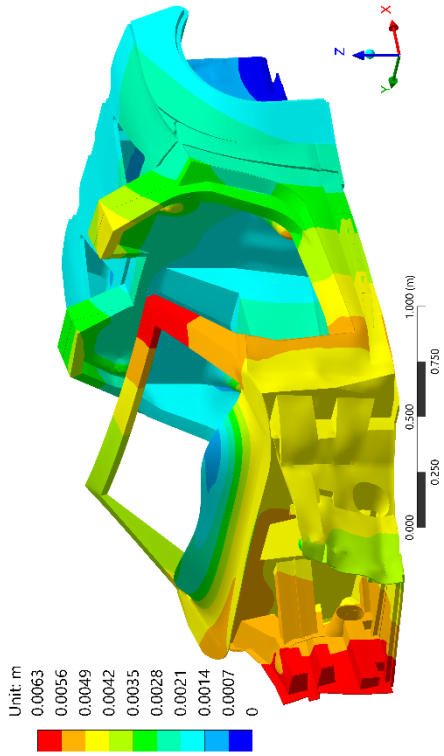

Figure 8.18 Total deformation for ECE R94 frontal collision, rigid REESS (amplified visualisation)

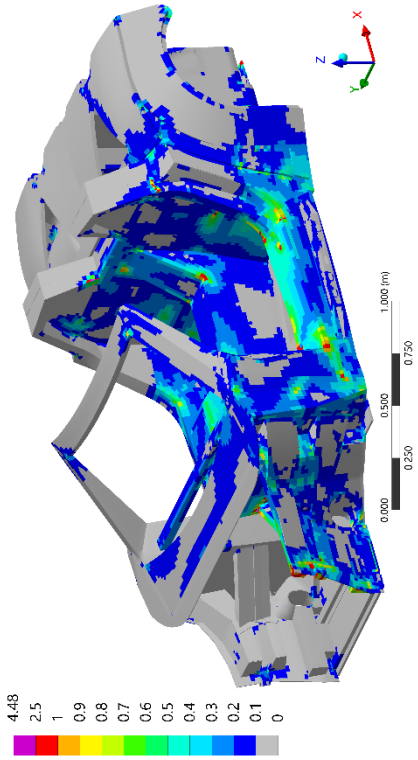

Figure 8.19 Inverse reserve factor for ECE R94 frontal collision, deformable REESS, view 1

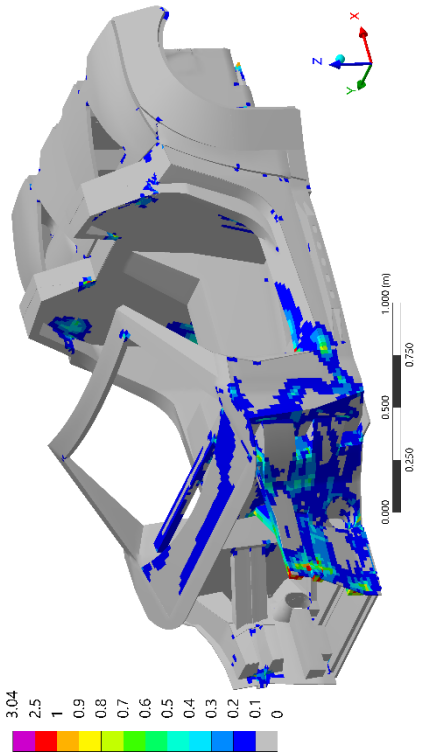

Figure 8.20 Inverse reserve factor for ECE R94 frontal collision, rigid REESS, view 1

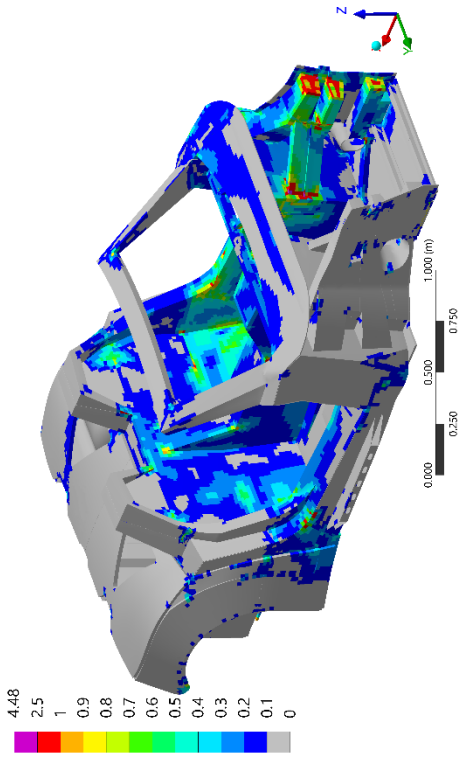

Figure 8.21 Inverse reserve factor for ECE R94 frontal collision, deformable REESS, view 2

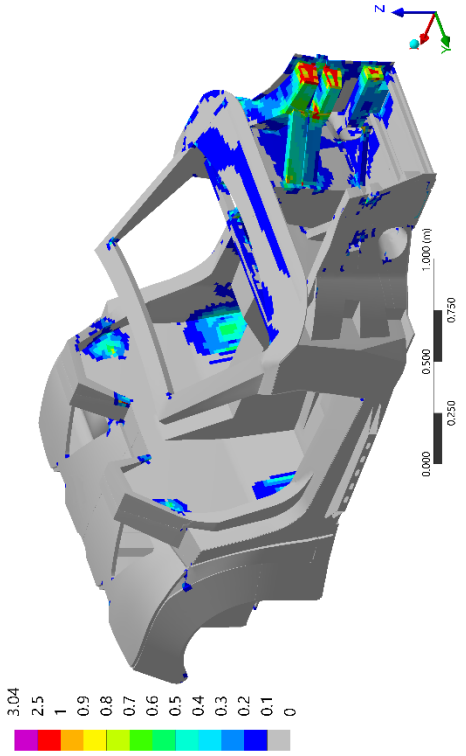

Figure 8.22 Inverse reserve factor for ECE R94 frontal collision, rigid REESS, view 2

8.3.3 Lateral Collision Analysis

Figure 8.23, Figure 8.25 and Figure 8.27 give an overview of the structural performance for the lateral collision, modelled with a deformable REESS. Figure 8.24, Figure 8.26 and Figure 8.28 show the analysis including a rigid REESS.

For the lateral collision one can directly see that the addition of the horizontal panel in the “B” pillar decreases the failure criteria. In Section 8.3.6 a clear overview will show the improvement in this section for the different chassis version. For Figure 8.25 to Figure 8.28 the core failure criterion was suppressed. This is done since under the involved loads, crushing of the core material at the impact zone is inevitable. This does result in irreversible damage and decrease of load bearing capabilities, but is assumed to be trivial during the described collision as long as the occupants are adequately protected.

When reviewing Figure 8.27 with respect to Figure 8.28, it can be seen that the behaviour of the REESS, as expected, does not influence the results at the zone of impact significantly. One can see that in the section around the middle tunnel the loads decrease. Since at the rear section of the middle tunnel a critical section is present for the deformable REESS, this load transfer via the REESS might be beneficial. To decrease the failure in the “B” pillar, in the next iteration two additional 630gsm layers are added as reinforcement, adding 0.8kg. These layers are placed to maintain a quasi-isotropic material, which is symmetric and balanced.

The horizontal plate inside the rear substructure is reinforced by 4 additional layers as well (2 additional layers on each side of the core), which adds approximately 1.3kg. Another option might be positioning a second plate within the “B” pillar. Due to the limited time available in this research, this solution was not analysed. It can be seen that the connection between the top of the “B” pillar and U-shaped cover shows an extremely high failure for this model as well. As explained for the original chassis, it is expected that failure in this component is not critical. Therefore it is concluded that this problem should be analysed using a more accurate geometry during the detailed design. At this moment, no further steps are taken to improve this performance at this position.

In Figure 4.5 (page 19), it can be seen that the “A” pillar, sill and “B” pillar are supported by additional sheet metal reinforcements. These are not visible in the shown figures, but show inverse reserve factures with maxima around 1.8. For this reason, the thickness of the sheet metal reinforcements in the sill is increased from 1.5 to 3mm steel. For the reinforcements in the “A” pillar and “B” pillar, the material

was changed from aluminium to steel, since only an increase in thickness would not suffice. Both changes add a total of approximately 3.5kg to the chassis weight.

For the failure on the most forward section of the sill, the behaviour should be reviewed in more detail first. From the directional deformation results it can be seen that the front of the sill is deforming inwards. The failing section is in line with the area of maximal deformation. Since the corner adds stiffness, this section cannot deform as easily as the section next to it, increasing stresses which cause failure.

Since the original strengthening profile (Figure 4.5 on page 19) is positioned too low for the lateral collision barrier, a solution might be to remove this profile and the indent of the sill it is mounted in. This way a better load transfer towards the bottom plate might be accomplished. It must be noted that for this solution, the chassis geometry is altered. The detailed design phase should give an insight in the realistic loads in this section and the influence of geometry alterations. At this point, a local increase in lay-up thickness of three additional 600gsm unidirectional layers in the x-direction will be included in Section 8.3.5, adding 0.7kg.

As explained earlier, analysis during detailed design should include the door. In practice this would increase the load on the hinge and latch, which means the “B” pillar would be loaded even more. The same holds for the “A” pillar. The addition of the door might also discharge the sill slightly, decreasing the stress peak at the front of the sill.

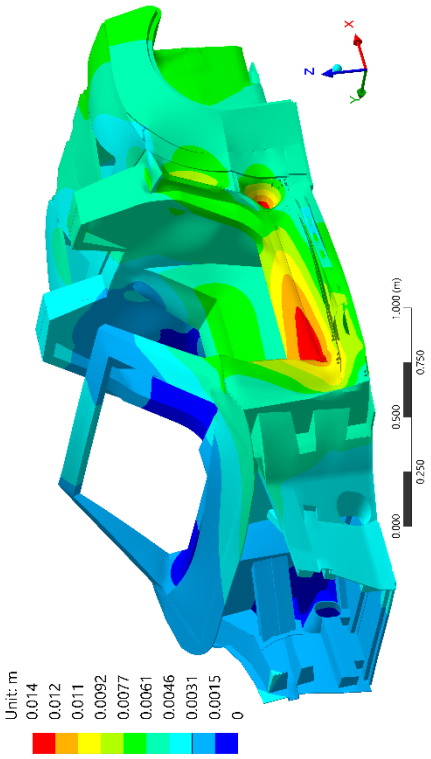

Figure 8.23 Total deformation for ECE R95 lateral collision, deformable REESS (amplified visualisation)

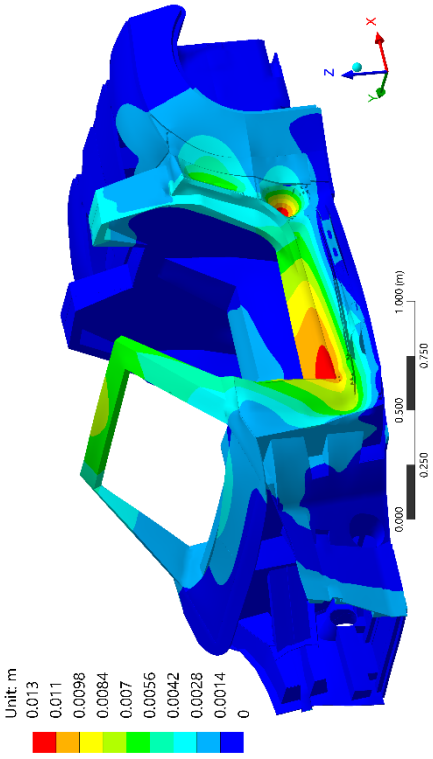

Figure 8.24 Total deformation for ECE R95 lateral collision, rigid REESS (amplified visualisation)

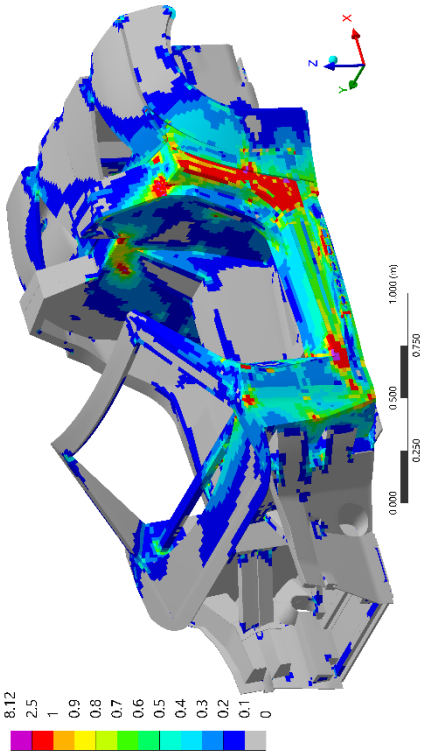

Figure 8.25 Inverse reserve factor for ECE R95 lateral collision, deformable REESS, view 1

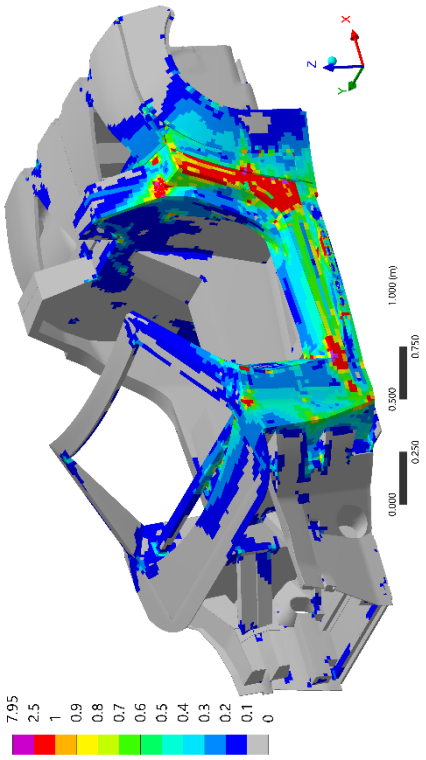

Figure 8.26 Inverse reserve factor for ECE R95 lateral collision, rigid REESS, view 1

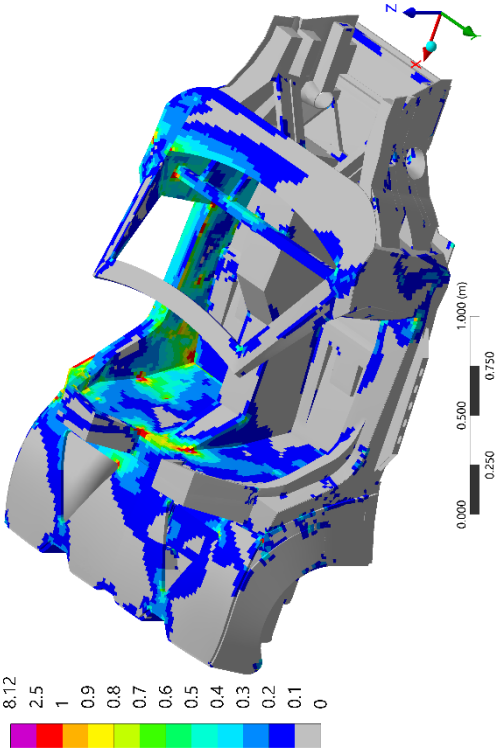

Figure 8.27 Inverse reserve factor for ECE R95 lateral collision, deformable REESS, view 2

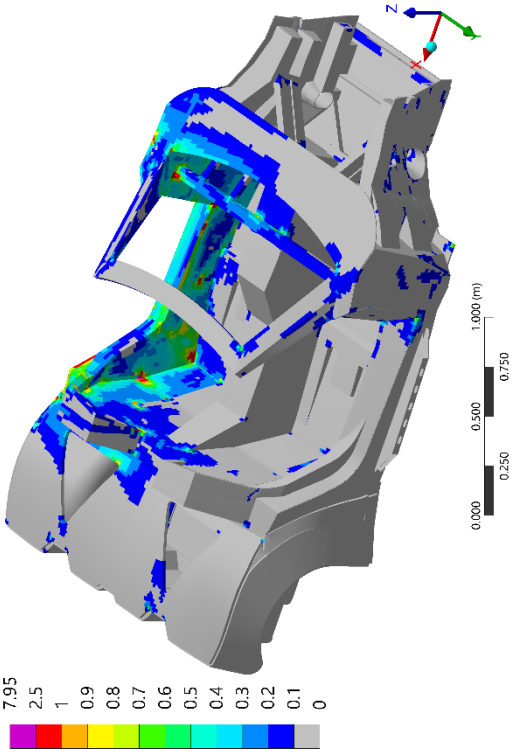

Figure 8.28 Inverse reserve factor for ECE R95 lateral collision, rigid REESS, view 2

8.3.4 Rear-end Collision Analysis

In this section the performance during a rear end collision will be evaluated. In order to be able to evaluate this, the crash attenuator concept will be revised. The rear crash attenuator in Figure 7.37 (page 70) has several weak spots which will be addressed first. With these weaknesses addressed accordingly, an analysis of the chassis is performed.

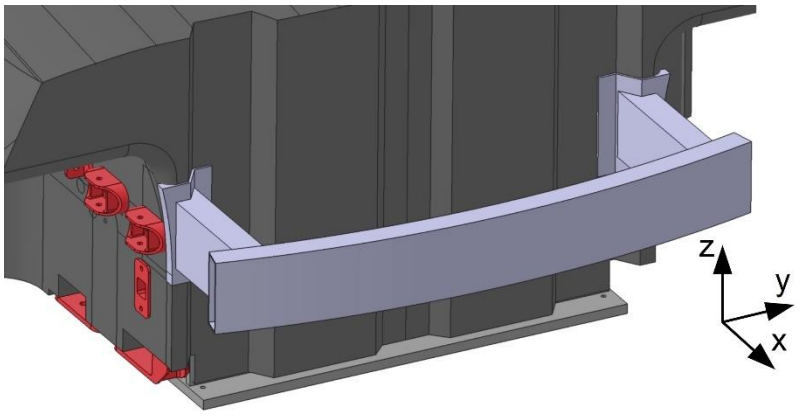

Figure 8.29 Rear crash attenuator configuration

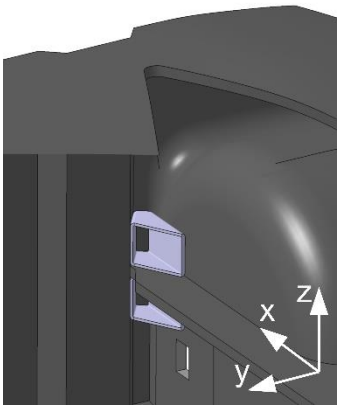

Figure 8.30 Internal braces for the left crash attenuator connection, cross-sectional view

Although in the attenuator concept of Figure 7.37 a strong and stiff adapter is constructed, it is locally prone to push through. To prevent this from happening, the spacing between the crash attenuator and chassis can best be removed. The most essential aspect during a rear-end collision is securing the REESS to prevent electrical shocks and fire. For this reason the connection points of the crash attenuators are moved more outwards. This places the crash attenuators besides the REESS, to make sure the crash attenuator cannot puncture the REESS under any load. The new concept for the crash attenuator position can be seen in Figure 8.29. A higher and slightly curved lateral beam were constructed in this figure for higher stability, based on experience at Roding Automobile GmbH and reference vehicles, such as the BMW i3. [7] The exact geometry and thickness of the profiles should be analysed during the detailed design phase. The weight of this aluminium attenuator is estimated to be approximately 4kg, based a measured rear crash attenuator for a vehicle of approximately the same weight. For the position of this crash attenuator in z-direction, the horizontal panel in the chassis was used as midplane. Sheet metal braces inside the attenuator connection are constructed and modelled to create a good load introduction in the rear panel, the wheel arch and the horizontal panel, as seen in Figure 8.30. In the detailed design this load introduction can be further improved by simplifying the chassis geometry at this point.

A first iteration of the load case from Section 6.1.4 is shown in Figure 8.31 and Figure 8.32. The braces were modelled as 2mm DIN 1.0984 steel. As expected, core failure was shown to be the critical failure mode in the section between the steel braces and the attenuator. Core failure can also be found in the rear substructure at the line next to the horizontal panel. Since this can be solved by using inserts or a local monolithic section, results were analysed excluding core failure. This shows critical values for the Tsai-Wu failure criterion. Figure 8.31 and Figure 8.32 show the results with suppressed core failure.

Besides the visualised failure, the horizontal inner panel and the braces show loads that are too high. The intended strengthening of this panel for the lateral collision will therefore have a beneficial influence on the behaviour during a rear-end collision as well. The material thickness of the braces is increased to 4mm to decrease stresses, resulting is a total weight of 2.8kg for both sides.

As expected, one can see a lot of differences between the rear-end collision modelled with a deformable and the one with a rigid REESS, since the load support is relatively close to one of the rigid supports. This means that besides the outer shell and the horizontal panel, the side walls of the REESS housing will transfer parts of the load. As long as this panel does not fail first, this might improve the ability to withstand rear-end collision significantly. Since out-of-plane loads are known to be more critical in composites, it is expected that the connecting section inbetween the crash attenuator and the REESS will give way first, to prevent catastrophic loads being introduced in the REESS.

Besides the stiffening effect of the crash attenuator joints, the REESS has an important local influence on the critical connections. It is important to understand this influence before adequate measures can be take. If further analyses show that measures must be taken, it is expected that local reinforcement will suffice to suppress the failure unveiled by the Tsai-Wu failure criterion. For this reason this is not seen as a major influence on the design in this conceptual phase and this will not be regarded further. Measures decreasing the loads in the internal horizontal panel will be reviewed accordingly in Section 8.3.6.

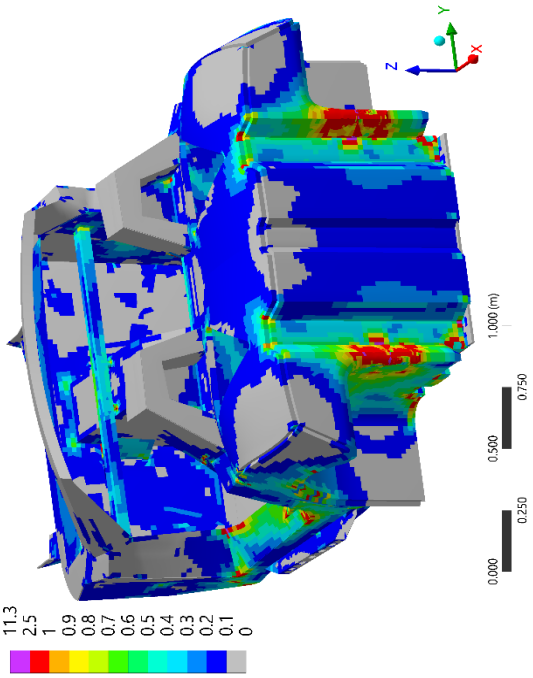

Figure 8.31 Inverse reserve factor for ECE R34 rear-end collision, deformable REESS

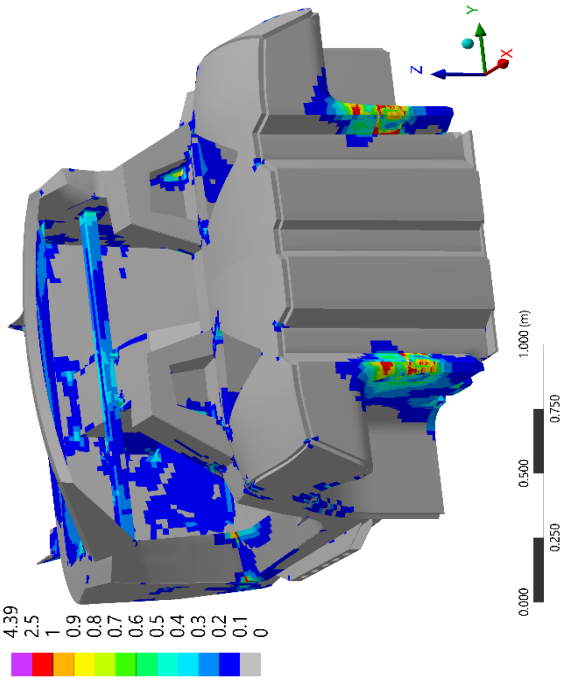

Figure 8.32 Inverse reserve factor for ECE R34 rear-end collision, rigid REESS

8.3.5 Extreme Driving Analysis

To estimate the range in which the REESS can add stiffness to the chassis, the extreme driving load case will be analysed in this section according to the description in Section 6.1.1. Since loads for cruising conditions are inferior to the extreme driving load case these will not be analysed during this phase of the design. Figure 8.33 and Figure 8.34 show the total deformation during the extreme driving load case for both a deformable and a rigid REESS, as was done for the collision load cases.

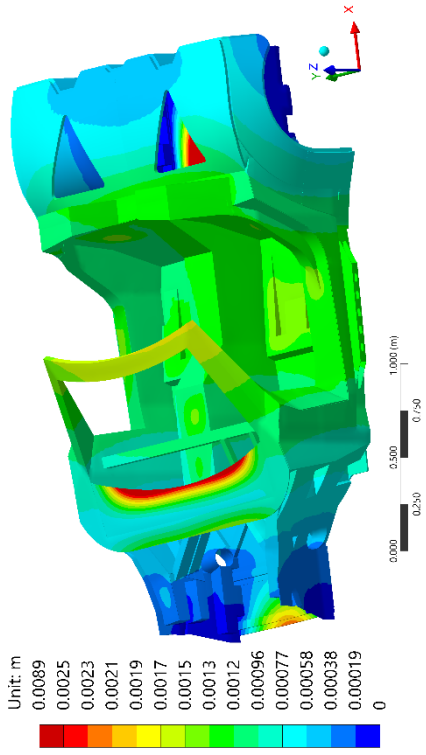

Figure 8.33 Total deformation for [1g,2g,4g] acceleration, deformable REESS (amplified visualisation)

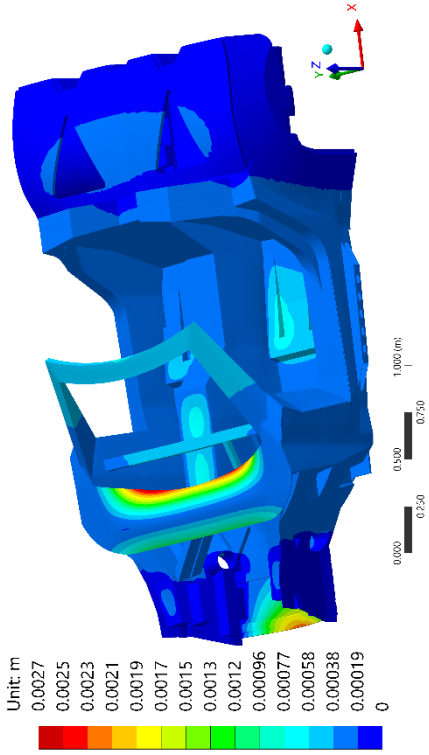

Figure 8.34 Total deformation for [1g,2g,4g] acceleration, rigid REESS (amplified visualisation)

At first glance it can be seen that the deformation is high in the water shield at the bottom of the windshield. This section has a higher geometrical stiffness in reality and will be supported by the windshield itself. For this reason, this extreme value is neglected. In Figure 8.33 a large deformation

can be seen through the cut-out in the rear substructure, in the bottom section below the rear REESS section. This extreme value is not relevant either, since the weight will not be supported by this middle section of the bottom plate. For this reason it is expected that deformation will be less extreme in this section. The deformation in the bottom part at the frontal substructure of both Figure 8.33 and Figure 8.34 is predominantly a deformation downwards. This is the result of the slight inward rotation of both sides of the frontal substructure. Deformations in this section do not exceed 2.1mm. The influence on the driving characteristics of this deformation should be investigated in more detail.

The directional deformations are reviewed for comparison as well. These show neglectable components for the driver compartment in both x and y-direction. For the right-front driver seat mounting point, the model with a deformable REESS shows a deformation of -1.5mm downwards, where the rigid model shows a deformation of -0.66mm downwards. This supports the fact that the REESS might increase the chassis stiffness significantly using the developed concept. Figure 7.11 (page 56) shows an increase in internal bending moments for the BEV with respect to the original vehicle. Because it is now shown that the REESS can add to the bending stiffness significantly, this effect can be compensated for. Furthermore, this increase in stiffness might facilitate weight reduction or improve vehicle handling. To quantify this more accurately, the REESS should be modelled along with the chassis. No changes on the chassis are derived from the results for this load case at this point, considering no strict requirements were constructed for this load case and an accurate quantification of the combined chassis/REESS performance is required.

Analysis of this load case using suspension loads might give more information on the vehicle behaviour during the detailed design phase. These loads can be counteracted by a similar set of accelerations, to bring the system in equilibrium. The advantage of this approach would be, that the analysis will result in a set of deformations at the suspension. These geometric changes can be used to assess the influence of the loads on the vehicle dynamics, using suspension analysis software such as Adams Car or Lotus Shark. [74, 75] The created model can be used to extract the support loads, required to create such analysis. This more elaborated analysis is beyond the scope of this project and is therefore not investigated further.

The inverse reserve factors for both versions of the model do not exceed 0.5, except locally at a single joint between the lateral profile and the frontal lower wishbone. Since this only point of attention is strengthened by the milled brace (as seen in Figure 4.5 on page 19), this result is not plotted in this research.

8.3.6 Improved Structural Performance

In this section the suggested improvements on the chassis construction are implemented. In Figure 8.35 and Figure 8.36 the results for the frontal collision are shown for both the deformable and the rigid REESS model. Figure 8.37 and Figure 8.38 show the lateral collision. Figure 8.39 and Figure 8.40 show the changes in the results for the rear end collision.

A decrease of failure criteria in the diagonal support beam can be seen for the frontal collision load case. An analysis including the REESS should provide more information on the loads within the monocoque connection of this beam.

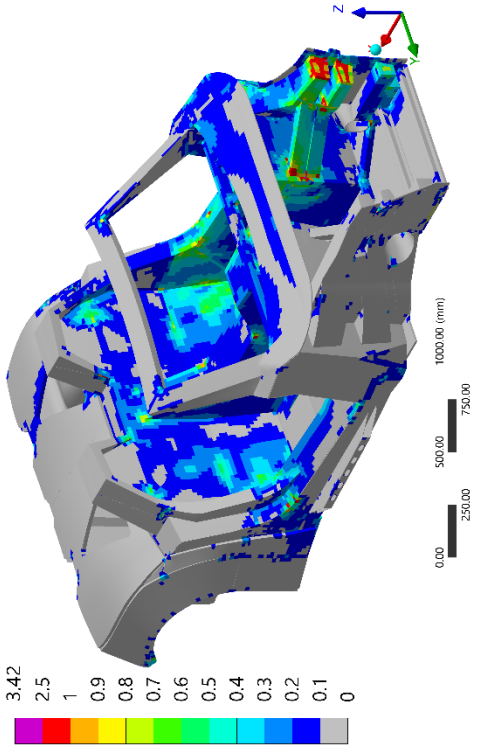

Figure 8.35 Inverse reserve factor for ECE R94 frontal collision with improved lay-up, deformable REESS

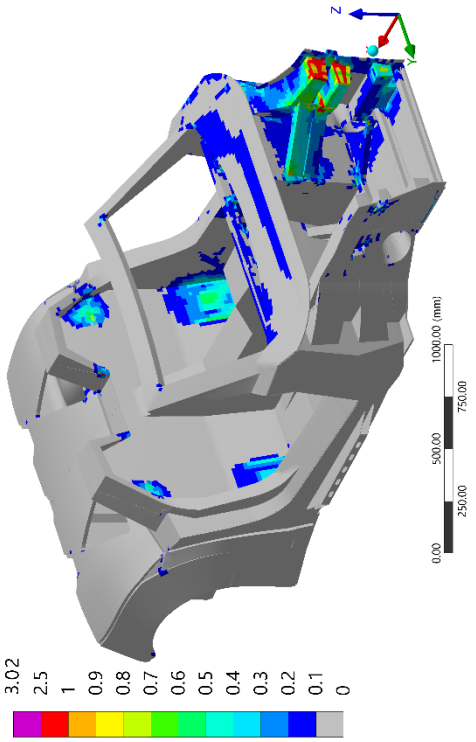

Figure 8.36 Inverse reserve factor for ECE R94 frontal collision with improved lay-up, rigid REESS

As stated before, Figure 8.37 and Figure 8.38 show the improved results for the lateral collision. To have a better view on the increase in performance for a lateral collision, Table 8.1 gives an overview of the decrease of the inverse reserve factor at two points in the most critical region of the “B” pillar. The points used for this comparison are shown in Figure 8.41. The change of materials and thickness of the sheet metal reinforcements in the “A” pillar, sill and “B” pillar decreased failure values from the mentioned 1.8 to maxima of 0.8 for lateral impact. This means that due to the alterations that were implemented, these components will not show any failure.

The increase of laminate thickness in the internal horizontal panel (Figure 8.5 on page 79) shows to be effective for both the lateral collision and the rear end collision. This is concluded since no failure is present anymore in this panel in both load cases. For the rear-end collision, the increase in material thickness of the braces also decreased the maximum inverse reserve factor from 1.9 to 0.7. As explained before, this section should be investigated in more detail using a more accurate model. For this reason critical loads are still shown in Figure 8.39.

With the chassis configuration and material layout it is assumed that most critical problems for type approval are addressed. Critical areas around connection points and chassis simplifications have to be addressed in a more detailed analysis which also includes a realistic behaviour of the REESS. For the rest of this research, the chassis as modelled in Figure 8.35 to Figure 8.40, will be used as the final version. The extracted weight of 124.9kg will be compared with the extracted ICE chassis weight in Chapter 9. As explained before, this research does not include any safety margins besides the conservative approach for determining the collision loads and the 1.25 load factor to include dynamic overshoot. For this reason, the sufficiency of close to failing components should be decided on during detailed design.

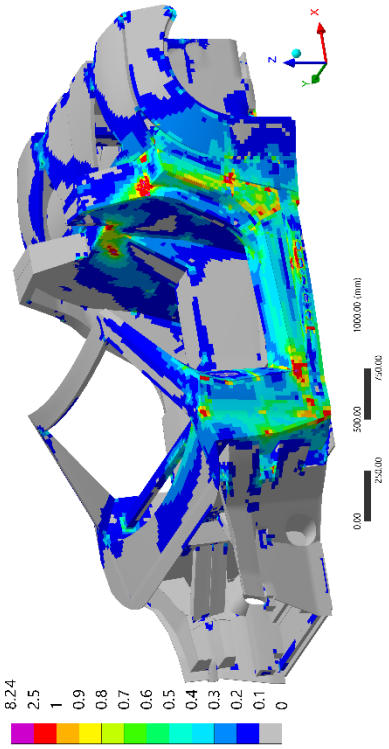

Figure 8.37 Inverse reserve factor for ECE R95 lateral collision with improved lay-up, deformable REESS

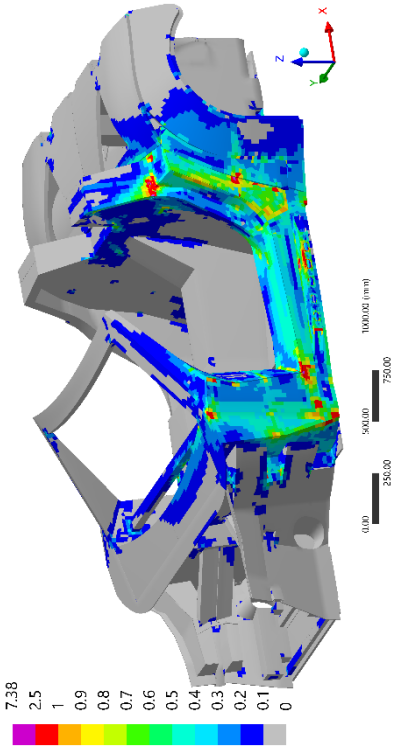

Figure 8.38 Inverse reserve factor for ECE R95 lateral collision with improved lay-up, rigid REESS

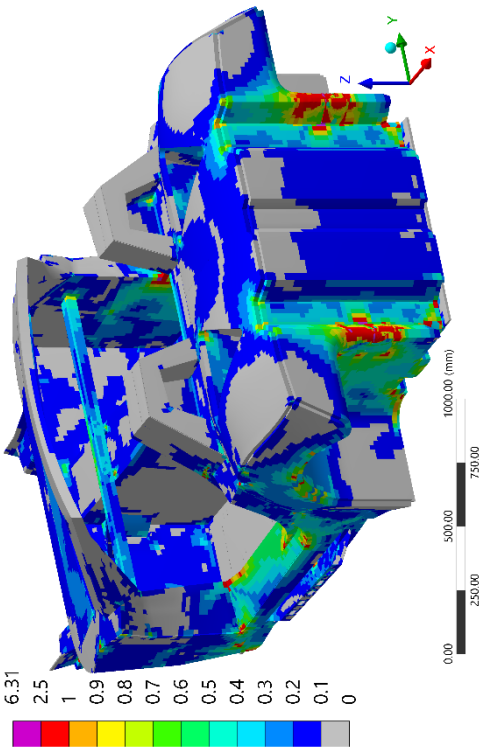

Figure 8.39 Inverse reserve factor for ECE R34 rear-end collision with improved lay-up, deformable REESS

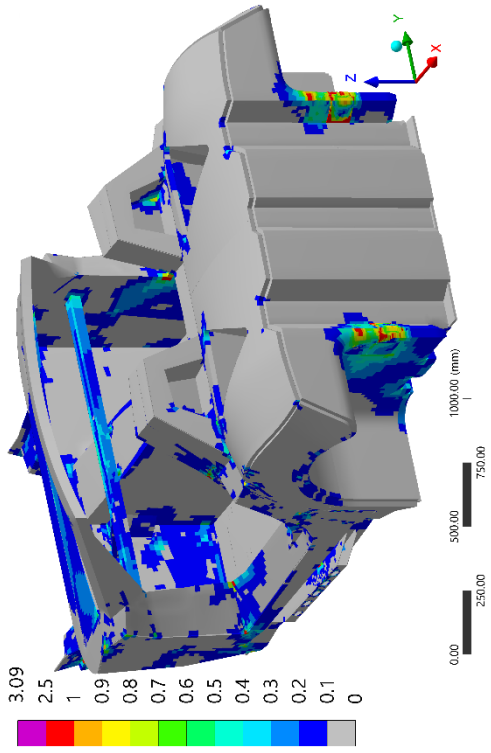

Figure 8.40 Inverse reserve factor for ECE R34 rear-end collision with improved lay-up, rigid REESS

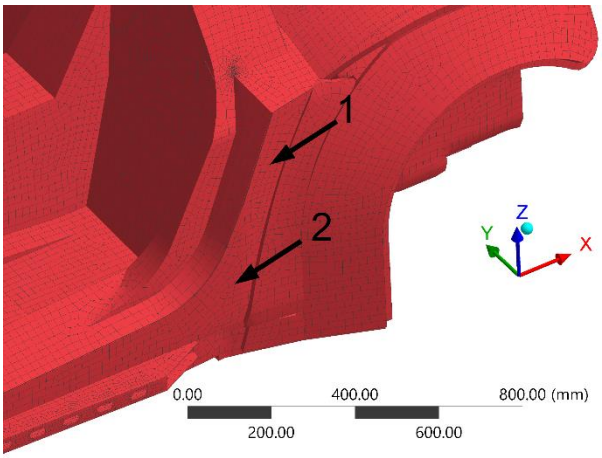

Figure 8.41 Visualisation of reference points used in Table 8.1

Table 8.1 Inverse reserve factor comparison for two positions in "B" pillar

Position	REESS behaviour	ICE-chassis (BEV weight distribution)	BEV-chassis first estimation	BEV-chassis improved lay-up
Point 1	Deformable REESS	3.40	1.25	0.71
	Rigid REESS	n/a	1.25	0.71
Point 2	Deformable REESS	1.69	1.47	0.73
	Rigid REESS	n/a	1.43	0.70

8.3.7 Analysis of the REESS Structure

To endorse a good estimation of the weight and performance of the modular REESS structure, a model was created. This model analyses a single layer of the structure in the main REESS compartment. In this model two load cases are analysed, being the extreme driving load case and the mechanical shock load case from Section 6.1. The mechanical shock load case was explained not to be mandatory when ECE R94 and ECE R95 are conducted. However, since it is difficult to create an accurate model combining the chassis and the REESS structure, in this phase of the design it is choses to analyse the REESS based on the component based test. This is assumed to be valid since for type approval these test are treated the same with respect to the REESS structure. If this concept would be approved under component based tests, it must be noted that compliance of the defined crush test becomes relevant as well.

To model the described accelerations in combination with the standard gravitational acceleration, six modules with a weight of 11.5kg each are modelled. This assumption is based on the total REESS weight and number of modules from Section 7.1. Although in practice the modules itself will add stiffness, in this model they were modelled as being deformable. This means that the modules do not add to the structural performance using the same method as was used for the complete REESS in the chassis analyses. In the model, the modules are supported by their entire footprint. This is done since for the actual module, inserts or mounts must be constructed suiting the specific module.

In Figure 8.42 one can see the structure of the model. For supports it was assumed that the mounting surface for the connectors are fixed, since these cannot rotate or translate in any direction within the housing. Supports between the layers are neglected, since only a single layer is analysed. This is done to analyse the worst case scenario. In practice, the next layer is important for the connection of the profile sections in x-direction, as described in Section 8.2.2. Since in this model the next layer is absent, the upper flange of the profiles in x-direction is modelled to be continuous. This creates a structural connection between the profile sections, which is per definition not stronger than the other flange sections.

For the first iteration, the profiles are assumed to be DIN 3.2315 aluminium, since Roding Automobile GmbH is experienced with extruded profiles from this aluminium alloy for structural components. The wall thickness is assumed to be 2mm. A sandwich construction is modelled for the horizontal panels containing the following lay-up:

- 2 layers of 630gsm carbon fibre epoxy biaxial prepreg [0, 45]
- 1 layer 7.5mm aluminium honeycomb
- 2 layers of 630gsm carbon fibre epoxy biaxial prepreg [45, 0]

For the mechanical shock load case the deformation is shown in Figure 8.43. The inverse reserve factor is visualised in Figure 8.44. From this figure it can be seen that most positions in the structure are far from critical. For this reason stiffness might be limiting. The maximum deformation of approximately 3mm occurs at a free corner of the layer. At the edge of the module this value is only approximately 2mm, which is not expected to damage to the module. The position of this maximum is as expected, due to the absence of profiles or supports in the corners. At these extreme loads, a deformation of 2mm is assumed to suffice. An additional support at the corners might be considered in the detailed design, since this can decrease the maximum deformation significantly. To apply this additional support, a similar extra support as discussed for the middle tunnel might be suitable. During the detailed design phase it should be determined if these supports can be cleverly combined with the construction of the REESS housing, to improve the performance without adding a lot of weight.

However the magnitude of the acceleration vector for the extreme driving load case is lower, this load case is analysed to check the behaviour under predominantly vertical accelerations. For this load case the maximum deformation was calculated to be approximately four times lower than for the mechanical shock load case. The maximum inverse reserve factor was calculated to be six times smaller. Since it was also found that the maxima in this analysis occur at the same position, the extreme driving load case is not analysed further.

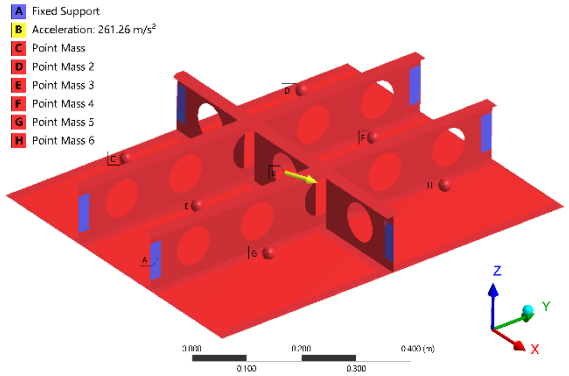

Figure 8.42 Supports for REESS structure analysis

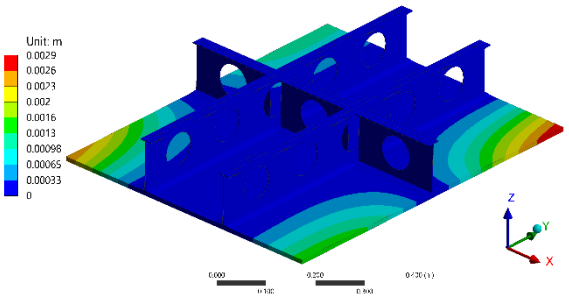

Figure 8.43 Total deformation in REESS structure analysis

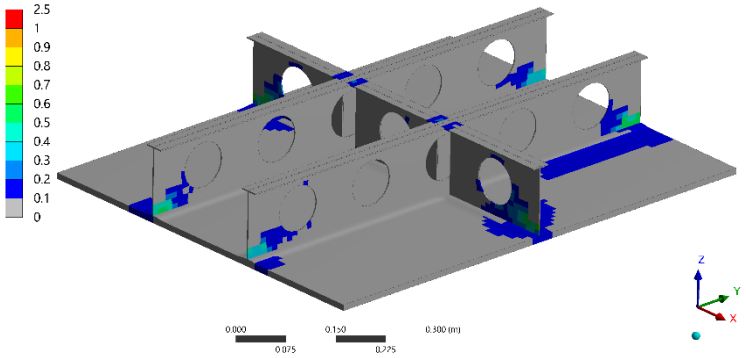

Figure 8.44 Inverse reserve factor in REESS structure analysis

Since stresses in the results are relatively low, it is tried to reduce the weight of the stacking system. For the aluminium profiles, it is tried to keep the thickness of the profile at least 2mm to create a durable and producible profile. For this reason it is tried to increase the size of the cut-outs. Also the geometry of the cut-outs is changed, to maximise their ability to resist bending. The sandwich panel lay-up is reduced in thickness. Both skins are modelled by the replacing two 630gsm layers by four 200gsm layers. The results for the REESS layer with reduced weight are shown in Figure 8.45 and Figure 8.46. It is assumed that the 4.2mm maximum deformation is within limits, since at the position of the module edge the maximum deformation is approximately 3mm. This value is expected to do no damage to the module. The model was also used to confirm that the profiles can withstand the load of the next layer before fastening, during installation. In this load case no critical loads occurred. Further weight and load optimisation is not effective at this point, since definitive modules should be chosen first to be able to create a model containing the entire REESS.

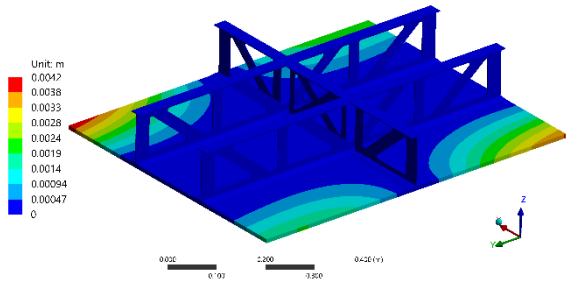

Figure 8.45 Total deformation in updated REESS structure analysis

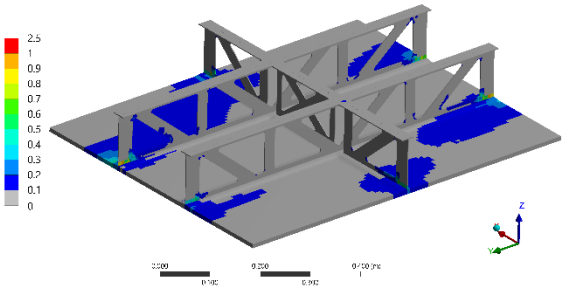

Figure 8.46 Inverse reserve factor in updated REESS structure analysis

With the applied changes, the modelled material weight decreased from approximately 3.85kg to 2.88kg. For all five layers of the main REESS compartment, this comes down to a weight reduction of 4.85kg. It must be noted that for the final weight calculation inserts, adhesive film and fasteners are not included.

To reduce complexity, the lay-up and materials used for the middle tunnel structure are set equal to the materials used in the main REESS compartment. Since spans are smaller, it is assumed that loads in this section of the REESS will be less critical. For this reason there is no purpose in creating a similar model to for this section of the REESS.

9 Concept Review

In Chapter 7, a composite rear substructure was decided to be the best concept in combination with four in-wheel motors. Chapter 8 was used to work out this concept in more detail. Using the gathered knowledge on the vehicle layout from these chapters, weight will be estimated in more accurately in this chapter.

After this estimation, the possibilities to project this concept on other vehicles will be discussed. This will be done to base the final conclusion and the recommendations on, which can be found in Chapter 10 and 11.

9.1 Weight Estimation

The chosen powertrain in combination with the replaced rear substructure resulted in the chassis, discussed in Chapter 7. An overview of this concept can be found in Figure 7.42 (page 75). In Chapter 8 steps were taken to argue the material usage of the redesigned chassis. In this section the material usage will be used to estimate the weight of the vehicle. A final overview of the weight breakdown of the total vehicle is given in Table 9.1.

Table 9.1 Weight estimation

Component	Source	Weight [kg]
Chassis as in model		124.9
Chassis remainder		68
Rear crash attenuator		4
Subtotal Chassis	-	197
REESS inner structure		35.5
REESS housing (excluding bottom)		16.5
REESS lids		5
REESS sealing		3
REESS modules	See App. A	500
Subtotal REESS	-	560
Motors	See App. A	144
Charger	See App. A	12
DC/DC Converter	See App. A	3
Wiring	See App. A	10
Auxiliaries	[32]	30
Suspension & wheels	[32]	95
Radiator & coolant	[32]	25
Auxiliary battery	[32]	20
Windscreen	[32]	15
Seats & safety belts	[32]	35
Pedals	[32]	10
Dashboard	[32]	15
Steering system	[32]	15
Special parts	[32]	30
Exterior, closures & miscellaneous	[32]	236
Bottom plate impact protection		14.5
TOTAL (vehicle empty weight)	**-**	**1467**

Based on the model parameters, the chassis weight is 124.9kg. This however excludes for example adhesives and fasteners. To estimate this additional weight for the BEV (Battery Electric Vehicle) chassis, the weight difference between the ICE (Internal Combustion Engine) chassis a modelled weight is used as a guideline. The weight difference between the model of the ICE Roding Roadster and the realistic weight is roughly 73kg. This weight includes for instance adhesives, fasteners, brackets, overlaps in material and the frontal crash attenuator. Although at first glance this value seems high, it is expected to be realistic based on the fact that several relatively heavy components are included in this mass. For example, the aluminium brackets for all four suspensions have an estimated weight of approximately 6kg (based on the volume of the brackets in Figure 8.4). The frontal crash attenuator is also measured to add approximately 7 kg. Based on the current chassis and these examples, it is assumed that 73kg is a fair estimation to include all unforeseen chassis components.

Since this remainder is a large weight component in comparison to the modelled chassis, it is expected that weight savings can be accomplished in this segment. However an accurate estimation of this remainder cannot be done in this phase of the design. For this reason the 73kg is expected to be equivalent in both versions of the chassis besides a 5kg deduction representing the cancellation of the bottom panel covering the rear substructure bottom. [32] For this reason 68kg will be used in Table 9.1.

For the REESS (Rechargeable Energy Storage System) weight estimation, the internal structure weight is estimated first, based on Section 8.3.7. The five module layers in the main REESS section have a total weight of approximately 14.4kg, excluding inserts, connectors and adhesive film. For the section in

the middle tunnel, this weight comes down to 3.5kg, based on 0.65m^2 sandwich panel and 1kg profiles. The adhesive film on both sides of the honeycomb core adds approximately 1.6kg, based on 3.2m^2 panel surface area and 250gsm. The guiding profiles add 8kg (Table 7.7) and inserts are included in the 8kg additional components and connectors (estimated in Section 7.4.1). This brings the inner REESS structure to only 35.5kg in total.

The square footage is used to calculate material weights for the REESS housing, based on Table 7.7. A measured 3.37m^2 surface area results in a weight estimation of 16.5kg. The weight of the REESS sealing is extracted from the estimation in Section 8.2.2. To include the O-ring and adhesive, this weight is rounded to 3kg. To close the seal, the lid weight estimation of 5kg is adopted from earlier estimations. This totals the REESS weight at 560kg, including 500kg modules.

It must be noted that the sheet metal plate protecting the bottom surface is not yet included in the estimated weight. The weight of this plate is estimated at 14.5kg, based on a 1.5mm thick aluminium plate covering 3.6m^2. The rest of the unchanged weights are adapted from the determined distribution in Section 7.1.2. For the exterior panelling, the measured 14kg reduction from Section 7.4.1 is subtracted. Adding all weights, the resulting kerb weight of the BEV Roding Roadster is estimated at 1467kg. When reviewing Table 9.1, the increase in weight with respect to the original Roding Roadster can be mainly imputed on the high capacity demand. Since this is based on external demands, this weight gain is regarded as inevitable as long as battery development does not result in higher energy density.

This weight estimation results in a vehicle which is 43kg heavier than the used weight distribution from Section 7.1. This 3% weight difference is assumed to be negligible due to the remaining uncertainties. For this reason it is not expected that a recalculation of the structural performance is required at this point to complete the iteration. Furthermore there is no ground to expect a significant change in the analysed weight distribution, since no major weight shifts were carried out. For this reason, it is concluded that the powertrain trade-off was carried out correctly and the chosen concept is valid.

9.2 Generic Chassis Development

During this research into a battery electric version of the Roding Roadster, it was tried to use a general approach applied to the Roding Roadster in particular. This resulted in a couple of methods which can be used more generic by Roding Automobile GmbH or other car manufacturers.

Concept Analysis

For the rough component layout, a method was developed to give a quick overview of major vehicle parameters based on the weight distribution. This method creates the possibility to get an overview of the influences of the vehicle layout on the weight distribution early in the development process. This method is vehicle independent and can be used for all vehicle configurations when target values for the vehicle parameters are changed accordingly.

Ergonomics and Regulation Analysis

A parametric CAD master part was created for the layout of the chassis around the component distribution. This model combines a visualisation of ergonomic standards, regulations and carry-over parts (unaltered components from other vehicles). These visualisations are based on either regulations, standards or supplier data. Since this model is built in a parametric way, this model can be used to suit all vehicles for the ergonomic section. For passenger cars subjected to type approval in the European Union, the regulations section of the model is directly applicable to proof direct vision regulations and check impact zones for collision tests. This is possible since vehicle dependent parameters are clearly defined and adaptable. This model is currently being applied at new Roding Automobile GmbH projects to check the compliance of these projects. For the detailed development of passenger vehicles it might be relevant to add additional visualisations and analyses to assess a vehicle more elaborately.

Collision Analysis

To estimate the structural performance during dictated collision tests, methods were combined to create a relatively simple model. For a static analysis, inertia relief was used to estimate load paths in the vehicle during impact. A universal method was used to set a lower load limit based on energy absorption and an upper limit based on the allowed occupant injury criteria. This method makes it possible for vehicle manufacturers to estimate the structural performance of a chassis during impact. Besides the fact that for composite chassis it is very complex to create a realistic dynamic analysis, this method

might also save costs by creating simple models for metal chassis. As explained before, a modal analysis is required for every chassis design to be able to use this generalisation. This should be done to guarantee the absence of a large dynamic overshoot.

Besides analysis of type approval in the European Union, this method can be extended to cover type approval collision tests for different countries as well. For example for type approval in the USA, the ratio between ASI (Acceleration Severity Index) and HIC (Head Injury Criterion) can be applied similarly to set the upper limit of the collision load. This can be done since the injury criteria are defined similarly within type approval for the USA. However, since barriers and test velocities are different, the energy absorption method can be used in a similar fashion to estimate the lower load limit. [76]

REESS Concept

During the literature study it was found that HV (High Voltage) components in electric vehicles must be grounded according to ECE R100. During this research, a cost and time efficient method to ground carbon fibre sandwich panels was developed and tested. Since these tests showed constant and reliable results, this method of grounding REESS compartments can be adapted for more vehicles. This principle can be easily combined with the modular stacking concept, which can be adapted to suit other REESS geometries and sizes.

Since this grounding concept cuts costs with respect to coating of CFRP material, it might influence the choice of materials. This influence on material choice can facilitate vehicle weight reduction, which results in a beneficial lower power consumption. Besides the REESS, this grounding method might also be adaptable to other high voltage components in electric vehicles or other high voltage systems where grounding is required and a low weight is relevant.

Chassis Concept

Besides design methods, the chassis concept can also be applied more generic. The suggested chassis layout is very suitable for the redesign of more mid-engine vehicles or novel vehicles with a similar layout. In the case of the Roding Roadster, the middle-tunnel was filled with battery modules, to accommodate the requested REESS capacity. Depending on the vehicle and its requirements, only the rear REESS compartment might suffice. This can result in a competitive chassis concept for electric sports vehicles, which uses a light but stiff structure due to the combined performance of the REESS and chassis.

10 Conclusion

Knowledge of composites and its usage in the automotive industry has increased significantly in the last years. Since the founding of Roding Automobile GmbH in 2008, the company has been developing the composite Roding Roadster. Besides the company its flagship, Roding Automobile GmbH was involved in the development of several electric prototype and test vehicles, parallel to CFRP (Carbon Fibre Reinforced Plastic) manufacturing for motorsport and other industries. To combine these technologies, this research was initiated to develop a chassis for a battery electric Roding Roadster concept, suitable for type approval process in the EU (European Union).

In this research, the chassis modification of the Roding Roadster has provided valuable knowledge on the use of a battery electric powertrain in sports cars. The replacement of the metal rear substructure by a composite structure is shown to be the best solution to combine the structural function of the chassis with an integral construction of the REESS (Rechargeable Energy Storage System). For the REESS, a modular system was developed to benefit from this combined structure with as less added complexity as possible. By combining this chassis concept with four in-wheel motors, the weight distribution could be modified to create ideal vehicle characteristics due to a more flexible design envelope.

It became clear that desired vehicle characteristics have a guiding role in the vehicle layout of electric sports vehicles. Furthermore it became clear that, to comply with regulations for type approval in the EU, mainly the lateral collision requires additional attention. It was discovered that these collision requirements could be averted at annual production numbers under 1,000 vehicles. Nevertheless compliance was estimated using static finite element analyses in combination with the inertia relief method to estimate the performance of the chassis during the impact. With the critical points addressed, a vehicle with a kerb weight of 1467kg was estimated to fulfil all requirements. The conclusion can be drawn that the addition in weight is mainly the consequence of a high capacity requirement.

Tests have been conducted to prove the adequate grounding of CFRP components such as the used REESS construction. It was shown that a cost effective method using a blind rivet nut can be used to guarantee adequate grounding via the aluminium honeycomb in typically sized sandwich panels. It is concluded that this method would be scalable and can be combined with the modular REESS concept. Either way, this concept can serve as a cost efficient solution to develop competitive battery electric vehicles for type approval.

For Roding Automobile GmbH the goal of this research was to get a better understanding of the implications of the integration of a battery electric powertrain on the current chassis layout and its type approval in the EU. This research has provided knowledge on the implications of different layouts and concepts and provided insight in a decision-making process. For Roding Automobile GmbH, it has become clear, that a battery electric version of the Roding Roadster for type approval in the EU is feasible, if a selected set of adjustments is made. It can be concluded that this project has provided valuable insight for the development opportunities of future vehicle projects at Roding Automobile GmbH and has provided Roding Automobile GmbH with several tools to simplify judgement during this development.

11 Recommendations

This research has shown the feasibility of a battery electric version of a composite sports car. Furthermore is has been explained how decision-making processes and concepts can be used in different vehicles or projects. In this section recommendations will be presented, which are endorsed for the continuation of this research. These recommendations are split into recommendations for the further development of the BEV (Battery Electric Vehicle) Roding Roadster and recommendations which are directed towards the generalisation of the research.

11.1 Project Specific Recommendations

This report presented a research concerning the development of a battery electric version of the Roding Roadster. For further development of this vehicle, the following recommendations are made.

Improve Structural Analysis

For the final version of the structural analysis, only a range could be provided where the results lie in. This was done to get an impression of the worst-case and best-case performance when including the REESS (Rechargeable Energy Storage System) in the structural performance of the chassis. Since for the extreme driving load case this range was big, it is recommended to improve the structural model by combining the chassis analysis with the REESS analysis. This way the influence of the REESS on the chassis stiffness can be estimated. In combination with more accurate load cases describing critical suspension loads, this will give a better understanding of the chassis. Using analysis software such as Adams Car or Lotus Shark, this information can be used to either improve vehicle dynamics or improve vehicle weight, which are both important aspects when reviewing sports cars. [74, 75]

Improve REESS Concept

A relatively universal REESS concept was developed in this research to create a REESS which can be easily assembled and adapted. Since no specific module was chosen, thorough optimisation was not performed. For further development of the BEV Roding Roadster, it is recommended to review the developed concept for a specific module. This way, clever solutions for module fixings might be combined with the rest of the concept. Furthermore, this means that the structural requirements of the construction can be defined more accurate.

Suspension Development

Since the chosen concept makes use of in-wheel motors, redesign of the suspension is inevitable. It is recommended that the AWD (All-Wheel Drive) aspect of the powertrain is addressed during the redesign of the suspension. This way, the dynamics of the electric vehicle can be influenced to improve the racing capabilities to the maximum extent.

Due to the use of in-wheel motors, the unsprung mass increases significantly. The effect of this added unsprung mass on the vehicle dynamics is negative, but can be neutralised when addressed properly in the suspension design. [11] It is recommended that this influence is minimised, when the suspension is revised to exploit the possibilities of the concept to the full extent.

11.2 General Recommendations

Besides recommendations which specifically apply to the Roding Roadster, a set of recommendations is made for the generalisation of this research as well. The most relevant recommendations will be discussed below.

Improve Structural Analysis

This research has provided a method to estimate the behaviour of the chassis during the collisions defined for type approval. Within the final version of the structural analysis some critical points could not be tackled properly. Since in practice, a finished vehicle will be used in a lateral collision for approval under regulation ECE R95, the behaviour of the door becomes very relevant. Understanding of its behaviour is required for further type approval of vehicles which do not fall under small series type approval. To increase the understanding, it is recommended to analyse the chassis including the realistic behaviour of the door early in the process. Along with realistic modelling of the REESS structure, this would improve accuracy of the performed analysis significantly.

Investigate and Include Safety Factors

As explained before, this research made use of a conservative approach for the determination of load cases. Besides that, no safety factors were introduced to report unbiased results. It is recommended that extra research should gather information on the deviation in material quality and the deviation in production quality at Roding Automobile GmbH. This should be done to account for any uncertainties in the produced vehicle. This should be done to ensure that every approved vehicle meets the set requirements for type approval. [1] Furthermore, it is recommended that the desired margin of safety is investigated for every load case. This will define how close to the failure limit each load case may be constructed. The uncertainties and inaccuracies within the analysis should be included within these margins.

Improve REESS Concept

For the general improvement of the REESS, its structural analysis should be reviewed. It was seen that the maximum deformation at the corners of each layer is the weakest point of the concept. It is recommended that this aspect of the concept is improved. It might be possible to combine additional supports of the corners with a revised design of the connection between the different walls of the REESS housing. It is expected that this can increase the efficiency of the structure significantly.

Resistance Measurements

A grounding concept using rivnuts was purposed to remove an additional process and decrease costs of grounding CFRP components in the HV (High Voltage) system. It is recommended that larger panels will be tested to validate the created relations. Along with these measurements, the durability of the used connection should be tested to guarantee adequate grounding throughout the lifetime of a vehicle. It is recommended that during these tests, the emphasis is placed on galvanic corrosion within the required connection and loss of connection due to vibrations and deformations.

References

[1] United Nations, Agreement concerning the adoption of uniform conditions of approval and reciprocal recognition of approval for motor vehicle equipment and parts, Geneva: United Nations, 1995.

[2] McLaren, “The Cars,” McLaren, [Online]. Available: http://cars.mclaren.com/legacy-cars. [Accessed 14 June 2016].

[3] Lucintel, "Growth Opportunities in Global Carbon Fiber Market 2016-2021," Lucintel, 2016, 2016.

[4] Lucintel, "Automotive Lightweight Materials Market 2014-2019," Lucintel, Irving, 2015.

[5] B. Bregar, “Price keeping carbon fiber from mass adoption,” *Plastic News,* 5 August 2014.

[6] R. N. Shame, T. Simha, K. Rai and G. Ravikumar, “Carbon composites are becoming competitive and cost effective,” Infosys, Pune, 2015.

[7] BMW, “The all-electric BMW i3,” [Online]. Available: http://www.bmw.com/com/en/newvehicles/i/i3/2016/showroom/index.html. [Accessed 20 June 2016].

[8] M. Trzesniowski, Rennwagentechnik, Wiesbaden: Vieweg + Teubner, 2008.

[9] R. N. Jazar, Vehicle Dynamics, Berlin: Springer, 2008.

[10] D. Prassel, “one massive go kart,” 10 08 2012. [Online]. Available: http://forums.steampowered.com/forums/archive/index.php/t-2963764.html. [Accessed 26 04 2016].

[11] A. Urlings, “Literature Study - An Introduction into Composite Chassis and Electric Vehicles,” TU Delft/Roding Automobile, 2016.

[12] European Parliament, Council of the European Union, *Directive 2007/46/EC of the European parliament and of the council,* Strasbourg/Brussels: European Union, 2007.

[13] European Parliament, Council of the European Union, “Supplementing and amending Regulation (EC) No 661/2009 of the European Parliament and of the Council as regards the inclusion of specific procedures, assessment methods and technical requirements, and amending Directive 2007/46/EC ...,” European Union, Strasbourg/Brussels, 2015.

[14] European Parliament, Council of the European Union, *Commission regulation (EU) 2016/1004,* Strasbourg/Brussels: European Union, 2016.

[15] European Parliament, Council of the European Union, “Amending Regulation (EC) No 661/2009 of the European Parliament and of the Council,” European Union, Strasbourg/Brussels, 2016.

[16] J. A. J. Wolf and M. F. Nelson, “The Use of Inertia Relief to Estimate Impact laods,” in *Conference proceedings: 2nd International Conference on Vehicle Structural Mechanics*, Southfield, 1977.

[17] L. Liao, “A Study of Inertia Relief Analysis,” AIAA, Denver, 2011.

[18] N. Pagaldipti and Y. Shyy, “Influence of inertia relief on optimal designs,” AIAA, Albany, 2004.

[19] G. Käsmeier, “Vehicle body and method for producing a vehicle body”. Germany Patent WO 2011/12808 A1, 20 October 2011.

[20] B. Riley, „Formula SAE anthropometric reference data 5th percentile female & 5th percentile male,“ SAE international, Warrendale, 2015.

[21] SAE International, „Surface Vehicle Standard J4002 - H-Point Machine (HPM-II) Specifications and Procedure for H-Point Determination,“ SAE International, Warrendale, 2010.

[22] Recaro Automotive Seating, Recaro Sportster CS, Kirchheim unter Teck: Recaro, 2015.

[23] S. Macey and G. Wardle, H-Point, The Fundamentals of Car Design & Packaging, Culver City: Designstudio Press, 2009.

[24] J. Grabner and R. Nothhaft, Konstruieren von Pkw-Karosserien, 3., erweiterte Auflage ed., Berlin: Springer, 2006.

[25] SAE international, “Surface Vehicle Standard J1052 - Motor Vehicle Driver and Passenger Head Position,” SAE International, Warrendale, 2010.

[26] R. Sturt and C. Fell, “The relationship of injury risk to accident severity in impacts with roadside barriers,” *International Journal of Crashworthiness,* pp. 165-172, 29 April 2009.

[27] M. Dr. Shojaati, “Correlation between injury risk and impact severity index ASI,” in *3rd Swiss Transport Research Conference*, Monte Virita, 2003.

[28] D. Gabauer and R. Thomson, “Correlation of vehicle and roadside crash test injury criteria,” in *19th International Technical Conference on the Enhanced Safety of Vehicles*, Washington, 2005.

[29] European Committee for Standardization, “Road restraint systems; Part 2: Performance classes, impact test acceptance criteria and test methods for safety barriers including vehicle parapets,” British Standards Institution, London, 2010.

[30] F. A. J. Smith and P. M. Hopkins, “Non-linear Internal Loads Modeling Methods,” *Proceedings of AHS International 62nd Annual Forum - Vertical Flight: Leading through Innovation – Proceedings, Vol. III,* pp. 1436-1455, 2006.

[31] Granta Material Intelligence, „CES EduPack 2016,“ Granta Design Limited, Cambridge, 2016.

[32] Roding Automobile GmbH, *Fertigungsartikel Stammdaten,* Roding, 2016.

[33] R. Mills, “Dexmet Expanded Materials,” Dexmet, Wallingford, 2016.

[34] ELV Elektronik AG, Bedienungsanleitung: Digital-Multimeter mit Datenlogger und PC-Link VC 98B, Hongkong: ELV Elektronik AG, 2010.

[35] R. A. Serway, J. W. Jewett and V. Peroomian, Physics for scientists and engineers with modern physics, Boston: Brooks/Cole, 2014.

[36] S. Streitbürger, “Einzigartige Composite Anwendung,” STB-GH-TEC (UG), Uchte, 2016.

[37] STB-GH-TEC (UG), *Quotation - SVS-kernmaterial,* Uchte: STB-GH-TEC (UG), 2016.

[38] bigHead Bonding Faseners Ltd., “bigHead catalogue,” bigHead Bonding Faseners Ltd., Bournemouth, 2015.

[39] Emil Lux GmbH & Co. KG, “Sicherheitsdatenblatt gemäß 1907/2006/EG, Artikel 31,” OBI, Wermelskirchen, 2013.

[40] Chemtronics, “CircuitWorks Conductive Pen Technical Data Sheet CW2200,” Chemtronics, Kennesaw, 2013.

[41] J. Pawlowski and G. Tidbury, Vehicle body engineering, London: Century, 1969.

[42] K. Newton, W. Steeds and T. Garrett, The Motor Vehicle, Oxford: Butterworth-Heinemann Ltd, 1989.

[43] J. C. Brown, J. Robertson and S. T. Serpento, Motor Vehicle Structures, Oxford: Butterworth-Heineman, 2002.

[44] Humanetics, “Hybrid III 50th Male Dummy,” Humanetics Innovative Solutions, 2016. [Online]. Available: http://www.humaneticsatd.com/. [Accessed 24 October 2016].

[45] European New Car Assessment Programme, “Full Width Frontal Impact Test Protocol v1.0.3,” Euro NCAP, Brussels, 2017.

[46] SAE Passenger Protection Commitee, Vehicle crashworthiness and occupant protection in frontal collisions, Warrendale: Society of Automotive Engineers, Inc., 1990.

[47] C. Schäfer und J. Prof. Dr.-Ing. Hirsch, *Aluminium Electro-Car Lightweight Design,* Oslo: Hydro, 2014.

[48] European New Car Assessment Programme, “Offset Deformable Barrier Frontal Impact Testing Protocol v7.1.1,” Euro NCAP, Brussels, 2016.

[49] CrashNet1, “Youtube - 2016 Honda Civic Crash Test (Side Crash),” 28 April 2016. [Online]. Available: https://www.youtube.com/watch?v=t4unqvp3N1E. [Accessed 10 December 2016].

[50] CrashNet1, “Youtube - 2016 Volvo XC90 Crash Test (Side Crash),” 5 May 2016. [Online]. Available: https://www.youtube.com/watch?v=C9NW8wPV_Hg. [Accessed 10 December 2016].

[51] EuroNCAP, “Youtube - Euro NCAP | Saab 9-5 | 2009 | Crash test,” 18 December 2009. [Online]. Available: https://www.youtube.com/watch?v=tdbbkov7QDc. [Accessed 10 December 2016].

[52] EuroNCAP, “Youtube - Euro NCAP | Fiat Multipla | 2001 | Crash test,” 19 August 2009. [Online]. Available: https://www.youtube.com/watch?v=PRCj7JnMxWU. [Accessed 10 December 2016].

[53] ANSYS Inc., “ANSYS-Material Library,” [Online]. [Accessed 10 November 2016].

[54] C. Kassapoglou, Design and Analysis of Composite Structures, 2nd ed., West Sussex: Wiley, 2013.

[55] R. Hibbler and K. B. Yap, Mechanics for Engineers - Dynamics - SI edition, London: Pearson, 2013.

[56] C. Smith, Tune to Win, Fallbrook: Aero Publischers, 1978.

[57] A. Khajepour, S. Fallah and A. Goodarzi, Electric and Hybrid Vehicles, West Sussex: Wiley, 2014.

[58] Roding Automobile GmbH, Roding Roadster R1 Preisliste, Roding, 2012.

[59] D. Hrovat, “Influence of Unsprung Weight on Vehicle Ride Quality,” *Journal of Sound and Virbration,* pp. 497-516, 1988.

[60] L. Ming-chun, Z. Chen-ning and W. Zhi-fu, “Research on the Influence of Unsprung Mass on Vehicle Handling Stability,” *Advanced Materials Research,* pp. 816-820, 30 August 2012.

[61] S. Black, “Composites World,” Composites Technology, 10 January 2013. [Online]. Available: http://www.compositesworld.com/. [Accessed 6 December 2016].

[62] H. Kals, Industriële productie : het voortbrengen van mechanische producten., Boom Uitgevers: Amsterdam, 2007.

[63] D. Booth, “Supercar Review: 2015 Porsche 918 Spyder,” Postmedia Network, 9 December 2013. [Online]. Available: http://driving.ca/. [Accessed 22 November 2016].

[64] F. Senécal-Tremblay, Director, *How its Made Dream Cars: The Porsche 918 Spyder.* [Film]. Canada: Discovery Channel, 2015.

[65] TenCate Advanced Composites, *TenCate Cetex and CFRT Thermoplastic Advanced Composites,* Morgan Hill: TenCate, 2016.

[66] Cars informations, “Cars Information,” [Online]. Available: http://carsinfox.com/. [Accessed 14 November 2016].

[67] Du Ponts Coating Solutions, “DuPont AQUA EC 3000,” Wilmington, 2012.

[68] E. Almeida, I. Alves, C. Brites and L. Fedrizzi, “Cataphoretic and autophoretic automotive primers: A comparative study,” Elsevier, Oxford, 2002.

[69] C. Nergiza, “BMW I3: Una opinión de primera mano,” 11 March 2015. [Online]. Available: http://nergiza.com/. [Accessed 22 November 2016].

[70] Gregor Hämel, “O-Ring Einbauberechnung,” Kremer GmbH, [Online]. Available: http://www.kremer-reiff.de/. [Accessed 19 December 2016].

[71] Stangl & Co., *Konstruktions Standards,* Roding: SK Group, 2016.

[72] The Taunton Press, “Start Woodworking,” The Taunton Press, 19 April 2012. [Online]. Available: http://www.startwoodworking.com/. [Accessed 21 December 2016].

[73] L. Meirovitch, Analytical methods in vibrations, New Jersey: Pearson, 1967.

[74] MSC Software, “Adams Car,” MSC Software, [Online]. Available: http://www.mscsoftware.com/product/adams-car. [Accessed 10 February 2017].

[75] Lotus Cars Ltd., Getting Started With Lotus Suspension Analysis, Norwich: Lotus Cars Ltd., 2013.

[76] Department of Transportation and Department of Homeland Security, “e-CFR Title 49, Chapter V, Part 571,” U.S. Government Publishing Office, Washington D.C., 2017.

[77] Fluke Corporation, *Fluke 83V and 87V Digital Multimeters Detailed Specifications,* Everett: Fluke Corporation, 2005.

[78] Voltcraft, “Labornetzgerät, Festspannung VOLTCRAFT FSP-11330 13.8 V/DC 30 A 415 W Anzahl Ausgänge 1,” Voltcraft, [Online]. Available: http://www.voltcraft.com/laboratory-power-supplies/. [Accessed 19 October 2016].

[79] Ohmite, “40 Series - Datasheet,” [Online]. [Accessed 19 October 2016].

Title Page Figures References

Image courtesy (from left to right):

Front page:	RA
Chapter 3:	http://library.nrhtx.com/
	http://www.autoexpress.co.uk/
	RA
Chapter 4:	RA
	http://www.projectmanagementod.co.uk/
	http://www.johnandtable.com/
Chapter 5:	http://www.destentor.nl/
	-
	http://itsocial.fr/
Chapter 6:	RA
	http://highroads.az.aaa.com/
	RA
Chapter 7:	RA
	http://lmtabogados.com/
	RA
Chapter 8:	RA
	http://www.businessinsider.com/
	-
Chapter 9:	RA
	http://reputationsavvy.com/
	http://www.jobacle.com/

Appendix A: Resistance Measurement Method

To measure resistance, a multimeter can only be used for accurate measurements higher than 0.1Ω. [77] For lower resistance a milliohm meter should be used. This method uses four measurement points to compensate for the contact resistants to create a reliable measurement. Due to limited resources within this research, an alternative method is used to achieve reliable results. To perform measurements, the specimens were connected in series with power source. A load was added to the circuit to prevent shortcuts along the low resistance specimen. This circuit is connected as shown in Figure A.1. Using this method, voltage and current are measured as shown. This creates more accurate results than direct resistance measurements, because measurement of small voltages can be done more accurate than resistance.

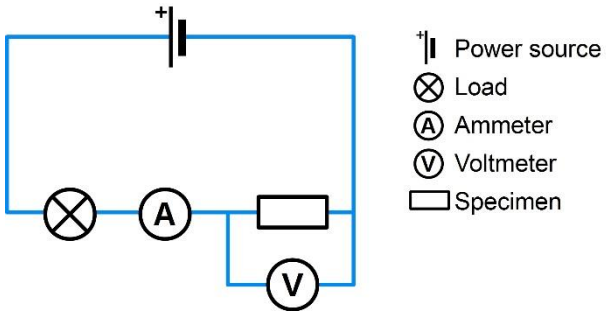

Figure A.1Schematic overview of measurement circuit

As power source a Voltcraft Fsp-11330 was used to provide 13.8V. [78] The load can be chosen randomly. For this project a Hella 2JA 009 037 interior light was used. For the current and voltage measurements an ELV VC 98B multimeter was used. [34] This measures voltage with a resolution of 0.001V and current was rounded to values of 0.05A. Using Ohm's law, the resistance can be calculated as in Formula A.1.

$$R = \frac{U}{I}$$

A.1 [35]

The multimeter which was used has an accuracy of less than 3% within the used spectrum for the combined current and voltage measurement. [34] This was additionally verified using a fixed resistor to check the accuracy. A resistor was chosen in the same measuring spectrum as the samples with an error of less than 1%, namely an Ohmite 40 series 100mΩ ±1% 10W. [79] For this resistor, a resistance of 100.2mΩ was measured, which verifies the accuracy of the measurement with an error less than 1.6%. This error is calculated by assuming a resistance of 99mΩ, because this would result in the largest error.

This method relies on a good connection between the set-up and the specimen. This means that a good connection must be made in the carbon fibre material, to measure CFRP (Carbon Fibre Reinforced Plastic) grounding concepts. Another solution is to eliminate the connection point in the composite material. This can be done by combining two identical samples into one symmetrical specimen. In this case, the measurement can be performed between two good connection points. By dividing the measured resistance by two, the resistance between the specimen midpoint and a ground wire is known. This principle is shown in Figure 5.15 (Page 29) and is based on the fact that two resistors in series have a total resistance equal to the sum of the connected resistors. [35] Results throughout this research are always given for half specimens, because these represent the values compared to regulations.

For the measurements in this report, the resistance was assumed to be independent of the absolute position of the connection points. Regarding this assumption no connections were made close to the edge of the substrate. For the measurements in Figure 5.17 (page 31), the angle between honeycomb interruption and the line connecting both rivnuts was limited between 80º and 110º. Within this range, the resistance was assumed to be independent of this angle. This is valid due to neutralisation any geometrical effects as a result of point symmetry.

Appendix B: Material Data

In this appendix an overview will be given of the materials which were used for the FE (Finite Element) analyses in this research. Isotropic materials can be found in Table B.1. The used material data for orthotropic materials can be found in Table B.2. The manufacturer only provided relevant material data for the honeycomb material. For this reason this set of data was completed with data from the ANSYS material database for honeycomb material, since these values are required to solve the model. This can be done because these values are not critical for the model but are required as an input. From the alignment, the source of the value can be found.

Table B.1 Isotropic material data

Material Property	Unit	1.0984 S500C	1.4301	3.2315 T6	3.3206 T6	3.3547 H323
Src.	-	[31]	[31]	[31]	[31]	[31]
Density	[kg/m^3]	7850	7905	2700	2700	2655
Young's Modulus	[GPa]	211	197	72	72	72
Poisson's Ratio	[-]	0.305	0.27	0.33	0.33	0.34
Yield Strength	[MPa]	545	603	265	215	326
Ultimate Compressive Strength	[MPa]	545	603	316	215	211
Ultimate Tensile Strength	[MPa]	625	949	310	245	247

Table B.2 Orthotropic material data

Material Property	Unit	Carbon-Epoxy Woven Prepreg	Carbon-Epoxy Unidirectional Prepreg	Aluminium Honeycomb
Src.	-	[53]	[53]	[53]
Density	[kg/m^3]	1480	1540	57.66
Young's Modulus X	[GPa]	91.82	209	0.001
Young's Modulus Y	[GPa]	91.82	9.450	0.001
Young's Modulus Z	[GPa]	9.00	9.450	0.634
Poisson's Ratio XY	[-]	0.05	0.27	0.49
Poisson's Ratio YZ	[-]	0.3	0.4	0.001
Poisson's Ratio XZ	[-]	0.3	0.27	0.001
Shear Modulus XY	[MPa]	19500	5500	1*10^{-6}
Shear Modulus YZ	[MPa]	3000	3900	137.9
Shear Modulus XZ	[MPa]	3000	5500	275.8
Tensile Strength X	[MPa]	829	1979	0
Tensile Strength Y	[MPa]	829	26	0
Tensile Strength Z	[MPa]	50	26	2.24
Compressive Strength X	[MPa]	-439	-893	0
Compressive Strength Y	[MPa]	-439	-139	0
Compressive Strength Z	[MPa]	-140	-139	-2.24
Shear Strength XY	[MPa]	120	100	0
Shear Strength YZ	[MPa]	50	50	0.896
Shear Strength XZ	[MPa]	50	100	1.4479
Max Strain Tension X	[-]	0.0086	0.0092	-
Max Strain Tension Y	[-]	0.0086	0.0031	-
Max Strain Tension Z	[-]	0.007	0	-
Max Strain Compression X	[-]	-0.0055	-0.0053	-
Max Strain Compression Y	[-]	-0.0055	-0.0172	-
Max Strain Compression Z	[-]	-0.012	0	-
Max Strain Shear XY	[-]	0.022	0.016	-
Max Strain Shear YZ	[-]	0.018	0	-
Max Strain Shear XZ	[-]	0.018	0	-

Appendix C: Powertrain Market Analysis